Numerical analysis of the effect of earth pressure balanced shield tunneling on soil stress–deformation behavior

October 2014

Alireza AFSHANI

Numerical analysis of the effect of earth pressure balanced shield tunneling on soil stress–deformation behavior

土圧式シールドトンネル工事が地盤の応力変形挙動に及ぼす影響に関する数値解析

by

Alireza AFSHANI

アリレザ アフシャニ

WASEDA University
Graduate School of Creative Science and Engineering
Department of Civil and Environmental Engineering
Research on Soil Mechanics

October 2014

Doctor of Philosophy Declaration

I, Alireza Afshani, declare that this PhD thesis entitled 'Numerical analysis of the effect of earth pressure balanced shield tunneling on soil stress–deformation behavior', is my original work, gathered and utilized especially to fulfil the purposes and objectives of this study, and has not been previously submitted to any other university for a higher degree. This thesis contains no material that has been submitted previously, in whole or in part, for the award of any other academic degree or diploma.

Alireza Afshani

Date: October, 2014

Signature:

Acknowledgements

I would like to give my special thanks to my supervisor Prof. Hirokazu Akagi for his insight, advices, and commitment through the past three years. He has been very supportive. In addition, I appreciate the freedom given to me to explore, the opportunities to shape my skills, and the effort and time he put into my thesis. I would also like to express my gratitude to my other mentors Prof. Kazuhito Komiya at Chiba Institute of Technology for his worthy advices and assistance during the thesis accomplishment, Dr. Hiroshi Dobashi at Metropolitan Expressway Company for his kind cooperation on preparing the required data, and also his thoughtful guidance on fulfillment of the thesis, and Dr. Shinji Konishi at Tokyo Metro Company for his helpful feedbacks and advices through the past years.

The financial support from my supervisor Prof. Hirokazu Akagi, and also from Department of Civil and Environmental Engineering at Waseda University is highly appreciated. This assistantship greatly expands my horizon in various aspects, and made the accomplishment of this thesis feasible for me.

I'm thankful to Mr. Osamu Yoshino for his support and aid for preparation of data needed for this thesis to be completed. I would like to thank every member of Prof. Akagi laboratory during these three years including my close friend Mr. Taichi Hyoudo. My thanks extended to Ms. Shio Ariura, Akagi laboratory's nice secretary who really was supportive and kind through these years. The author also wishes to thank his referees, Prof. Komine and Prof. Kiyomiya for their advice, insight and comments in better development of the thesis.

I express my sincere thanks to my family, their love, support, and encouragement during these years. I thank God for the many blessing he has always bestowed on me.

Tokyo, Japan

October 2014

Abstract

Reliable prediction and control of ground movements represent an essential component of underground construction projects in congested urban environments to prevent possible damage to adjacent structures and utilities. In urban environments, the impact of the tunnel construction process on the surrounding underground has to been kept minimal due to the presence of sensitive and valuable surface and sub-surface structures. Therefore, lowering of the groundwater table is often prohibited and the resulting surface settlements have to been kept below the given admissible limits. Shield supported tunnel construction is an appropriate way to fulfil these requirements.

An important subject in tunnel engineering is to analyze the stress-deformation behavior of soil during tunnel construction. In engineering practice, different design methods tend to be used, varying from simple empirical and analytical formulations to advanced finite element analyses.

To achieve a realistic reproduction of behavior of the soil due to the shield tunneling, the excavation simulation usually accounts for the coupling between the pore fluid flows and pressures and the soil matrix deformations and stresses in partially and fully saturated conditions. In the case of large FEM meshes, finite element analysis calculation especially for three dimensional models needs powerful computer and long computation time. Consequently, in the case of EPB tunneling which is common and safe practice in Japan, this study attempts to perform the three-dimensional FEM analysis with a total stress analysis under a simple drainage condition instead of a complicated effective stress analysis considering soil-water coupling and then verify the stress-deformation behavior by comparing FEM outputs with the field measurement results.

The current thesis reports the results of numerical analysis with 3D FEM of EPB shield tunneling by considering various realistic conditions, such as an advance rate of

the tunnel face, the consolidation coefficient of the soil and the overburden depth of the tunnel. This simplified numerical analysis procedure of shield tunneling in this case is mainly used for the settlements predictions of the soil due to tunneling construction.

This thesis develops, implements, and applies an efficient simple procedure for the ground response computation by earth pressure balanced shield tunneling. This study is divided into three main parts; in the first part, the effect of EPB shield tunneling on the soil effective stress path is investigated. In the second part, the effect of EPB tunneling on the drained and undrained behavior of the soil is examined. In the last part, EPB shield tunneling simulation case studies are introduced. In this way, a simplified finite element procedure using useful empirical formulae, which enable a simple total stress analysis under simple drainage condition instead of a complicated effective stress analysis considering soil-water coupling, have been proposed by organizing the many parametric study analysis results. The proposed FE method have been verified by comparing the 3D FEM analysis results of EPB shield tunneling with the field measurement record obtained from the large diameter and the deep EPB shield tunneling within the stiff ground.

Keywords

Earth pressure balanced shield tunneling, Hydraulic condition of soil, Stress-path analysis, Shield tunneling case study

Contents

Doctor of Philosophy Declaration ..... **i**

Acknowledgements ..... **ii**

Abstract ..... **iv**

Keywords ..... **v**

Contents ..... **vi**

List of Figures **8**

List of Tables **12**

Chapter 1 Introduction **13**

1.1 Background 13

1.2 Thesis structure 16

1.3 Objectives of the research 20

References: 21

Chapter 2 Literature review **22**

2.1 Introduction 22

2.2 Shield tunneling 22

2.2.1 Shield tunneling types 22

2.2.2 Grouting during EPB tunneling 27

2.2.3 Shield tunneling support pressure 28

2.3 Shield tunneling advancement simulation using finite element analysis 29

2.4 Shield tunneling effects on hydraulic condition of the soil 35

2.5 Summary 36

References 37

Chapter 3 EPB Shield tunneling effects on stress-state and hydraulic condition of soil **40**

3.1 Introduction 40

3.2 Earth Pressure Balanced tunneling principals 41

3.3 Effect of EPB shield tunneling on the soil stress-path 43

3.3.1 Numerical model and used parameters 44

3.3.2 Stress path analysis 45

3.4 Effect of EPB shield tunneling on the hydraulic condition of the soil 65

3.4.1 Drained and undrained condition of the soil during EPB tunneling 65
3.4.2 Method 66
3.4.3 Parametric study 67
3.4.4 Numerical experimental equation for soil drainage determination during EPB tunneling 73
3.5 Proposed simplified finite element method 78
3.6 Summary 80
3.7 Appendix A (2D tunneling chart method proposed by Chen and Tseng, 2010) 81
References: 85
Chapter 4 Case study 86
4.1 Introduction 86
4.2 Project Overview 86
4.3 Geological and hydrological specification of the site 90
4.4 Monitoring sections 92
4.5 Measurement data 94
4.6 Summary 97
References: 98
Chapter 5 Comparison and verification 99
5.1 Introduction 99
5.2 FEM numerical model 100
5.3 Comparison and verification 103
5.3.1 General 103
5.3.2 Vertical soil displacement comparison 103
5.3.3 Comparison of computational time 105
5.4 Summary 107
References: 109
Chapter 6 Conclusion 110
6.1 Achieved results 110
References: 113
LIST OF PUBLISHED PAPERS 114

List of Figures

Figure 1.1. Structure of the thesis..... 16

Figure 2.1. Schematic representation of SPBM 24

Figure 2.2. Schematic representation of EPBM 24

Figure 2.3. Range of suitable soil for EPB and SPB machines. 26

Figure 2.4. Sliding mechanism in front of TBM machine 29

Figure 3.1. Equilibrium forces in front of EPBM..... 43

Figure 3.2. Three dimensional PLAXIS model 46

Figure 3.3. Effective principal stress variation at point c40 for soil type 1 during active loading.50

Figure 3.4. Effective principal stress variation at point s40 for soil type 1 during active loading.51

Figure 3.5. Effective principal stress variation at point c40 for soil type 2 during active loading.51

Figure 3.6. Effective principal stress variation at point s40 for soil type 2 during active loading.52

Figure 3.7. Effective principal stress variation at point c40 for soil type 3 during active loading.52

Figure 3.8. Effective principal stress variation at point s40 for soil type 3 during active loading.53

Figure 3.9. Effective principal stress variation at point c40 for soil type 1 during static loading.53

Figure 3.10. Effective principal stress variation at point s40 for soil type 1 during static loading.54

Figure 3.11. Effective principal stress variation at point c40 for soil type 2 during static loading.54

Figure 3.12. Effective principal stress variation at point s40 for soil type 2 during static loading.55

Figure 3.13. Effective principal stress variation at point c40 for soil type 3 during static loading.55

Figure 3.14. Effective principal stress variation at point s40 for soil type 3 during static loading.56

Figure 3.15. Effective principal stress variation at point c40 for soil type 1 during passive loading. 56

Figure 3.16. Effective principal stress variation at point s40 for soil type 1 during passive loading. 57

Figure 3.17. Effective principal stress variation at point c40 for soil type 2 during passive loading. 57

Figure 3.18. Effective principal stress variation at point s40 for soil type 2 during passive loading. 58

Figure 3.19. Effective principal stress variation at point c40 for soil type 3 during passive loading. 58

Figure 3.20. Effective principal stress variation at point s40 for soil type 3 during passive loading. 59

Figure 3.21. Stress path of point c40 in unique normalized deviatoric plane for soil type 1 during active loading. 60

Figure 3.22. Stress path of point s40 in unique normalized deviatoric plane for soil type 1 during active loading. 60

Figure 3.23. Stress path of point c40 in unique normalized deviatoric plane for soil type 2 during active loading. 60

Figure 3.24. Stress path of point s40 in unique normalized deviatoric plane for soil type 2 during active loading. 60

Figure 3.25. Stress path of point c40 in unique normalized deviatoric plane for soil type 3 during active loading. 61

Figure 3.26. Stress path of point s40 in unique normalized deviatoric plane for soil type 3 during active loading. 61

Figure 3.27. Stress path of point c40 in unique normalized deviatoric plane for soil type 1 during static loading. 61

Figure 3.28. Stress path of point s40 in unique normalized deviatoric plane for soil type 1 during static loading. 61

Figure 3.29. Stress path of point c40 in unique normalized deviatoric plane for soil type 2 during static loading. 62

Figure 3.30. Stress path of point s40 in unique normalized deviatoric plane for soil type 2 during static loading. 62

Figure 3.31. Stress path of point c40 in unique normalized deviatoric plane for soil type 3 during static loading. 62

Figure 3.32. Stress path of point s40 in unique normalized deviatoric plane for soil type 3 during static loading. 62

Figure 3.33. Stress path of point c40 in unique normalized deviatoric plane for soil type 1 during passive loading. 63

Figure 3.34. Stress path of point s40 in unique normalized deviatoric plane for soil type 1 during passive loading. 63

Figure 3.35. Stress path of point c40 in unique normalized deviatoric plane for soil type 2 during passive loading. 63

Figure 3.36. Stress path of point s40 in unique normalized deviatoric plane for soil type 2 during passive loading. 63

Figure 3.37. Stress path of point c40 in unique normalized deviatoric plane for soil type 3 during passive loading. 64

Figure 3.38. Stress path of point s40 in unique normalized deviatoric plane for soil type 3 during passive loading. 64

Figure 3.39. Shield tunnel face advancement toward monitoring section. 67

Figure 3.40. Average degree of consolidation at monitoring section (y = +40 m) assuming v =1 m/day, H = 12 m. 70

Figure 3.41. Average degree of consolidation at monitoring section (y = +40 m) assuming v =2 m/day, H = 12 m. 70

Figure 3.42. Average degree of consolidation at monitoring section (y = +40 m) assuming v =5 m/day, H = 12 m. 70

Figure 3.43. Average degree of consolidation at monitoring section (y = +40 m) assuming v =10 m/day, H = 12 m. 70

Figure 3.44. Average degree of consolidation at monitoring section (y = +40 m) assuming v =20 m/day, H = 12 m. 70

Figure 3.45. Average degree of consolidation at monitoring section (y = +40 m) assuming v =1 m/day, H = 18 m. 71

Figure 3.46. Average degree of consolidation at monitoring section (y = +40 m) assuming v =2 m/day, H = 18 m. 71

Figure 3.47. Average degree of consolidation at monitoring section (y = +40 m) assuming v =5 m/day, H = 18 m. 71

Figure 3.48. Average degree of consolidation at monitoring section (y = +40 m) assuming v =10 m/day, H = 18 m. 71

Figure 3.49. Average degree of consolidation at monitoring section (y = +40 m) assuming v =20 m/day, H = 18 m. 71

Figure 3.50. Average degree of consolidation at monitoring section (y = +40 m) assuming c_v =33.61 m^2/day, H = 18 m. 72

Figure 3.51. Average degree of consolidation at monitoring section (y = +40 m) assuming c_v =33.61 m^2/day, v = 5 m/day. 72

Figure 3.52. Drained-undrained condition with respect to advance rate of tunnel face and soil coefficient of consolidation. 74

Figure 3.53. Dimensional analysis by plotting π_1 against π_3 for U = 60%, $\pi^2 = H/D$ = 1. 75

Figure 3.54. Dimensional analysis by plotting π_1 against π_3 for U = 70%, $\pi^2 = H/D$ = 1. 75

Figure 3.55. Dimensional analysis by plotting π_1 against π_3 for U = 80%, $\pi^2 = H/D$ = 1. 75

Figure 3.56. Dimensional analysis by plotting π_1 against π_3 for U = 60%, $\pi^2 = H/D$ = 1.5. 76

Figure 3.57. Dimensional analysis by plotting π_1 against π_3 for U = 70%, $\pi^2 = H/D$ = 1.5. 76

Figure 3.58. Dimensional analysis by plotting π_1 against π_3 for U = 80%, $\pi^2 = H/D$ = 1.5. 76

Figure 3.59. Dimensional analysis by plotting π_1 against π_3 for U = 60%, 70%, and 80%, with $\pi_2 = H/D$ = 1 and 1.5. 77

Figure 3.60. a) Mohr–Coulomb criterion; b) π-plane; c) relationship of principal stresses in deviatoric plane. 83

Figure 3.61. Unique normalized deviatoric plane. 84

Figure 4.1. Yokohama Circular Northern Route 87

Figure 4.2. Plan view of the Kohoku interchange (starting point) and Namamugi Junction (End point) of the tunneling route (Photo was made by data from Google map, 2014). 88

Figure 4.3. Starting shaft location in shin-Yokohama 89

Figure 4.4. Entrance of tunneling route down through the shaft below the shin-Yokohama area 89

Figure 4.5. Used EPB shield machines for tunneling of Yokohama Circular Northern Route 90

Figure 4.6. Geological profile (soil types are shown in Fig. 4.7). 90

Figure 4.7. Stratigraphic classification (geological profile is shown in Fig. 4.6) 91

Figure 4.8. Layout of the approximate first 350 m of the tunneling routes (west and east lines), ring numbers (shown by R), launching shaft, and monitoring locations (MS1, MS2, and MS3). . 93

Figure 4.9. Measurement points in monitoring section 1 (MS1). 93

Figure 4.10. Measurement points in monitoring section 2 (MS2)..... 94

Figure 4.11. Measurement points in monitoring section 3 (MS3)..... 94

Figure 4.12. Date of excavation, ring numbers (shown by R), and monitoring sections. 95

Figure 4.13. Measurement of vertical soil displacement by date of construction in monitoring points of MS1 (west and east lines)..... 95

Figure 4.14. Measurement of vertical soil displacement by date of construction in monitoring points of MS2 (west and east lines)..... 96

Figure 4.15. Measurement of vertical soil displacement by date of construction in monitoring points of MS3 (west and east lines)..... 96

Figure 5.1. Layout of the site plan, launching shaft, west and east lines including MS3 (investigated are shown in this figure). 100

Figure 5.2. Developed 3D FEM mesh of the case study introduced in chapter 4. 101

Figure 5.3. Comparison of FEA results with field measurement data for monitoring section MS3.104

Figure 5.4. Schematic of loading steps and type of analyses in soil-water coupling analyses program (PLAXIS)..... 105

List of Tables

Table 2.1. Optimum TBM for various ground condition[1]..... 26

Table 3.1. Properties of the soil and concrete lining..... 45

Table 3.2. Soil types assumed for stress path analyses during EPB tunneling. 47

Table 3.3. Loading cases for face support and tail grouting pressure assumed for stress path investigations during EPB tunneling..... 47

Table 3.4. Values of parameters employed in the parametric study..... 69

Table 3.5. Typical values of the coefficient of consolidation 69

Table 4.1. Soil parameters and stratification of studied site obtained from field tests[1]. 91

Table 4.2. Lining specification of the tunnel..... 92

Table 5.1. Comparison of computation time of analyses between soil-water coupling program and the program using presented simplified FEM procedure..... 106

Chapter 1 Introduction

1.1 Background

The development and extension of infrastructure for transport and supply is a big challenge in view of a growing world population, progressive urbanization and an increase in passenger and cargo traffic. In particular in the metropolises like Tokyo still an efficient and economic infrastructure is required for the improvement of both the mobility in the city centers and the quality of urban life. The use of underground space for traffic infrastructure is connected, in contrast to surface infrastructure, with low surface space consumption and offers the possibility to efficiently control the sound level and the other traffic related emissions. In urban environments, the impact of the tunnel construction process on the surrounding underground has to be kept minimal due to the presence of sensitive and valuable surface and sub-surface constructions. Therefore, lowering of the groundwater table is often prohibited and the resulting surface settlements have to be kept below given admissible limits. Shield supported tunnel construction is an appropriate way to fulfil these requirements. By the continuous support of the surrounding underground, the shield supported tunnel advance allows for tunnel construction with minimal surface settlements and a high safety against loss of stability of the soil. Furthermore, the automation of the construction process leads to a fast and economic advance. These features, along with minimal requirements for aboveground space of the construction site, have made the shield supported tunnel construction the predominantly used method in urban environments.

Among the shield machines, Earth balance pressure (EPB) tunnel shields are used in excavating and advancing tunnels through any type of soft ground or soil condition, particularly below the water table. This method which was developed in Japan in the 1960s, devolved the primary method of mining in soil. The EPB method has actually revolutionized soft-ground tunneling as the technique has become widely applied in

constructing shallow, soft-ground, close-to-the-surface tunnels in heavily congested urban areas. Today, earth balance pressure machines (EPBMs) are commonly used in the excavation and driving of rail and highway tunnels, metropolitan subway systems, and other civil works projects that require tunneling in a soft soil, below the water table. The technique enables the construction of near-surface tunnels in poor ground conditions, such as running or flowing ground, with minimal surface effects and permits tunneling in urban areas under which tunnels could not be previously mined.

Deformation behavior of the soil during shield tunnel construction is an important subject which needs to be analyzed in tunnel engineering. In engineering practice, different design methods tend to be used, varying from simple empirical and analytical formulations to advanced finite element analyses. Depending on the tunneling method, e.g. conventional or closed shield tunneling, different procedures have been adopted through the years for the excavation sequence modeling. The method of analysis needs to take into consideration the actual soil behavior during the tunneling, proper mechanical and hydraulic boundary condition, type and specifications of boring machine, and so forth.

The shield supported tunnel advance constitutes an inherently three dimensional and time variant problem due to the construction process, the multi-phase composition of the soil. Besides, it is complex and heterogeneous as different components are involved – the TBM, the lining tube, the grouting mortar and the (layered) soil. Considering these characteristics, analytical methods can only be used for a simplified description of certain aspects of the advancement process, whereas, in contrast, numerical methods like the Finite Element Method (FEM) are capable to realistically describe the soil and the construction process and can be used to obtain a reliable prognosis of the soil-process interactions taking into account various process and soil parameters (Gioda and Swoboda 1999, Potts 2003, Schweiger 2008). Whereas such simulations are often restricted to the use in academia due to their complexity and their numerical effort, the continuous increase of computer resources and advances of user-friendliness of simulation software increase the attractiveness of such models for the engineering practice (Grose and Yeow 2005). With the rise of computers ‘capacity, complex numerical methods came into the realm of design practice and tunneling can thus be simulated more realistically. The consideration of the multi-phase nature of the soil within a numerical simulation to model its time variant behavior allows for transient description of consolida-

tion processes and make a distinction into a drained and undrained situation dispensable (Habte et al. 2009).

To achieve a realistic behavior of the soil due to the shield tunneling, excavation simulation usually accounts for the coupling between the pore fluid flows and pressures and the soil matrix deformations and stresses in non-, partially and fully saturated conditions. In the case of large meshes, finite element analysis calculation especially for three dimensional models needs powerful computer and long calculation time. Therefore, in the case of EPB tunneling which is common and safe practice in Japan, there is an attempt to perform and then verify the stress-deformation analysis of shield tunneling with a simple total stress analysis under simple drainage condition instead of a complicated effective stress analysis considering soil-water coupling by organizing many analysis results.

In this way, a continuous monitoring of the ground response is generally used in tunneling construction for safety verification of excavation process or to take other suitable counter measures. By monitoring the ground displacement during TBM construction, ground response induced by tunnel excavation can be observed. Comparison between field measurement data and FEM computation results can also be done.

The current thesis reports results of numerical analysis with 3D FEM of EPB shield tunneling by considering various realistic conditions such as advance rate of the tunnel face, consolidation coefficient of the soil, and overburden depth of the tunnel. Numerical analysis method of shield tunneling in this case is mainly used for settlements predictions of the soil due to tunneling construction.

The research is divided into three parts; in the first part, the effect of EPB shield tunneling on the stress path of the soil around the tunnel face is investigated. In the second part, the effect of EPB tunneling on the hydraulic condition of the soil around the tunnel face is examined. In the last part, EPB shield tunneling case studies are introduced. In this way, a useful set of numerical experimental equations are presented for drainage determination. Conclusively, by using of the presented numerical equation, a simplified 3D FEM simulation procedure of EPB shield tunneling have been proposed which enables a simple total stress analysis under simple drainage condition instead of a complicated effective stress analysis considering soil-water coupling. The proposed FEM procedures have been verified by comparing the 3D FEM analysis results of EPB shield tunneling with the field measurement records.

1.2 Thesis structure

The thesis structure schematically is shown in Fig. 1.1. Main part of the thesis is presented in chapter 3. Chapters of the thesis are as follow:

Chapter 1 gives an introduction to the whole objective of thesis, and introduces the structure of the thesis.

Chapter 2 presents the previous researches relating to shield tunneling history. It starts with introducing the various types and applications of shield tunneling including earth pressure balanced shield tunneling, and then gives a condensed overview of the modern tunneling methods especially shield tunneling technology. Finite element analysis practices for shield tunneling simulation are also reviewed.

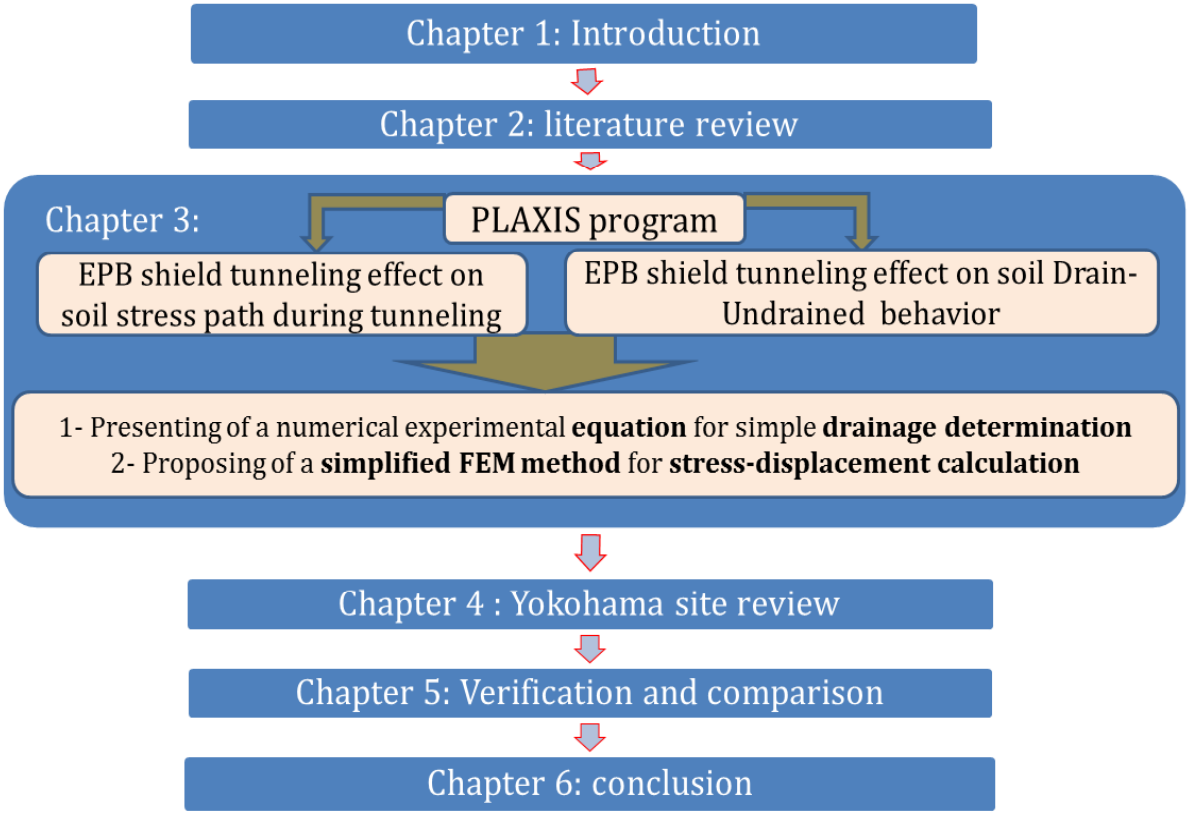

Figure 1.1. Structure of the thesis

Chapter 3 presents the main part of the research. Firstly, the effect of EPB shield tunneling on the soil stress path is investigated. Using the elastic perfectly plastic constitutive model with the Mohr–Coulomb (M-C) failure criterion, the 3D stress distribution of the area near the crown and spring line of the tunnel is investigated, after which the soil stress path with respect to the M–C yielding surface is presented. In this part, a numerical modeling of an EPB shield tunneling using PLAXIS program is introduced. To generalize the investigation, three different soil types which cover wide range of the soils that may be encountered in urban tunneling and three different types of the TBM face pressure loading cases are considered. In total, nine analyses were conducted in this part for combination of the three soil types and three loading cases. In the introduced numerical simulation, TBM advances along a tunnel path and then through a section named as a 'monitoring section'. By considering two monitoring points at the spring line and the crown of the tunnel in the monitoring section, the principal effective stress values at these points were obtained throughout the tunnel advancement, after which the stress paths were plotted for different analysis cases. Effective stress paths with respect to Mohr-Coulomb failure criterion are drawn for monitoring points throughout the entire tunnel advancement. The results of analyses in this part show that all stress paths are inside the yielding surface. With the assumptions made in this part of chapter, it was observed that in the case of EPB shield tunneling, where the TBM operations are made to maintain the face pressure as close as possible to in situ earth and hydraulic pressure, the soil around the cutter head is kept in the elastic domain.

In the next part of this chapter, the effect of EPB tunneling on the drained and undrained behavior of the soil is examined. A parametric study is conducted and a numerical experimental equation is proposed for determination of drained and undrained condition of the soil during shield tunnel advancement. Drained or undrained condition of a soil during tunneling is a matter that has been discussed mostly in relation to stability of the open tunnel face. However, if the soil to be analyzed is of medium and low permeability, the factors such as soil type and advance rate of the TBM face can greatly affect the hydraulic condition of the ground. In the case of saturated soil, both the generation and dissipation of pore water pressure should be considered simultaneously by using the soil–water coupling theory. For a relatively rapid TBM driving within the fine

grained soil, undrained deformation may be assumed. For the case of the soil with high permeability and a relatively slow TBM driving, drained deformation could be assumed. Depending on the soil type and an advance rate of the TBM face, soil stress–deformation behavior may vary from fully drained to fully undrained condition. Although FEM analyses in saturated soil can be carried out by using soil–water coupling consolidation programs, they can also be accomplished by using the so called total stress method in either of the above cases. In this part, three significant factors—a) advance rate of the TBM face, b) consolidation coefficient of the soil and c) overburden depth of the tunnel—are considered first in conducting a parametric study and then proposing a numerical experimental equation for drained and undrained determination of soil stress–deformation behavior during EPB shield advancement in soil. In this part, a series of undrained analysis followed by a consolidation analysis, in which the generation and dissipation of excess pore water pressure is taken into consideration, were carried out using the PLAXIS program and the same finite element model introduced in the previous part. By using the results of parametric study, the relationship among the introduced parameters is then found using dimensional analysis. Finally in this part, useful set of numerical experimental equations for the specific horizontal distance L between the TBM face and the monitoring section is proposed by organizing the many analysis results.

By the use of the simplified simulation procedures, the time period required to obtain the FEM simulation results of the same problem is shown to be reduced by approximately 50% compared with the soil-water coupling procedures. Conclusively, the simplified 3D FEM simulation procedures of EPB shield tunneling have been proposed as follows based on the parametric study.

1) Three dimensional finite element mesh of the analyzed region including monitoring sections is prepared.
2) The soil constitutive model employed in the FEM calculation is an ideal elastic model.
3) According to the horizontal distance x between the TBM face and the monitoring section, the acting in-situ earth pressure and the soil Poisson's ratio are selected as follows by using the specific distance L mentioned above.

If x>L, the soil undrained deformation condition is assumed and the acting in-situ earth pressure and the soil Poisson's ratio can be obtained using soil total stress analysis.

If 0<x<L, the soil drained deformation condition is assumed and the acting earth pressure and the soil Poisson's ratio can be obtained using soil effective analysis.

By using the soil stress condition and the material properties mentioned above, the total stress FEM analysis is carried out without soil-water coupling.

4) The soil stress change due to the previous step TBM face pressure loading is used to obtain the in-situ earth pressure at the current step TBM face pressure loading.

Chapter 4 presents the case study of the EPB shield tunneling related to Yokohama Circular Northern route. In this chapter, general description of the site, geological profile of tunnel path, geotechnical property of soil, and monitoring data are fully covered. Data on vertical displacements of the soil in a monitoring section measured by displacement gauges are collected and presented in this chapter.

Chapter 5 presents the comparison and verification results of computed FEM output with field measurement data. In this chapter, using the case study data introduced in chapter 4, the proposed simple FE procedure is verified. Using the case study data, the displacement of the corresponding measurement points in the monitoring section induced by EPB tunneling is calculated by simplified 3D FE method, after which the vertical displacement of the measured data and the computational results of the FEM are compared.

The results display that the values of vertical displacement anticipated by FEM analyses highly conform to the field measurement data. Hence, good prediction of vertical soil displacement can be achieved with the proposed equation to determine the drainage condition by use of a simple total stress analysis without soil–water coupling of the soil during EPB tunneling. Furthermore, a comparison is made to obtain the difference between computation time of analyses for cases of analyses performed with soil-water coupling method and simplified proposed FEM procedure.

Finally, **chapter 6** summarizes and concludes findings, and recommends future directions of the numerical modeling of shield tunneling.

1.3 Objectives of the research

Computation time for large scale 3D tunneling analysis usually is too lengthy, and prohibits the adoption of complicated advanced soil models and more accurate modeling. One of the main goals of the research is to perform the calculation with a simple total stress analysis under simple drainage condition instead of a complicated effective stress analysis considering soil-water coupling. Therefore, the objectives of the research can be summarized as follows:

I. To simulate shield tunneling advancement using finite element method.

II. To investigate the effects of earth pressure balanced tunneling on the stress path of the soil around TBM.

III. To investigate the effects of earth pressure balanced tunneling on the hydraulic condition of the soil around TBM.

IV. To evaluate the effect of some influential parameters on the hydraulic behavior of the soil during EPB tunneling by carrying out a parametric study.

V. To presents an empirical formulae for drainage determination of soil.

VI. To compile and collect the data of EPB tunneling case.

VII. To present a simplified FEM procedure for stress-deformation calculation of EPB tunneling.

References:

1) Gioda, G. and Swoboda, G. : Developments and applications of the numerical analysis of tunnels in continuous media, International Journal for Numerical and Analytical Methods in Geomechanics, Vol. 23, No. 13, pp. 1393-1405, 1999.
2) Potts, D. M. : Numerical analysis: a virtual dream or practical reality?, Geotechnique, vol. 53, No. 6, pp. 535-573, 2003.
3) Schweiger, H. F. : The Role of Advanced Constitutive Models in Geotechnical Engineering, journal of Geomechanics and Tunnelling, vol. 1, No. 5, pp. 336-344, 2008.
4) Grose, B., Macklin, S., and Yeow, H. C. : Numerical tunnel design: How far have we come?, journal of tunnels and tunneling international, Vol. 37, No. 5, pp. 40-43, 2005.
5) Habte, M., and Khalili, N., and Valliappan, S. : Multi-phase Modelling of Unsaturated Soils, ECCOMAS Multidisciplinary Jubilee Symposium, pp. 49-61, 2009.
6) Anagnostou, G. : Modelling seepage flow during tunnel excavation, International Symposium-EUROCK 93, 1993.
7) Vermeer, P. A, Ruse, N. and Marcher, T. : Tunnel heading stability in drained ground, Felsbau, Vol. 20, No. 6, pp. 8–18, 2002.

Chapter 2 Literature review

2.1 Introduction

This chapter starts by introducing various types and applications of shield tunneling including earth pressure balanced (EPB) shield tunneling. It gives a condensed overview of the modern tunneling methods especially EPB shield tunneling technology. Past researches on finite element analysis practices for shield tunneling advancement simulation, as well as shield tunneling effects on hydraulic condition of the soil are also reviewed.

2.2 Shield tunneling

2.2.1 Shield tunneling types

Among the tunneling boring methods, tunnel boring machines (TBMs) and associated back-up systems are used to automate the entire tunneling process, and reducing tunneling costs. In certain predominantly urban applications, tunnel boring is viewed as quick and cost effective alternative to laying surface rails and roads. Expensive compulsory purchase of buildings and lands, with potentially lengthy planning inquiries, is eliminated.

The first record of a working TBM was a machine patented by Charles Wilson in 1856, called Wilson's patented Stone-Cutting Machine. Wilson's second, "improved" machine was built in 1857 and was used to build the 7645 m Hoosac tunnel in western Massachusetts. Following these three decade of TBM development in mechanized tunneling, no practical advances were achieved until James Robbins, in 1953, built an 8 m diameter machine for the Oahe Dam project in South Dakota. The machine, referred to as the "Mittry mole", was 27.4 m long and the cutter head was comprised of two counter-

rotating heads. The first successful application of a TBM in medium hard rock was at the Humber River sewer project. In 1956, for this project in Toronto, a 3.3 m diameter machine was built for the Foundation Company of Canada (Hamphill 2012).

There are a variety of TBM designs that can operate in a variety of conditions, from hard rock to soft water-bearing ground. Two types of the shield machines are the *open shield* TBMs, and the *closed shield* TBMs. The shield TBMs are supported by a minimum of two circular ribs and longitudinal and vertical beams. Among the closed shield types of TBMs, the slurry pressure balance machine (SPBM) and earth-pressure balance machines (EPBMs), have pressurized compartments at the front end, allowing them to be used in difficult conditions below the water table. This pressurizes the ground ahead of the TBM cutter head to balance the water pressure. In hard rock, either shielded or open-type TBMs can be used but in soft ground, EPBMs, slurry shield and open-face type are used. Both types of closed machines operate like single shield TBMs, using thrust cylinders to advance forward by pushing off against concrete segments. The greatest load to which the shield will be subject is from the jacks. The number and location of the jacks are determined by the size of the shield. The jacks push against the installed primary liner to advance the shield. Jacks are equally spaced around the periphery; however, sometimes there are more put in the bottom to counteract the tendency of the shield to dip.

Slurry pressure balanced machines stabilize the tunnel face by applying pressurized bentonite slurry, as illustrated in Fig. 2.1. In soft ground with very high water pressure and large amounts of ground water, slurry shield TBMs are needed. These machines offer a completely enclosed working environment. During operation, soil is mixed into the slurry and at the end the soil is removed from the slurry in a separation plant. For the slurry pressure it is important that a more or less impermeable mud layer is formed, the so called filter cake, which is sealing the tunnel face. It ensures that the slurry does not totally flow into the ground, keeping a certain pressure on the tunnel face. Soils are mixed with bentonite slurry, which must be removed from the tunnel through a system of slurry tubes that exit the tunnel. Large slurry separation plants are needed on the surface for this process, which separate the dirt from the slurry so it can be recycled back into the tunnel.

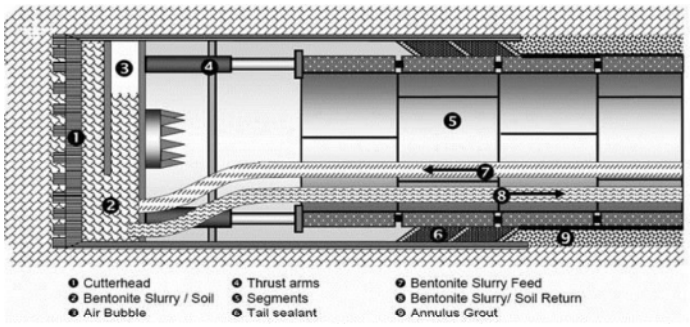

Figure 2.1. Schematic representation of SPBM

Earth pressure balanced machines apply support pressure to the tunnel face by suing the excavated soil as shown in Fig. 2.2. Various additives are often used to ensure appropriate muck properties. This is of particular importance for the screw conveyer, which is extracting the soil from the chamber behind the tunnel face. The screw conveyer is controlling the pressure at the tunnel face by its advance rate. For tunneling underneath the ground water table, the length of the screw conveyer has to be designed for the hydrostatic water pressure. It should be long enough in order to reduce the water pressure to atmospheric pressure. EPBMs are used in soft ground with less than 7 bar of pressure. The EPB gets its name because it is capable of holding up soft ground by maintaining a balance between earth pressure and chamber pressure. The TBM operator and automated systems keep the rate of soil removal equal to the rate of machine advance. In Japan, because of the very permeable sandy to gravelly ground, an EPB shield with suspension back pressure was developed in the 1970s.

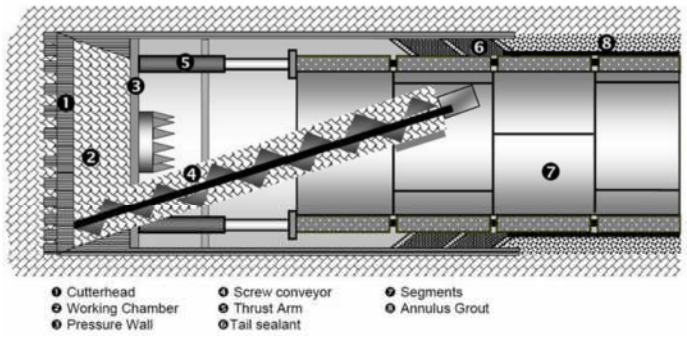

Figure 2.2. Schematic representation of EPBM

The decision to choose between Earth pressure balanced machines (EPBMs) and slurry pressure balance machine (SPBM) can be assessed by following conditions:

Selection Criteria Based on Particle Size Distribution and Plasticity: An SPBM is ideal in loose water bearing granular soils that are easily separated at the separation plant. By contrast SPBMs have problems dealing with clays and some silts.

Permeability: As a general guide the point of selection between the two types of machines is a ground permeability of 1×10^{-5} m/s, by using SPBMs applicable to ground of higher permeability and EPBMs for ground of lower permeability. However, an EPBM can be used at a permeability of greater than 1×10^{-5} m/s by using an increased percentage of conditioning agent in the plenum. The choice will take into account the content of fines and the ground permeability.

Hydrostatic Head: High hydrostatic heads of groundwater pressure along the tunnel alignment add a significant concern to the choice of TBM. In situations where a high hydrostatic head is combined with high permeability or fissures it maybe be difficult to form an adequate plug in the screw conveyor of an EPBM. Under such conditions, an SPBM may be the more appropriate choice especially as the bentonite slurry will aid in sealing the face during interventions under compressed air.

Settlement Criteria: Both types of machine are effective in controlling ground movement and surface settlement - providing they are operated correctly. While settlement control may not be overriding factor in the choice of TBM type, the costs associated with minimizing settlement should be considered. For example, large quantities of conditioning agent may be needed to reduce the risk of over-excavation and control settlement if using EPBM in loose granular soils.

Final Considerations: Other aspects to consider when making the choice between the use of an SPBM or an EPBM include the presence of gas, the presence of boulders, the torque and thrust required for each type of TBM and, lastly, the national experience with each method. These factors should be considered but would not necessarily dictate the choice.

Table 2.1 illustrates the various types of shield machines and the type of geologic condition for which they are best suited.

Basically EPB machines can be used for all soil type especially in the presence of suitable additives. The use of either the EPB TBM or the SPB TBM is possible in a full range of ground conditions. Traditionally the EPB machine has been selected for finer grained soils and the SPB for coarser grained soils.

Table 2.1. Optimum TBM for various ground condition[1]

Type of machine	Approximate diameter	Optimum Ground
Pipe jacking machines	Up to 3-4 m	any ground
Small bore unit, microtunnel	Up to 2 m	any ground
EPB TBMs	2-14 m	Fine-grained soft ground below the water table
Slurry TBMs	2-14 m	Coarse-grained soft ground below the water table
Hard-rock TBMs	2-14 m	Hard rock

1 Adopted from Kessler and Moore (1996).

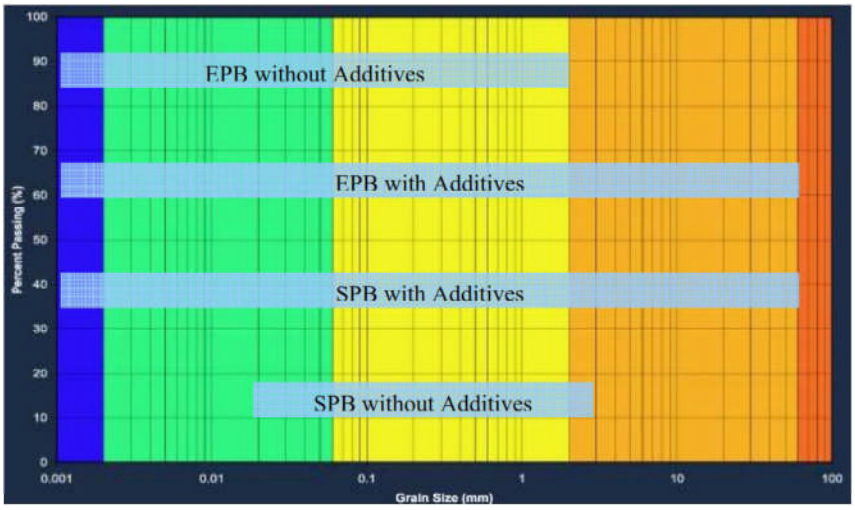

Figure 2.3. Range of suitable soil for EPB and SPB machines.

In recent years, increased development of additives and additive injection systems have allowed the two types of machines to excavate a broader range of soil conditions to the point where the type of soil is no longer the most critical item in the decision making process of EPB vs SPB (Fig. 2.3).

2.2.2 Grouting during EPB tunneling

The objective of grouting is to reduce the permeability of the rock, reduce the compressibility of the ground, compress the ground to provide stability, and seal the soil and rock.

The types of grouting include jet grouting, permeation grouting, consolidation grouting, compaction grouting, pre-grouting, post-grouting, backfill grouting, and contact grouting; each has its purposes and techniques (Hamphill 2012). Among these grouting types, compensation and backfilling grouting are well known in shield tunneling.

Compensation Grouting

When a tunnel is being driven under structures or a shaft is being sunk near a structure and there is a danger of causing surface settlement, grout is injected between the tunnel or shaft being excavated and the foundations of structures on the surface. The quantities are calculated to offset the settlement caused by material removed by the tunnel or shaft. This is generally used in soft ground. The settlement can often be propagated from the gap over the tail shield. The zone of disturbed soil extends up and horizontally until the ground surface is reached. Depending on the depth of the tunnel or the distance from the shaft to the structure, this settlement can occur quickly or over an extended period of time. This settlement can affect not only foundations but also buried utilities.

Backfilling

Among the most important reasons for backfill and concrete grouting is to stabilize the lining by transferring the load from the lining to the adjacent ground or the load from the adjacent ground to the lining (Henn, 2003). When mining with a TBM, there is a gap between the TBM and the walls of the excavation. The gap is the result of oversizing the peripheral cutters of the cutter head to permit space for steering and the conical shape of the shield diameter from the face toward the rear of the shield to provide for forward movement and reduce the chances of the shield binding. The outside diameter of the segment ring must be smaller than the inside diameter of the tail shield to enable

the assembly of the segments within the tail shield and the wire brush seal between the segments and the tail shield. This annular space has to be filled.

The purpose of backfill grouting during tunnel excavation by a TBM with precast segmental lining erected in the tail shield is to make the lining of a tunnel tight enough against the surrounding ground to ensure stability. The way this is accomplished is by backfilling the annulus between the tunnel lining and the ground. Backfilling will reduce the deformation of the rock around the tunnel and will help reduce settlement above the tunnel. Filling the annulus puts the liner in contact with the surrounding ground, which helps to stabilize the liner during construction, thus securing the lining and making it more stable for thrusting during TBM advance. In addition to providing some corrosion protection, backfilling will reduce the flow of groundwater around the tunnel lining, reducing the potential for void formation.

The timing of the backfilling depends on the standup time of the material. When TBMs in soft ground use non-expansive precast concrete segmental lining systems mining in soil below the water table or with low standup time, the annulus must be backfilled simultaneously with the mining.

2.2.3 Shield tunneling support pressure

As the tunnel boring machine advances, the soil is removed from the tunnel face. The soil mass in front and above the tunnel face exerts active earth pressure. The presence of infrastructures or surcharge also contributes as additional earth pressure. For the tunnel alignment below the groundwater table, water pressure is another significant component of pressure acting at the tunnel face. Shield machine should sustain loading from the soil and water above it. With the operating load, the shield is stressed by the soil excavation, the thrust caused by the push jacks, the weight of the components, and the erection of the lining segments. The body of the shield machine usually is a steel cylindrical plate about 2.5–3 m long (Hamphill 2012).

Excavation of tunnel machine and soil mass movement in front of the machine face alike to the model introduced by Horn (Horn 1961) which was originally inspired by

silo-theory by Janssen (Janssen 1895). The failure mechanism developed by Horn consists of a wedge and an overlying right-angled prism as shown in Figure 2.4.

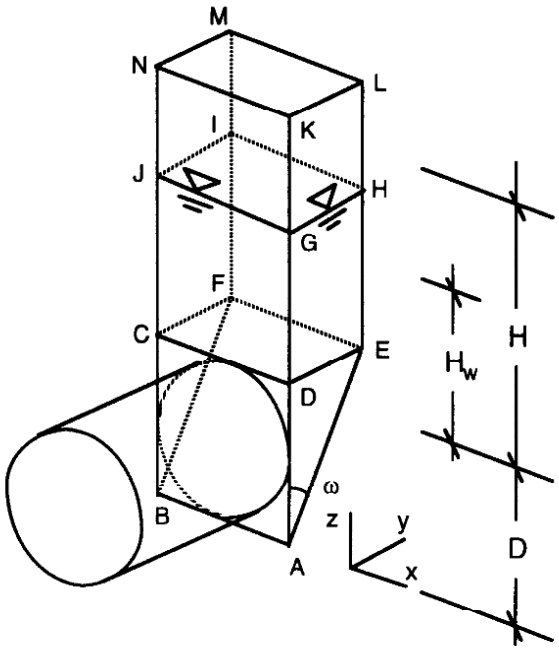

Figure 2.4. Sliding mechanism in front of TBM machine

Based on the first proposed Horn model, Anagnostou and Kovari introduced a three dimensional model in 1994 for slurry shield tunneling support pressure computation. They stated that the wedge in front of the tunnel face (Figure 2.4), is acted upon by: (a) its weight; (b) the resultant normal and shear force along failure surfaces of ADE, BCF, and ABFE; (c) the resultant support force of the slurry over the surface of ABCD, (d) the vertical force of right-angle prism at the interface DEFC. By solving the limit-equilibrium equations of the wedge, support pressure for the specific collapse mechanism is obtained (Anagnostou and Kovari 1994).

2.3 Shield tunneling advancement simulation using finite element analysis

Ground deformation are inevitably induces by all tunnel construction procedures. In the case of open face tunneling, there is full release or redistribution of stress around the tunnel heading. Ground deformation around a closed face TBM occurs due to the differential pressure acting at the face, over cut, pitching of cutter head, the tail void

between shield and segmented lining, and shearing at the soil-shield interface. There are also movements caused by grout injection into the tail void. If undesirable surface settlement did occur due to tunnel construction, active measures such as compensation grouting can be performed to control and even reverse the surface settlement. Compensation grouting injects grouts into the ground to compensate the ground loss caused by underground construction and stress relief, and has been successfully applied to several underground construction projects such as Jubilee Line extension project (Harris et al. 1996). In general, evaluation of deformation induced by shield tunneling ranges from empirical data from prior projects to simplified analytical methods and numerical computation, particularly using finite element method (FEM).

Two dimensional (2D) plane-strain finite element analyses, which consider the initial and final configuration of tunneled ground, have been extensively used to estimate the transverse settlement troughs caused by tunneling. The FEMs developed for simulation of shield tunneling at the first were proposed in 2D formats (Clough et al. 1983, Finno et al. 1985, Bernat et al. 1998). Clough et al. (1983) and Finno et al. (1985) investigated the influence of the face pressure of 2D analyses in both longitudinal and transverse sections (Clough et al. 1983, Finno et al. 1985). There are subtly three various techniques used to represent the excavation and lining support in 2D FE tunneling:

- Load reduction techniques
- Stiffness reduction techniques
- Displaced boundary techniques

The *load reduction method* in also known as convergence-confinement method (Panet and Guenot 1982). The method first removes the finite elements representing the excavated ground and applies a set of equilibrating forces to the nodes on the tunnel cavity such as no displacement occurs. These equilibrating forces are then activated, and then remaining equilibrating forces is reduced to zero. The prescribed load reduction factor can be estimated from prior experience of similar projects (Bernat et al. 1997) from back analysis. The volume loss method (Addenbrook et al. 1997) is a special load reduction technique which involves unloading to prescribed volume loss. The *stiffness reduction technique* (Swoboda 1979) reduces the stiffness of the ground being excavated in

the finite element mesh with a certain prescribed reduction factor α. After reaching the targeted stiffness, the elements representing the excavation are removed and lining elements are activated. The *displayed boundary technique* prescribes a displacement boundary condition at the tunnel cavity. After imposing the prescribed displacement and achieving the equilibrium, lining elements are activated, and the soil structure interaction starts (Rowe and Lee 1992). Commercial programs such as PLAXIS also provide the capability to specify a uniform contraction parameter that prescribes a uniform radial displacement to simulate the ground loss. Abu-Farsakh (1999) developed two-dimensional computational model to simulate the continuous advance of the EPB Shield during the tunneling process in cohesive soils. The model is based on the combination of the plane strain transverse-longitudinal sections that can incorporate the three dimensional (3D) deformation of the soil around and ahead of the shield face. The model is capable of predicting the soil response due to the shield tunneling before the event, especially in soft ground conditions.

However, tunneling is intrinsically a three dimensional problem with three-dimensional ground deformation, stress redistribution, and flow around the tunnel heading. Approximation techniques for 2D plane strain analyses are highly empirical, do not necessarily account for the three-dimensional, and require major judgments to determine appropriation factors that incorporate three-dimensional effect as discussed by Lee et al. (1992). Predictions of strain around the tunnel heading will clearly be affected by inelasticity, path dependent material modeling. For example, as the material yields, the yield surface evolves with change of strain or stresses, and the evolution of the yield surfaces can be very different between 3D and plane-strain analyses. Nakai and Xu (1995) conducted both 2D (plane-strain) and full 3D finite element analyses with constitutive models for sands and clays considering hardening behavior of soil. Their results show significant difference between plane-strain models and 3D models. In the early 1990s, Lee et al. developed the first three-dimensional (3D) FEM for shield tunneling, assuming undrained soil conditions and using a Mohr–Coulomb material model for the soil. He developed techniques for estimating surface settlements caused by tunneling in soft ground. A 3D elasto-plastic finite element formulation developed to allow simulation of the construction sequence and subsequent ground displacements and

stress patterns around the tunnel face and at the ground surface. Yu and Rowe (1999) incorporated plasticity in an analytical solution for tunneling by using cavity contraction analyses with the Mohr–Coulomb yield criterion. Their results showed that soil plasticity affects the prediction of ground movement up to one radius beyond the tunnel cavity.

Ohtsu et al. (1999) compared 3D finite element (FE) analysis with coupling of deformation and water flow to 2D analysis with plane strain condition. For elastic material, they found that stress path in the ground are different between 2D and 3D models. They concluded that for elasto-plastic analyses, the stress path in 2D FE analysis would have satisfied the yield condition, whereas that in 3D analysis remains in the elastic regime owing to drainage from the tunnel face. Therefore, the difference between 2D and 3D analyses depends on the permeability of the soil and the advance rate of the tunnel face. Ohtsu et al. demonstrated that the change in pore water pressure and effective stress varies greatly according to the permeability of the ground and advance rate of the tunnel face. They also found that the more permeable the ground is, the farther away the stress path is from the failure envelope.

Shield tunneling modeling using 3D FEM usually incorporated with active face support in order to minimize ground loss caused by ground deformation associated with face intrusion. However, these construction technologies are also difficult to incorporate realistically. Akagi and Komiya (1996), and Komiya et al. (1996) proposed the concept of “excavation elements” to represent distorted material in front of the shield tunnel boring machine (TBM) in conjunction with a re-meshing procedure for modelling the excavation of the tunnel face. The operation of shield advancement is simulated using re-meshing technique for the finite elements at each time step of the analysis.

More or less severe idealizations are often being made in the numerical simulation of mechanized tunnel advance, e.g. by assuming the surrounding underground to behave in a drained or undrained manner to its process induced loading, by modelling its deformation behavior using a simple material law or by neglecting single interactions between the soil and the construction process. Even if such idealizations are applied the computational effort in terms of computation time and memory consumption of full

scale, three dimensional computer models for the analysis of shield supported tunnel advance is huge (Golser 1999). The size of the problem and its geometrical complexity require for a large number of elements, due to its time variant nature a series of loading or construction steps has to be simulated, the multiple non-linearities demand for an iterative solution of the equilibrium if the study shall be performed in an implicit way and the matrices to be solved are in general ill-conditioned, non-symmetric and badly ordered so that an iterative solution of the resulting equation system is hardly applicable.

To evaluate the influence of tunnel excavation on existence building, full finite element models including buildings and tunnels without lining (Burd et al. 2000) and with lining (Mroueh and shahrour 2003) have been used, and significant interaction between tunnels and building have been observed.

Other application of 3D finite element analysis (FEA) include complex geometries with two tunnel intersecting at 45° (Tsuchiyama et al. 1988); complex ground support interaction including fore-pole, shotcrete, steel ribs, and rock bolt (Aydan et al. 1988).

Sugimoto and Sramoon (2002) proposed a kinematic shield model to simulate shield TBM behavior during excavation on the basis of equilibrium conditions by considering ground displacement around the shield. They developed a closed-type shield tunneling together with computer-aided automatic control systems. A model of the theoretical dynamic load acting on the shield during excavation developed, and shield tunnel engineering practices; i.e., the excavated area, the tail clearance, the rotation direction of the cutter face, sliding of the shield, ground loosening at the shield crown, and the dynamic equilibrium condition were taken into consideration. They conclude that the proposed model represents the shield behavior reasonably well. They then extended their investigation to shield tunneling behavior along a curved alignment in a multilayered ground and found that the excavated area including the area generated by copy cutter is a predominant factor affecting the shield behavior, and the ground displacement, at the excavated surface plays an important role in the surrounding ground movements during shield tunneling (Sugimoto et al. 2007).

Franzius and Potts (2005), investigate the influence of the geometry and the dimension of a 3D finite element model on tunnel-induced surface settlement predictions. They considered vertical boundaries influence on results and demonstrates that reasonable results can be obtained by increasing the length of incremental tunnel excavation and by scaling back the settlement values to give a required tunnel volume loss.

Moller (2006) analyzed tunnel induced settlements and structural forces in linings, considering both elementary methods of analysis and the Finite Element Method. He presented a three dimensional FE model for the analysis of open and closed face shield tunneling with special emphasis on the study of lining forces yield surface. Two material laws – the Hardening Soil Model and an elastic-perfectly plastic model with Mohr-Coulomb yield surface – are applied to model the stress-strain behavior of the surrounding underground that is assumed to be unsaturated. At the heading face, a high pressure is applied to simulate the heading face support. To the soil around the excavated volume a radial, lower pressure is applied representing the contact pressure between TBM and soil or the presence of a pressurized fluid within the steering gap. Both of these pressures increase hydrostatically with depth. Behind the TBM, the elements representing the lining tube are activated, whereas the tail gap is first modelled as free space. To the soil elements in the area of the tail gap, first a radial pressure is applied representing the grouting pressure, whereas the soil is free to deform until it gets in contact with the newly activated lining elements.

Considering the influence of previous stress history and stress path direction during tunneling, Grammatikopoulou et al. (2008) studied the ground surface settlement trough induced by tunneling and concluded that a more realistic undrained settlement trough induced by tunneling can be simulated if the effect of previous stress history is taken into account.

A study of EPB machine's chamber pressure effect on driving efficiency was performed by Fang et al. (2011) by creating a 3D FEM of EPB shield tunneling in gravely soil. To do so, they investigated the resistance distribution around shield. By analysis of field test data, the relationship of cylinder thrust, chamber earth pressure and driving efficiency was obtained. The results showed that decreasing the chamber pressure to a certain extent can achieve a high driving efficiency.

2.4 Shield tunneling effects on hydraulic condition of the soil

Shield tunneling effect on hydraulic condition of the TBM around soil is a matter that has been discussed mostly in relation to stability of the open tunnel face (Anagnostou 1993, Vermeer et al. 2002). During tunnel excavation in a water-bearing ground, seepage flow towards the open-type shield tunnel takes place and heading of the tunnel acts as a groundwater drain. The seepage flow may lead to a drawdown of the water level, to a decrease in the discharge (or even a drying up) of wells, or to unacceptably severe subsidence due to consolidation. The loss of hydraulic head in the vicinity of the tunnel face does not take place immediately after excavation. The lower the permeability, the more the time required to achieve a steady state. Apart from the borderline case of highly permeable ground or very slow excavation, the excavation advance rate of shield tunnel face must be taken into consideration.

Anagnostou (1995) proposed a method for computing the effect of tunneling on the piezometric head field during tunnel construction. The proposed method can easily be implemented into existing finite element codes. He concluded that the effect of continuous tunnel excavation on the piezometric head can be analyzed by reformulating and solving the diffusion equation within a frame of reference which is fixed to the advancing tunnel face. He suggest that proposed method can be applied to other time-dependent problems, e.g. the analysis of the surface settlement caused by tunneling in a saturated, low-permeability, soft ground. He proposed that with typical advance rates being lower than 500 m/month, common steady-state seepage analyses are accurate enough for practical purposes when the soil permeability is higher than 10^{-6} m/s.

Anagnostou and Kovari (1996) studied EPB-shield tunneling face failure mechanism under the drained conditions. They concluded that the water pressure in the chamber reduces the hydraulic head gradient in the ground and consequently the seepage forces acting in front of the face. The face is thus stabilized both by the direct support of the pressurized muck and by the reduction of the seepage forces in the ground. They showed that relationships between the effective support pressure required and the hydraulic head in the muck for a given geotechnical situation. They concluded that tunneling using an earth pressure shield machines, both the effective support pressure and the pore

water pressure should be controlled and adjusted according to the hydrological and soil mechanics conditions encountered. Because both parameters depend on the characteristics of the excavated ground, the way the ground is mixed in the work chamber, the rotational speed of the screw conveyor, and the excavation advance rate, both geotechnical and operational aspects will affect tunnel face stability.

2.5 Summary

This chapter summarizes a brief history of the previous researches related to shield tunneling construction. Various types of shield tunneling, different types of shield machines including slurry and EPB shield machines were briefly described and their specific applications were covered. 2D and 3D shield tunneling advancement simulations were reviewed, and finally Earth pressure balanced (EPB) shield effect on hydraulic condition of the soil was also recalled.

References

1) Hemphill, G. B. : Practical tunnel construction, John Wiley and Sons, 2012.
2) Kessler, P. N. and Moore, C. J. : Tunneling by Tunnel Boring Machine, Transfield Tunneling, Australia, 1999.
3) Henn, R. W. : AUA guidelines for backfilling and contact grouting of tunnels and shafts, American Underground Construction Association, ASCE, 2003.
4) Horn, M. : Alagutak homlokbiztositasara hato vizszintes foldnyomasvizsgdlat nehany ered-mdnye. Az orszdgos medlyepitoipari konferencia eldaddsai, Kozlekeddsi Dokumentacios Va11alat, Budapest, 1961. (in Hungarian)
5) Janssen, H. A. 1895. Versuche uber Getreidedruck in Silozellen. Zeitschrift des Vereins deutscher Ingenieure, Band XXXIX, No. 35, 1045-1049 (in German).
6) Anagnostou, G. and Kovari, K. : The face stability of slurry-shield-driven tunnels, Tunnelling and Underground Space Technology, Vol. 9, No. 2, pp. 165-174, 1994.
7) Harris, D. I., Pooley, A. J., Menkiti, C. O., and Stephenson, J. A. : Construction of low level tunnels below waterloo station with compensation grouting for Jubilee Line Extension, Proceedings International Symposium Geotechnical Aspects of Underground Construction in Soft Ground, Mair and Taylor, London, pp. 361-66, 1996.
8) Clough, G. W., Sweeney, B. P., and Finno, R. J. : Measured soil response to EPB shield tunneling, Journal of Geotechnical Engineering, Vol. 109, No. 2, pp. 131–149, 1983.
9) Finno, R. J., Clough, G. W. : Evaluation of soil response to EPB shield tunneling. Journal of Geotechnical Engineering, Vol. 111, No. 2, pp. 155–173, 1985.
10) Bernat, S., Cambou, B. : Soil – structure interaction in shield tunneling in soft soil, Journal of Computers and Geotechnics, Vol. 22, No. 3, pp. 221–242, 1998.
11) Panet, M and Guenot : Analysis of convergence behind the face of a tunnel: proceedings of the 3rd international symposium, Brighton, pp. 197-204, 1982.
12) Bernat, S., Cambou, B. and Santosa, P : Modeling of soil-structure interaction during tunneling in soft soil, Computer Methods and Advanced in Geomechanics, 1997.
13) Addenbrooke, T. I., Potts, D. M. and Puzrin, A. M. : The influence of pre-failure soil stiffness on the numerical analysis of tunnel construction, Geotechniques, Vol. 47, No. 3, pp. 693-712, 1998.
14) Swoboda, G : Finite element analysis of the new Austrian tunneling method (NATM), Proceedings of the 3rd International Conference on Numerical Methods in Geomechanics, Vol. 2, pp. 581-86, 1979.
15) Rowe, R. K. and Lee, K. M. : Subsidence owing to tunneling. II. Evaluation of a prediction technique, Canadian Geotechnical Journal, Vol. 29, No. 6, pp. 941-54, 1992.
16) Abu-Farsakh, M. Y., Voyiadjis, G. Z. : Computational model for the simulation of the shield tunneling process in cohesive soils, International Journal for Numerical and Analytical Methods in Geomechanics, Vol. 23, No. 1, pp. 23–44, 1999.
17) Lee, K. M., Rowe, R. K. and Lo, K. Y. : Subsidence owing to tunneling. I. Estimating the gap parameter, Canadian Geotechnical Journal, Vol. 29, No. 6, pp. 929-40, 1992.
18) Lee, K. M, Rowe, R. K. : Finite element modelling of the three-dimensional ground deformations due to tunneling in soft cohesive soils: part I – method of analysis, Computers and Geotechnics, Vol. 10, No. 2, pp. 87–109, 1990.

19) Yu, H. S., and Rowe, R. K. : Plasticity solutions for soil behavior around contracting cavities and tunnels, International Journal for Numerical and Analytical Methods in Geomechanics, Vol. 23, No. 12, pp. 1245–1279, 1999.
20) Ohtsu, H., Ohnishi, Y., Taki, H., and Kamemura, K. : A study on problems associated with finite element excavation analysis by the stress-flow coupled method, International Journal for Numerical and Analytical Methods in Geomechanics, Vol. 23, No. 13, pp. 1473–1492, 1999.
21) Akagi, H., and Komiya, K. : Finite element simulation of shield tunneling processes in soft ground, International Symposium on Geotechnical Aspects of Underground Construction in Soft Ground, pp. 447–452, 1996.
22) Komiya, K., Soga, K., Akagi, H., Hagiwara, T., and Bolton, M. D. : Finite element modelling of excavation and advancement processes of a shield tunneling machine, Soils and Foundations Journal, Vol. 39, No. 3, pp. 37–52, 1999.
23) Golser, H. : Application of Numerical Simulation Methods on Site, Vol. 1, pp. 21-25, 1999.
24) Burd, H. J., Houlsby, G. T., Augarde, C. E. and Liu, G. : Modelling tunneling-induced settlement of masonry buildings, Proceedings of the ICE-Geotechnical Engineering, Vol. 143, No. 1, pp. 17-29, 2000.
25) Mroueh, H. and Shahrour, I. : Three-dimensional finite element analysis of the interaction between tunneling and pile foundations, International Journal for Numerical and Analytical Methods in Geomechanics, Vol. 26, No. 3, pp. 217-30, 2002.
26) Tsuchiyama, s., Hayakawa, m., Shinokawa, t. and Konno, h. : Deformation behavior of the tunnel under the excavation of crossing tunnel, proceedings of the sixth international conference on numerical methods in geomechanics, vol. 1-3, 1988.
27) Aydan, O., Kyoya, T., Ichikawa, Y., Kawamoto, T., Ito, T. and Shimizu, Y. : Three-dimensional simulation of an advancing tunnel supported with forepoles, shotcrete, steel ribs and rockbolts, Proc. Numerical Methods in Geomechanics, Vol. 1, pp. 1481-6, 1988.
28) Sugimoto, M., and Sramoon, A. : Theoretical model of shield behavior during excavation. I: Theory, Journal of Geotechnical and Geo-environmental Engineering, ASCE, Vol. 128, No. 2, pp. 138–155, 2002.
29) Sugimoto, M., Sramoon, A., Konishi, S., and Sato, Y. : Simulation of shield tunneling behavior along a curved alignment in a multilayered ground, Journal of Geotechnical and Geoenvironmental Engineering, ASCE, Vol. 133, No. 6, pp. 684–694, 2007.
30) Franzius, J. N. and Potts, D. M. : Influence of mesh geometry on three-dimensional finite-element analysis of tunnel excavation, International journal of Geomechanics, ASCE, Vol. 5, No. 3, pp.256-66, 2005.
31) Moller, S. : Tunnel induced settlements and structural forces in linings, PhD thesis, University of Stuttgart, 2005.
32) Grammatikopoulou, A., Zdravkovic, L. and Potts, D. M. : The influence of previous stress history and stress path direction on the surface settlement trough induced by tunneling, Geotechnique Journal, Vol. 58, No. 4, pp. 269–281, 2008.
33) Fang, Y. ,He, C., and Xu, G., and Jiang, Y. and Wang, Y. : Study on Thrust of Earth-Pressure-Balanced Shield Tunneling in Gravel, ASCE, Proceedings of the International Conference on Pipelines and Trenchless Technology, pp. 1938-1946, 2011.
34) Anagnostou, G. : Modelling seepage flow during tunnel excavation, International Symposium-EUROCK 93, 1993.

35) Vermeer, P. A, Ruse, N. and Marcher, T. : Tunnel heading stability in drained ground, Felsbau, Vol. 20, No. 6, pp. 8–18, 2002.
36) Anagnostou, G : The influence of tunnel excavation on the hydraulic head, International journal for numerical and analytical methods in geomechanics, Vol. 19, No. 10, pp. 725-46, 1995.
37) Anagnostou, G. and Kovari, K. : Face stability conditions with earth-pressure-balanced shields, Tunnelling and Underground Space Technology Journal, Vol. 11, No. 2, pp. 165-73, 1996.

Chapter 3 EPB Shield tunneling effects on stress-state and hydraulic condition of soil

3.1 Introduction

Finite element analysis is an essential tool for engineering design. However, large scale –non-linear finite element analysis are computationally expensive. The cost is expressed in term of computational resources and solution time associate with the both large number of unknown and iterative solution of material. EPB tunnel shields are used in excavating and advancing tunnels through any type of soft ground or soil condition, particularly below the water table. A subject of interest in tunnel engineering is to analyze the deformation behavior of soils, which may be fully or partially saturated with water. In the analysis of such kind of material, three types of behavior are generally to be distinguished, that is the long term fully drained behavior, the undrained behavior under rapid loading and the coupled behavior for intermediate time values. When the saturation is very low, or the permeability of the soil is high, or the load is applied very slowly, drained deformation can be assumed, and the pore pressure may be neglected, so that the analysis is quite similar to that of an ordinary solid mechanics problem. The other extreme case is that the drainage conditions are very low, or the load is applied in a relatively short period, so that undrained deformation can be assumed. In all of the intermediate situations, the deformation is coupled with the flow of the pore water. This kind of behavior is generally called soil-water coupling analysis.

So, it was matter of interest to perform the calculation with a simple total stress analysis under simple drainage condition instead of a complicated effective stress analysis considering soil-water coupling. Therefore, in this chapter a simplified analytical meth-

od is developed for stress-deformation analysis of shield tunneling. The method is described step by step in this chapter.

In this chapter, the effect of earth pressure balanced (EPB) tunneling on the soil stress-state and also hydraulic conditions of the soil during shield tunnel advancement are explained. The content of this chapter is divided into two main parts:

1) In the first part (section 3.3), the effect of EPB shield tunneling on the soil stress-path around the tunnel is investigated. Using the Mohr–Coulomb elasto-plastic criterion, the 3D stress distribution of the area near the crown and spring line of the tunnel is investigated, after which the soil stress path with respect to the M–C yielding surface is presented.

2) In the second part (section 3.4), the effect of EPB tunneling on the hydraulic condition of the soil around the tunnel is examined. Taking into account the three significant factors of a) advance rate of the tunnel face, b) consolidation coefficient of the soil, and c) overburden depth of the tunnel, a parametric study is conducted and a numerical experimental equation is proposed for simple determination of drainage condition of the soil during shield tunnel advancement.

3.2 Earth Pressure Balanced tunneling principals

As a primary mean of ground supports, pure mechanical support first was used but this was limited only to stable grounds. More challenging types of ground conditions often require the use of pressurized tunneling, where excavated material itself is used to support the face of the excavation. EPB TBMs have a proven track record for excavation in soft ground that requires immediate and continuous support at the excavation face.

Earth pressure shields provide continuous support of the tunnel face using freshly excavated soil, which under pressure completely fills up the work chamber (Fujita 1981; Nishitake 1990). The supporting pressure is achieved through control of the incoming and outgoing materials in the chamber, i.e., through regulation of the screw conveyor rotation and of the excavation advance rate. Considerable experience with earth-pressure shields has been gained in Japan, where this construction method was developed (Stack 1982). In 1980, earth-pressure shields were used for 27.8% of the total

length of tunnel constructed in Japan, and by 1985 this figure had risen to 68% (Nishitake 1990).

The tunnel face is supported with an earth paste formed by the excavated soil. For better conditioning of the soil, water and some additive (i.e. foam) are mixed with the excavated soil in the cutter head. This technique improves soil consistency and workability thereby reducing the required cutter head torque. In "closed mode operation", the working chamber is completely filled with conditioned excavated material, the earth paste. The support pressure is transmitted to the soil by pressurizing the earth paste through the thrust force transfer into the bulkhead. The pressure level is controlled by the inflow of excavated soil due to the forward movement of the TBM in relation to the outflow of soil from the discharging screw conveyor. It is measured by the readings of the earth pressure sensors at the bulkhead. In order to minimize the ground displacement during tunnel movement, face pressure and tail void grouting pressure keep close to that of earth pressure in front of machine. EPB TBM machine control the settlement by control of the EPB pressure in the excavation chamber. Because of the close magnitude of face and earth pressures, sometime amount of settlement during passing of tunnel is smaller than the secondary settlement after passing of tunnel. Combined ground and water pressure at the TBM face must be equally balanced with the pressure of the excavated material inside the cutting chamber. The pressure in chamber must be neither high nor low to prevent occurrence of ground heave and settlement. At the same time, it should be as low as possible to reduce the cutter torque and wearing (Yang et al. 2009). Failure to equalize these pressures will result in either:

• Surface settlement in the event when the pressure inside of the cutting chamber is lower than in-situ pressure

• Surface heave in the event when chamber pressure is higher than in-situ pressure. For the deeper tunnel, over pressurizing the cutting chamber may affect reliability of the TBM sealing system.

To determine the required support pressure at the tunnel face, information about the stratification of soil layers in the section, loads on the surface and head of groundwater will be necessary. The weights of permanent structures like buildings, dams, dykes, fills,

etc. above the section are considered constant loads. Loads of vehicles like cranes, trucks, etc. will be considered as temporary loads. Both of these loads will increase soil pressure, but only the constant load contributes against blow out and ground heaving. Geological conditions are key factors governing the construction of a tunnel. In addition to the grain size distribution, the soil stratification and the strength parameter of each layer will be important to determine the face support pressure.

Equilibrium forces are schematically shown in Fig. 3.1.

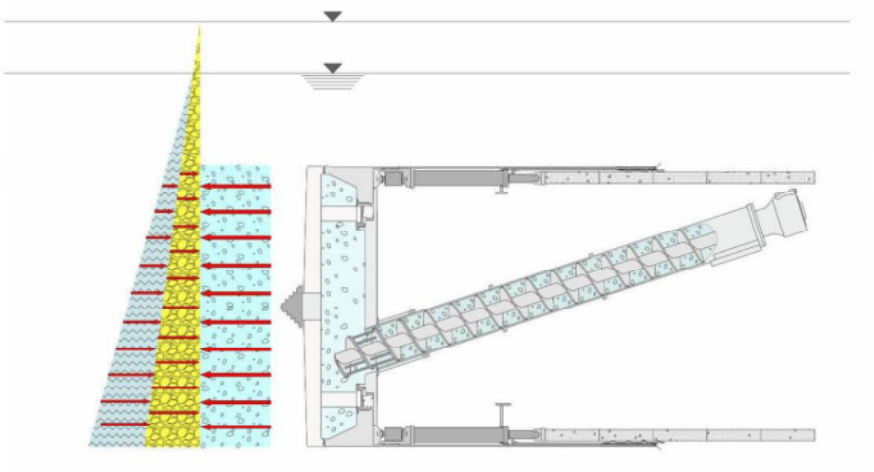

Figure 3.1. Equilibrium forces in front of EPBM

3.3 Effect of EPB shield tunneling on the soil stress-path

In this section, the soil stress path around tunnel face during EPB shield tunnel advancement is investigated. By using the Mohr–Coulomb elasto-plastic criterion, the 3D stress distribution of the area near the crown and spring line of the tunnel due to EPB shield construction is presented, after which the stress path with respect to the M–C yielding surface is drawn.

In order to investigate the EPB shield tunneling effects, a numerical model is developed using PLAXIS program. In the developed model, a monitoring section including monitoring points is considered. Stress path analysis is carried out by tracing of effective principal stress components of monitoring points in the introduced model when TBM advanced through the monitoring section. Stress-state of the monitoring points is

tracked before arrival, during and after passing of TBM through the monitoring section. To generalize the stress-path investigation, different types of the soil and loading cases are introduced for the numbers of analyses. Effective principal stresses variation of monitoring points for all analysis cases are shown in graphs and then more discussion and conclusion in this section are presented.

3.3.1 Numerical model and used parameters

To generate the tunnel stress path during TBM face advancement, a 3D model was created by numerical code PLAXIS 3D.

A tunnel of diameter D in a uniform soil deposit with an overall thickness of 4D, a width of 2.5D, and a length of 6.67D is assumed. Only one symmetric half is included. The three dimensional model and its mechanical boundaries are shown in Fig. 3.2. Regarding hydraulic boundaries, at x = 0.0 m, x = -2.5D m, y = 0.0 m, y = 6.67D m, and z = -4D m closed flow boundaries, and at z = 0.0 m free surface boundary were used. Numerical analyses were performed for a tunnel (with an outside diameter of D = 12 m) that advances in the y-direction for 25 steps (from y = +20 m to y = +70 m in Fig. 3.2). On each step, the tunnel face moves forward by Δy = +2 m. The length of the TBM is assumed to be 10 m, and lies from y = +10 m to y = +20 m before the start of the first step. The tunnel is assumed to be excavated by the EPB shield method. As the TBM advances, a monitoring section (y = +40 m) is considered for measurement purposes mid-way into the tunnel path, as shown in Fig. 3.2.

The elastic perfectly plastic constitutive model, using the Mohr–Coulomb failure criterion and a drained condition is used for soil modeling. Therefore, pore water pressure changes with the time are not taken into consideration. The tunnel lining is modeled as linear elastic and assumed to be 30 cm thick which is placed immediately following the next round of advancement. The water table is 4 m below ground level at z = –4 m. Table 1 lists the properties of the soil and concrete lining used in the analyses.

Table 3.1. Properties of the soil and concrete lining

Soil parameters used for stress path investigation	Value	Unit
Young's modulus (E_s)[1]	10, 30, 200	MN/m^2
Poisson's ratio (υ_s)	0.35	-
Total unit weight (γ_t)	19.5	kN/m^3
Cohesion (c)[1]	10, 20, 100	kN/m^2
Friction angle (φ)	30	°
Soil parameters used for drained-undrained analysis		
Young's modulus (E_s)	298	MN/m^2
Poisson's ratio (υ_s)	0.3	-
Total unit weight (γ_t)	19.5	kN/m^3
Cohesion (c)	60	kN/m^2
Friction angle (φ)	30	°
Permeability (k)[2]	8.64×10^{-4}, 8.64×10^{-3}, 8.64×10^{-2}, 8.64×10^{-1}, $8.64\times10^{+1}$	m/day
Lining parameters		
Young's modulus (E_l)	26.1	GN/m^2
Poisson's ratio (υ_l)	0.1	-
Total unit weight (γ_t)	27	kN/m^3

[1] Three different values of elastic modulus and cohesion were taken for three soil types assumed in Table 2.

[2] Five different values of permeability were taken for parametric study of soil coefficient of consolidation assumed in section (3.4).

3.3.2 Stress path analysis

a) General

Mechanical behavior of soil is not only dependent on the current stress state, but also associated with soil type, stress history and stress paths. The relationships between the various stress space displays may be illustrated by considering a relatively simple stress history. Progressive changes in the state of stress will plot as a series of points in J space, p-q space and $\boldsymbol{\sigma}$ space, defining a line meandering through the different stress spaces. It is refers as stress path. Stress path method provides a reasonable method that studies the strength and deformation behavior of soil under different loading conditions. Stress path method can be used to provide insight into the stresses developed in a soil mass under field loading. Stress path is also used to identify the soil element condition whether it is in elastic or plastic state.

To generalize the investigation, three different soil types and three different loading cases were considered in this research, as presented in Tables 3.2 and 3.3, respectively.

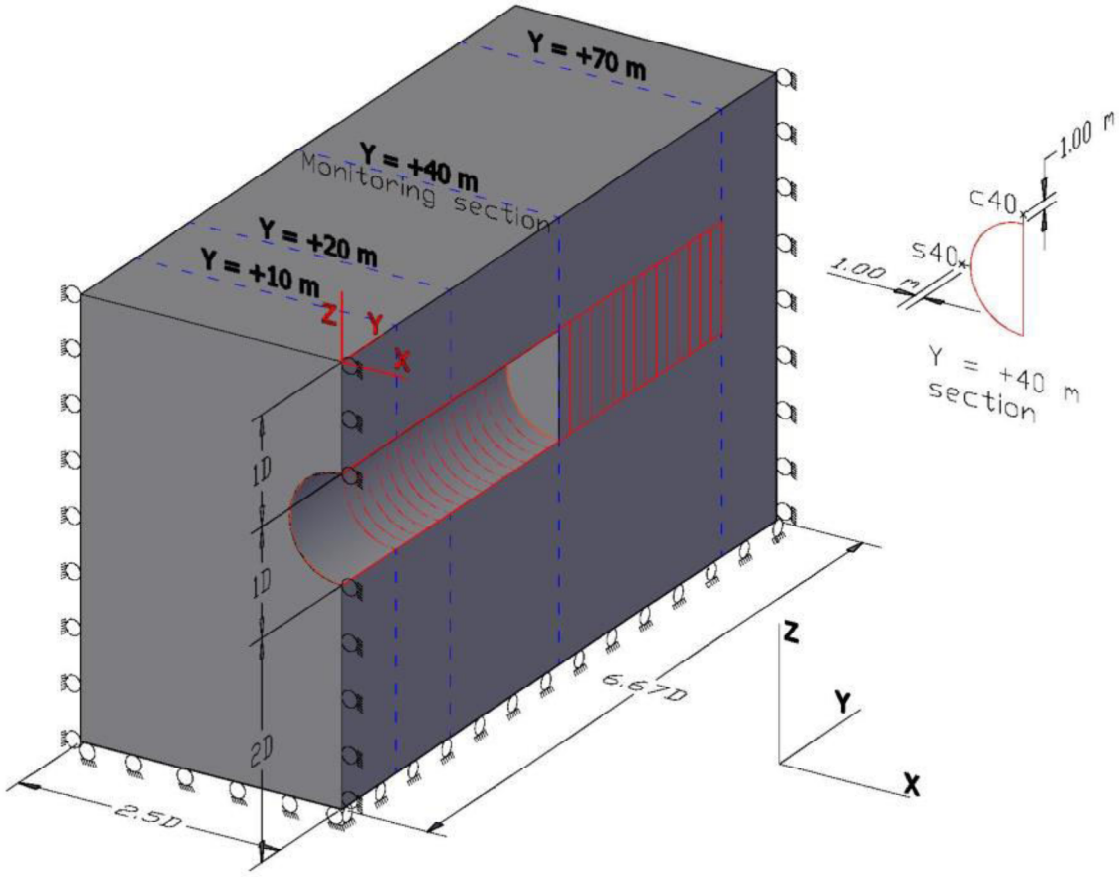

Figure 3.2. Three dimensional PLAXIS model

In Table 3.2, Poisson's ratio, total unit weight, friction angle, and permeability of the soil are taken to be constant for the three soil types. The values listed in Table 3.2 cover a wide range of soils that may be encountered in urban tunneling, from hard clay and very dense sand or dense gravel (Type 1) to soft silt, firm clay or loose sand (Type 3), although rock material is excluded. Regarding the face pressure in the case of EPB tunneling, the chamber pressure at the excavation face is generally controlled within a range between the active earth pressure and the earth pressure at rest; otherwise, ground settlement or heave occurs (Qu et al. 2009). As the maximum case, passive earth

pressure is also taken into consideration. The loading case values listed in Table 3.3 for face pressure are obtained by considering the active, static, and passive earth pressures as well as the hydrostatic pressure in the tunnel crown at z = –12 m, and in the tunnel invert at z = –24 m. The face pressure acts perpendicularly to the tunnel face and increases with depth according to the rates of increment presented in Table 3.3. The potential upper bound for the tail void grouting pressure is also the overburden pressure at the tunnel crown (Thompson et al. 2009).

Table 3.2. Soil types assumed for stress path analyses during EPB tunneling.

Soil types	Young's modulus (E_s), MN/m^2	Poisson's ratio (υ_s)	Total unit weight (γ_t), kN/m^3	Cohesion (c), kN/m^2	Friction angle (φ), °
Type 1	200	0.35	19.5	100	30
Type 2	30	0.35	19.5	20	30
Type 3	10	0.35	19.5	10	30

Table 3.3. Loading cases for face support and tail grouting pressure assumed for stress path investigations during EPB tunneling.

Loading case	Face pressure	Tail grouting pressure
Active	128 kPa at tunnel crown (z = –12 m), and increase with 13.1 kPa/m in depth	226 kPa at tunnel crown (z = –12 m), and increase with 19.5 kPa/m in depth.
Static	153 kPa at tunnel crown (z = –12 m), and increase with 14.75 kPa/m in depth	226 kPa at tunnel crown (z = –12 m), and increase with 19.5 kPa/m in depth
Passive	517 kPa at tunnel crown (z = –12 m), and increase with 38.5 kPa/m in depth	226 kPa at tunnel crown (z = –12 m), and increase with 19.5 kPa/m in depth

Therefore, in the three loading cases, values of the tail grouting pressure were assumed to be constant and equal to the ground overburden pressure values at the tunnel crown and invert. The grouting pressure is applied radially and increases with depth according to the values listed in Table 3.3.

In Table 3.3, the coefficients of active, static, and passive earth pressures were set to 0.33, 0.5, and 3, respectively, by assuming $\phi = 30^{\circ}$ and by using Jaky's equation and Rankine theory.

In total, for each soil type listed in Table 3.2, along with each loading case listed in Table 3.3, numerical analyses were conducted for nine cases.

b) Monitoring points for analyses

According to Fig. 3.2, two monitoring points were considered on the spring line and crown of the tunnel at y = +40 m section as follows:

(i) s40: a point one meter away from the tunnel spring line in the horizontal direction at y = +40 m.
(ii) c40: a point one meter away from the tunnel crown in the vertical direction at y = +40 m.

The principal effective stress values at points s40 and c40 were obtained throughout tunnel advancement, after which the stress paths were plotted for the nine analysis cases. In each of the nine cases of the analyses, stress history of the two monitoring points are calculated, recorded and shown in each loading step as the TBM moves toward the monitoring section and passes by it.

c) 2D tunneling chart of stress path

The 3D stress redistribution of shield tunneling is discussed in this section. In order to evaluate the safety of status of the tunnel advancement, stress state of the monitoring points should be compared in the extent of well-known failure criterion. Each round of tunnel advancement loading can be shown by a stress point in 3D stress axes. Superposing unique deviatoric planes, corresponding to differing tunneling rounds, together with tracing the 3D stress path are impossible, using these limited techniques. By allowing these deviatoric planes to map into a unique normalized deviatoric plane, the stress path can thereon be traced with simplicity. In order to investigate the stress-path analysis of two monitoring points s40 and c40 by tunnel advancement, proposed 2D tunneling chart method by Chen and Tseng (2010) is used in this part. They proposed a 2D tunneling chart obtained from redistributed 3D principal stress paths for the Mohr–

Coulomb criterion and mapped all deviatoric planes into a unique normalized deviatoric plane in which the stress path could be easily traced. By using the proposed tunneling chart and the Mohr–Coulomb criterion, the soil stress paths of the monitoring points during tunneling were obtained.

The 2D tunneling chart method used here, proposed by Chen and Tseng (2010), is described in detail in Appendix A of this Chapter.

As it was mentioned already, altogether, nine types of analyses were conducted in this section. Figs. 3.3 through 3.20 show the variations of the effective principal stress at points c40 and s40 of the monitoring section y = + 40m during TBM face advancement for all analyses. For instance, Figs. 3.3 and 3.4 show the variations in the effective principal stress at points c40 and s40 of the monitoring section for soil type 1 in the case of active loading. The negative sign in Figs. 3.3 to 3.20 represent the compression state of the soil. In Fig. 3.3, the major effective principal stress (σ'_1) at c40 increases and converges with the two other minor and intermediate effective principal stresses as the tunnel face approaches the monitoring section at y = +40 m. In Fig. 3.4, the effective principal stresses undergo a gradual decrease as the tunnel face approaches and passes the monitoring section. A small decrease due to tail void grouting is also noticeable 10 m after passing the monitoring section.

Clearly, great stress redistribution occurs when the working face closely approaches the monitoring points. The 3D stress redistribution becomes especially pronounced when the analyses closely approach and recede from the monitoring points.

In all of the Figs. 3.3 through 3.20, great stress redistribution occurs when the working face closely approaches the monitoring points. In the crown of the tunnel in point c40, the most severe variation happens for the passive loading case. For instance, in the case of soil type 3 and passive loading (Fig. 3.19), major effective principal stress (σ'_1) shifts from -140 toward -315 kPa as the tunnel working face approaches the monitoring section. After passing of the tunnel face, again the main effective principal stress value retreat back from the value of -315 kPa to -200 kPa. Intermediate and minor stresses show a milder variation in comparison with major principal stress when the working face of TBM passes through the monitoring section. So, in the crown of the tunnel, varia-

tion in the case of effective principal stress are larger than the other two minor and intermediate effective stresses. In the case of monitoring point s40 at tunnel spring line (Fig. 3.20), major effective principal stress (σ'_1) does not change as much as two other intermediate and minor effective stresses of σ'_2 and σ'_3 change.

Later on, by using of the data presented in the stress-path graphs and Mohr-Coulomb failure criterion, normalized deviatoric stress paths are obtained for all analysis cases.

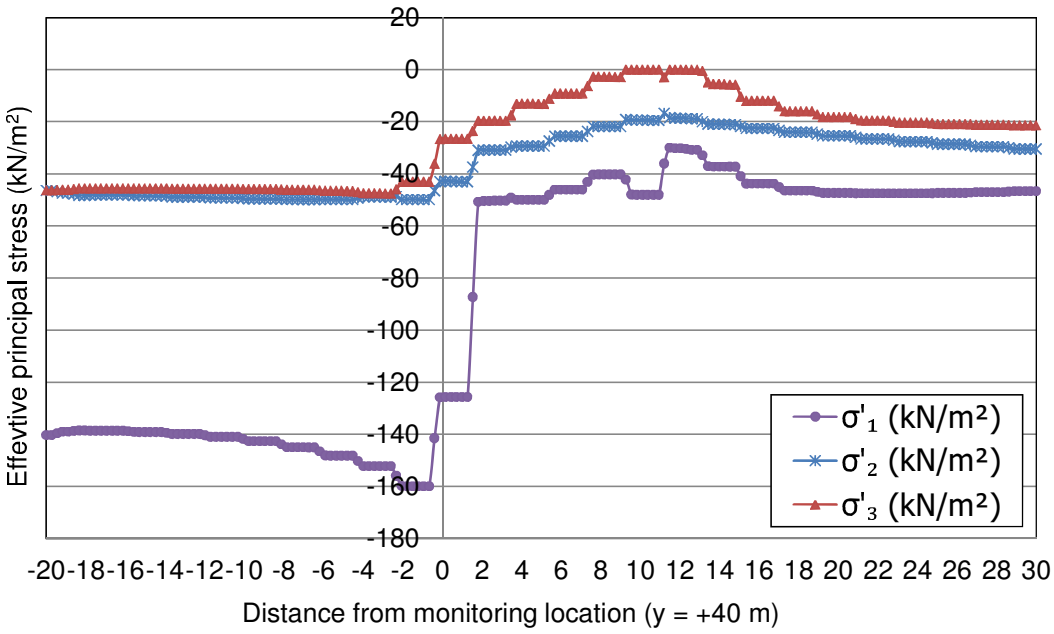

Figure 3.3. Effective principal stress variation at point c40 for soil type 1 during active loading.

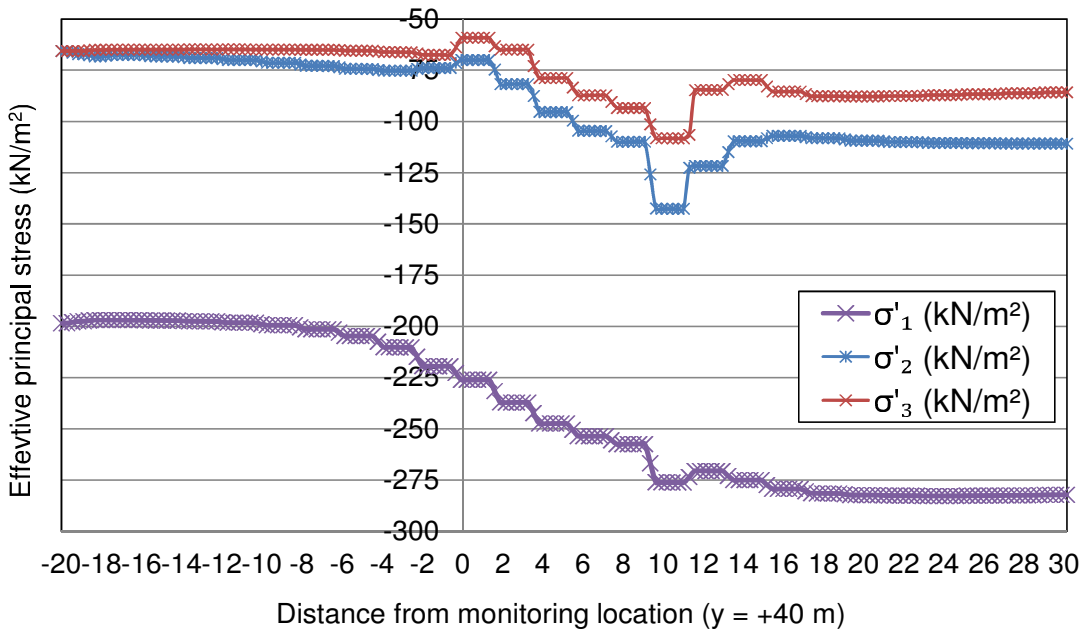

Figure 3.4. Effective principal stress variation at point s40 for soil type 1 during active loading.

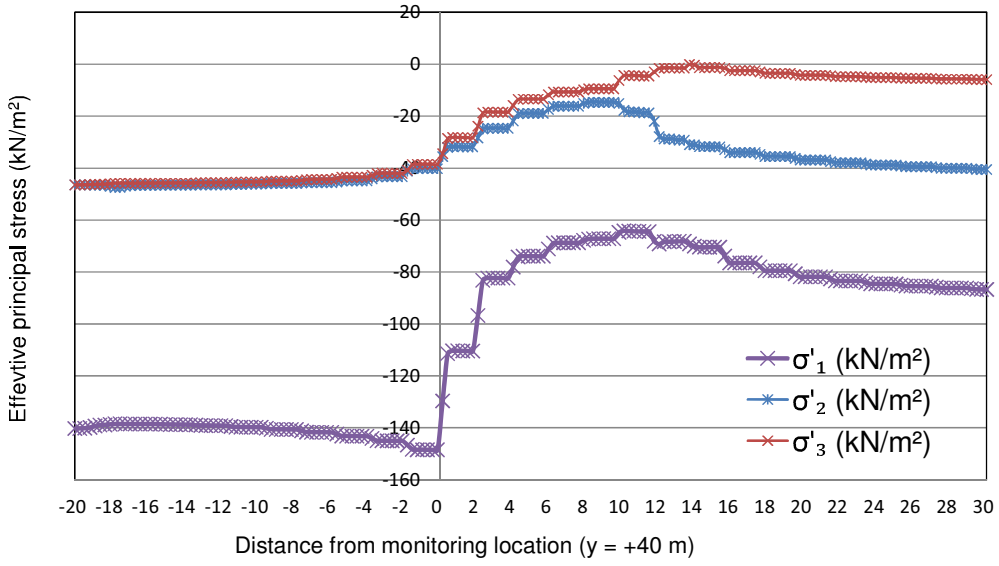

Figure 3.5. Effective principal stress variation at point c40 for soil type 2 during active loading.

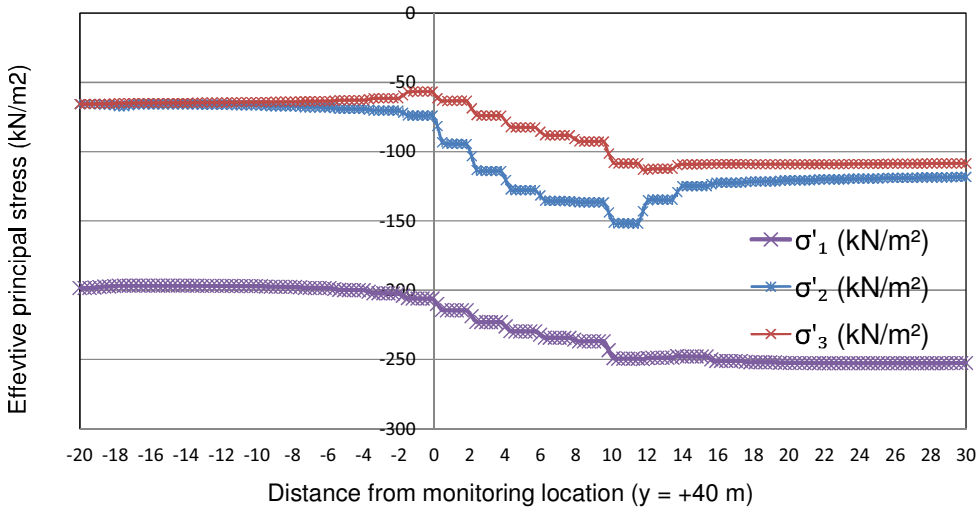

Figure 3.6. Effective principal stress variation at point s40 for soil type 2 during active loading.

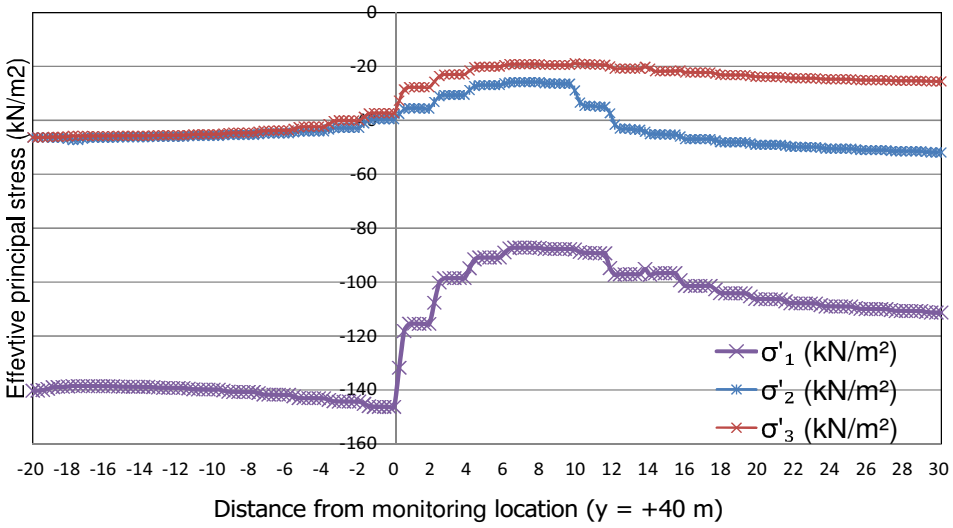

Figure 3.7. Effective principal stress variation at point c40 for soil type 3 during active loading.

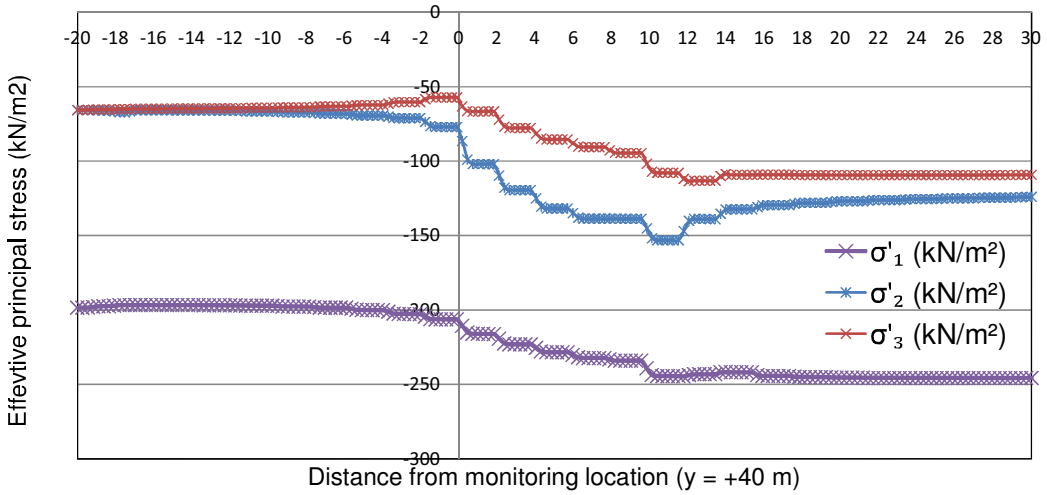

Figure 3.8. Effective principal stress variation at point s40 for soil type 3 during active loading.

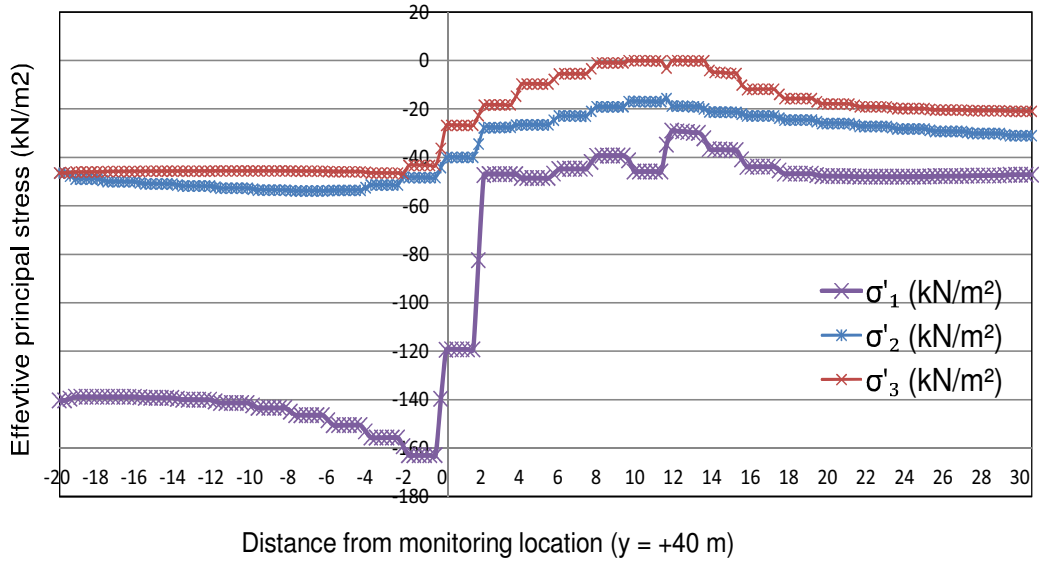

Figure 3.9. Effective principal stress variation at point c40 for soil type 1 during static loading.

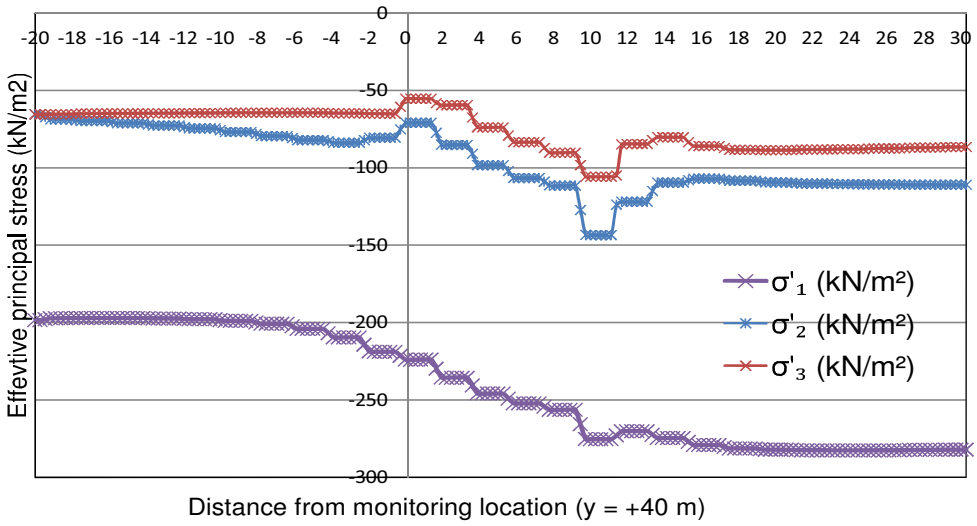

Figure 3.10. Effective principal stress variation at point s40 for soil type 1 during static loading.

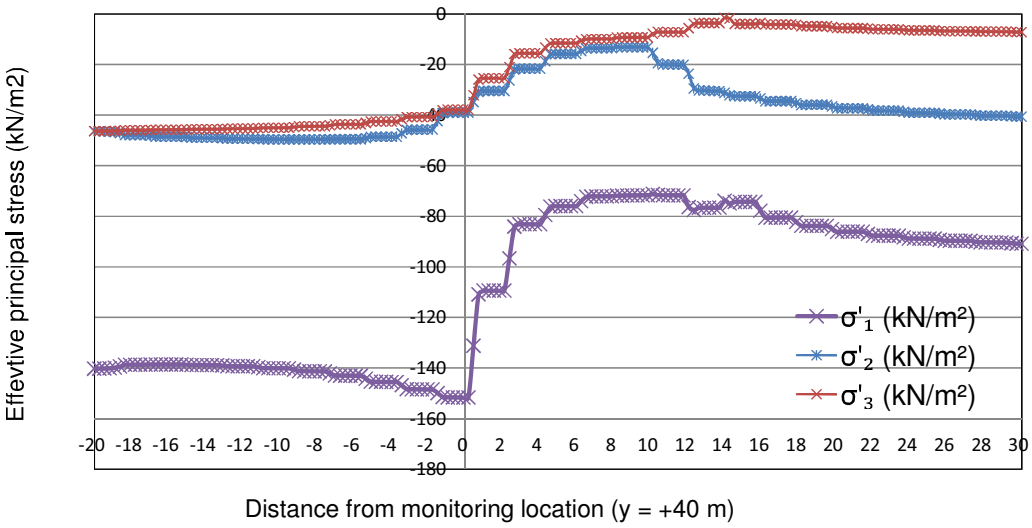

Figure 3.11. Effective principal stress variation at point c40 for soil type 2 during static loading.

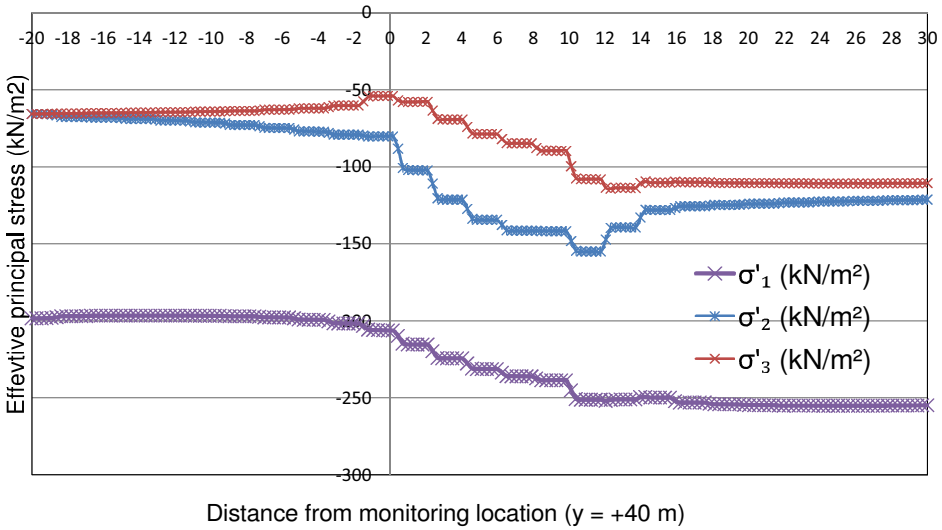

Figure 3.12. Effective principal stress variation at point s40 for soil type 2 during static loading.

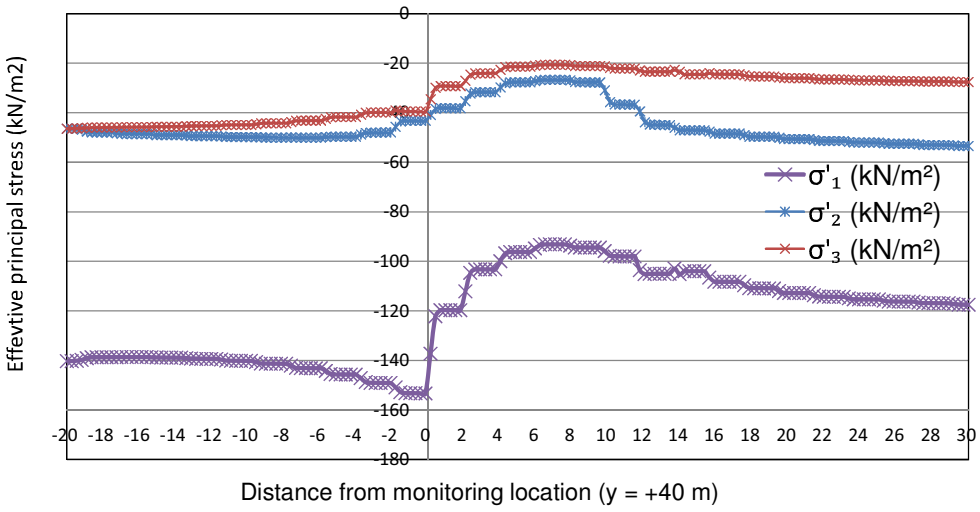

Figure 3.13. Effective principal stress variation at point c40 for soil type 3 during static loading.

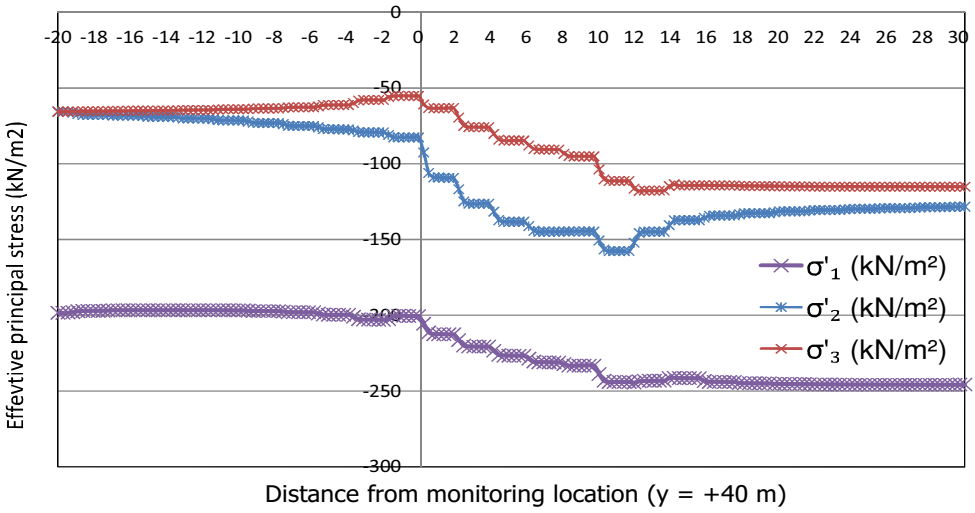

Figure 3.14. Effective principal stress variation at point s40 for soil type 3 during static loading.

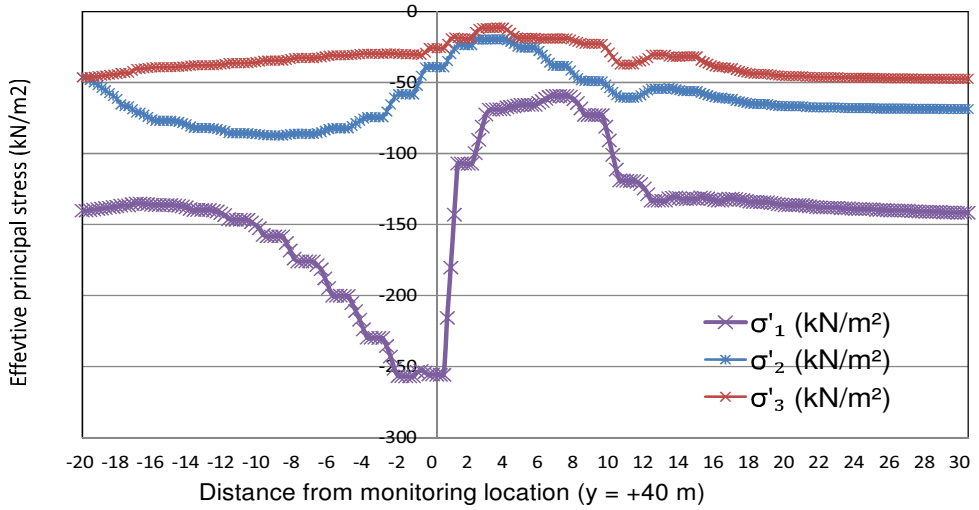

Figure 3.15. Effective principal stress variation at point c40 for soil type 1 during passive loading.

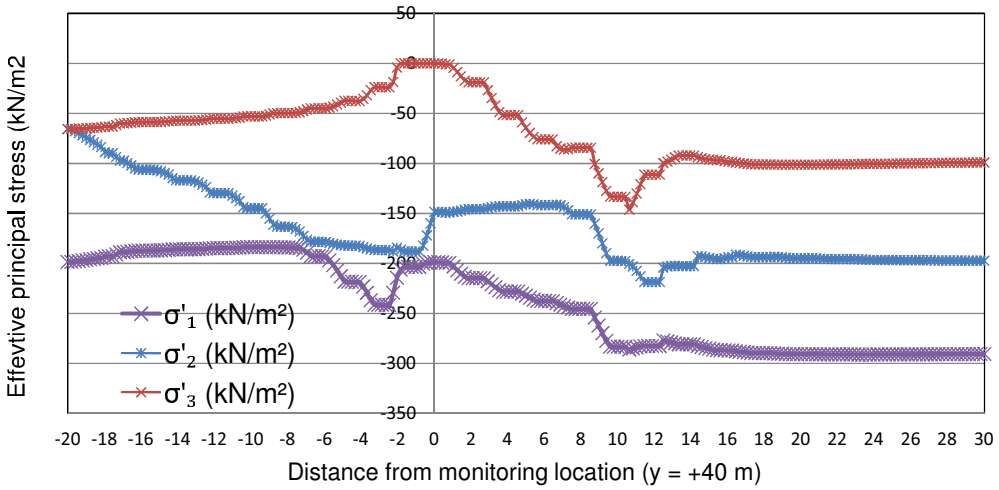

Figure 3.16. Effective principal stress variation at point s40 for soil type 1 during passive loading.

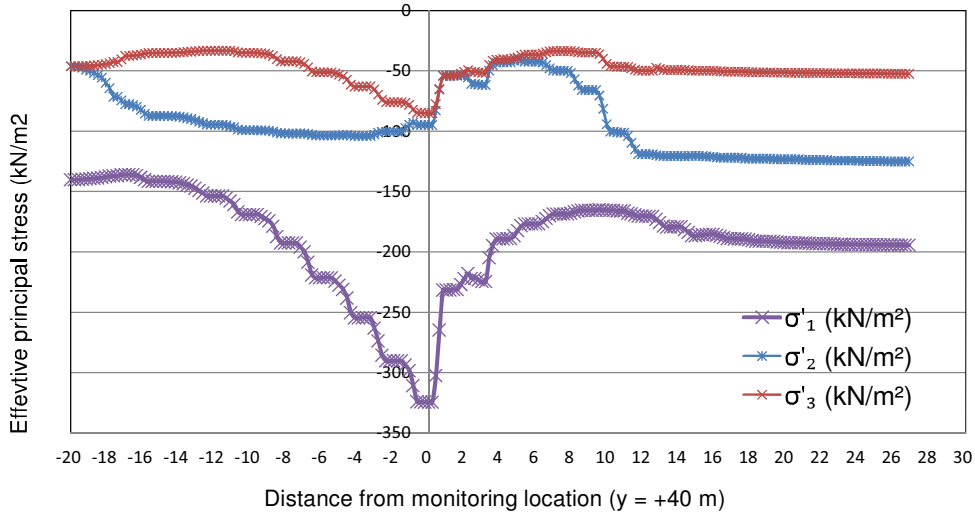

Figure 3.17. Effective principal stress variation at point c40 for soil type 2 during passive loading.

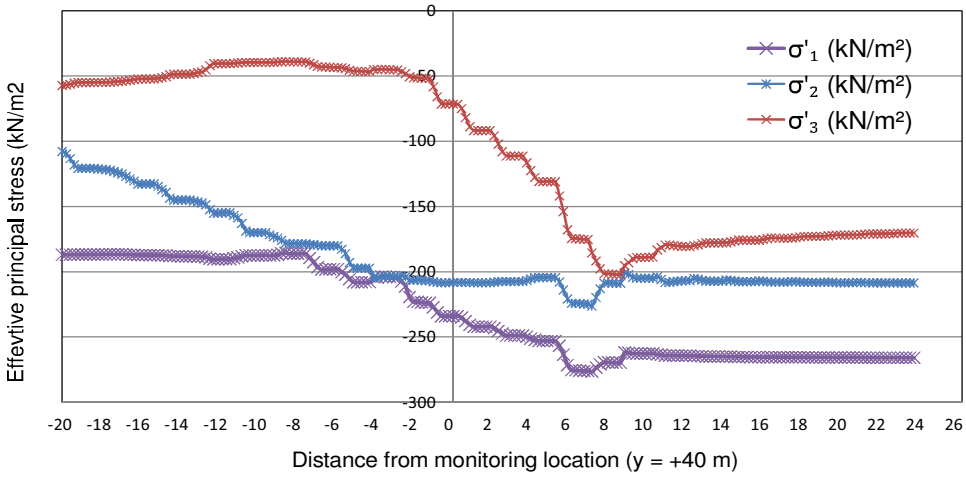

Figure 3.18. Effective principal stress variation at point s40 for soil type 2 during passive loading.

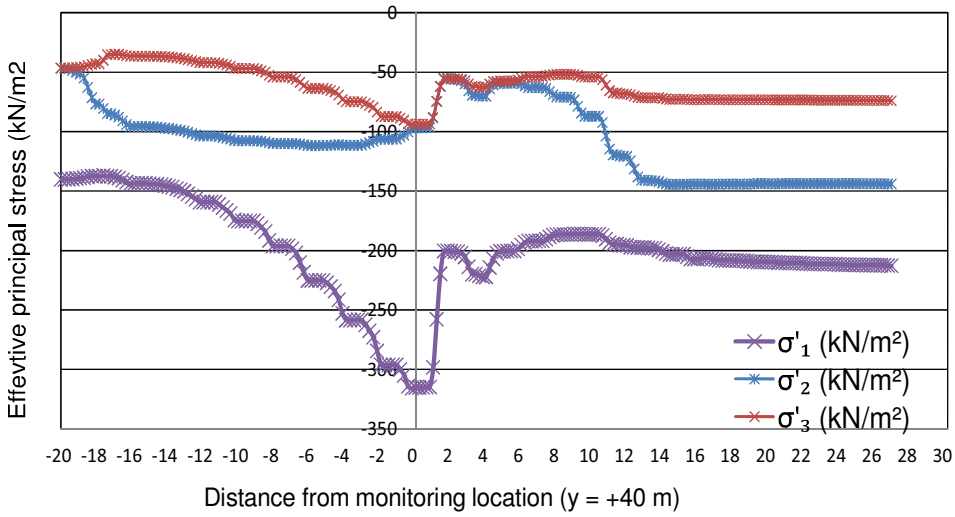

Figure 3.19. Effective principal stress variation at point c40 for soil type 3 during passive loading.

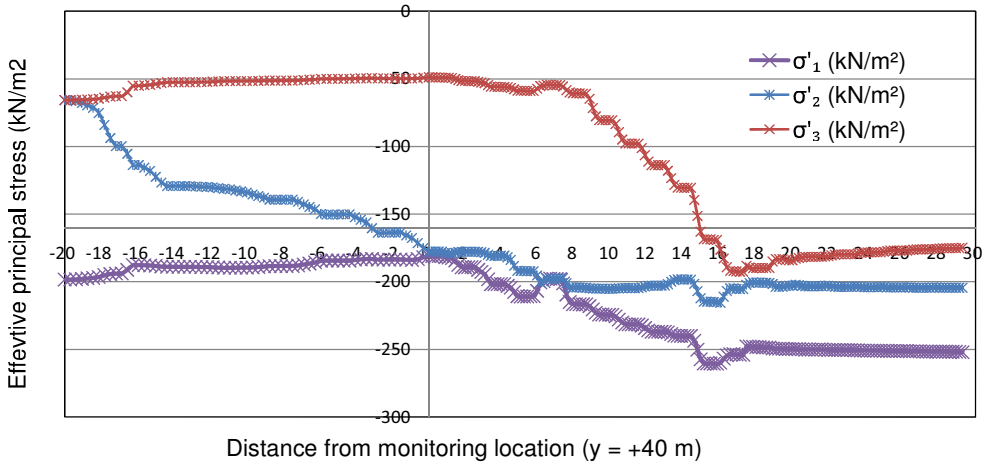

Figure 3.20. Effective principal stress variation at point s40 for soil type 3 during passive loading.

By using the 2D tunneling chart method, the normalized deviatoric stress paths of the points c40 and s40 for all nine analysis cases are presented in Figs. 3.21 through 3.38. As it was mentioned already, 2D tunneling chart proposed by Chen and Tseng, are created from the 3D principal stress redistribution (Figs. 3.3 through Figs. 3.20). The failure envelope intersecting normalized forms of the axes are used here for better comparison.

To obtain normalized deviatoric plane, $\sigma_1(\xi)$ and $\sigma_3(\xi)$ axes in the deviatoric plane are replaced respectively by normalized ratios $\sigma_1(\xi)/\rho_t(\xi)$ and $\sigma_3(\xi)/\rho_t(\xi)$ as shown in the axes of Figs. 3.21 to Figs. 3.38. The ξ parameter lies on the hydrostatic axis of stresses within the deviatoric plane, showing the distance from the origin. Parameters of ρ_t and ρ_c show the radius of extension in the deviatoric plane distance ξ from origin.

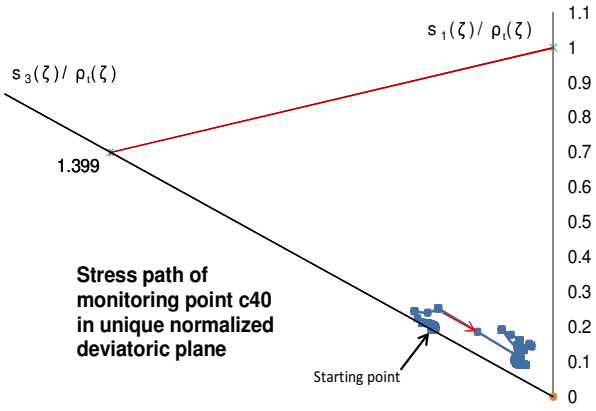

Figure 3.21. Stress path of point c40 in unique normalized deviatoric plane for soil type 1 during active loading.

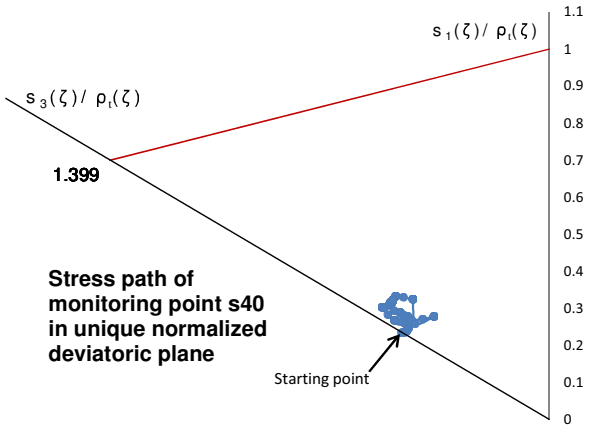

Figure 3.22. Stress path of point s40 in unique normalized deviatoric plane for soil type 1 during active loading.

For instance, in Figs. 3.21 and 3.22, normalized deviatoric stress paths at the points c40 and s40 for soil type 1 in the case of active loading are shown respectively.

As these figures show, the tunnel stress paths are inside the yielding surface during TBM advancement. In Fig. 3.21, as the TBM face approaches the monitoring location, the stress path moves away from the yielding surface. This is because according to Fig. 3.3, stress component values tend to converge, whereas in the case of Fig. 3.22, the difference between principal stress component values tend to be constant, which is the reason for the concentrated shape of the stress path at point s40.

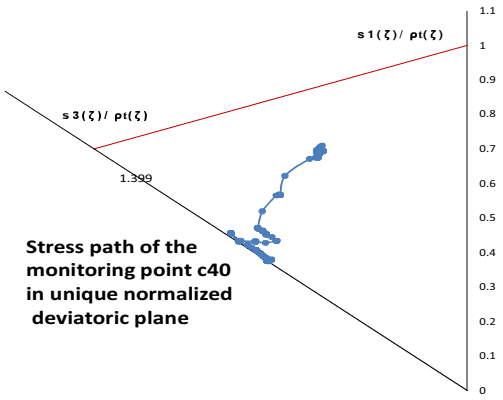

Figure 3.23. Stress path of point c40 in unique normalized deviatoric plane for soil type 2 during active loading.

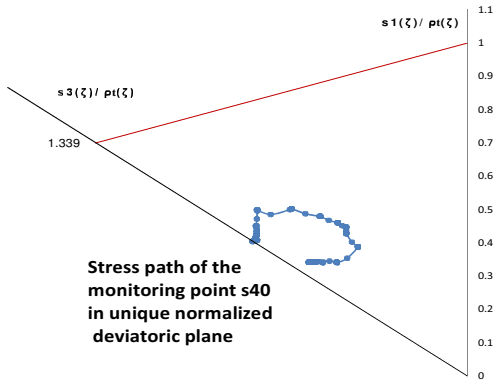

Figure 3.24. Stress path of point s40 in unique normalized deviatoric plane for soil type 2 during active loading.

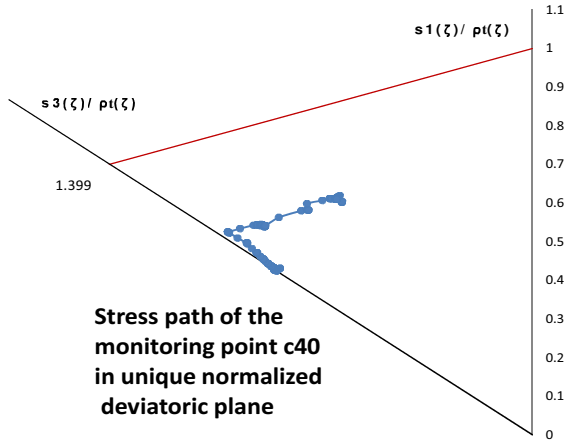

Figure 3.25. Stress path of point c40 in unique normalized deviatoric plane for soil type 3 during active loading.

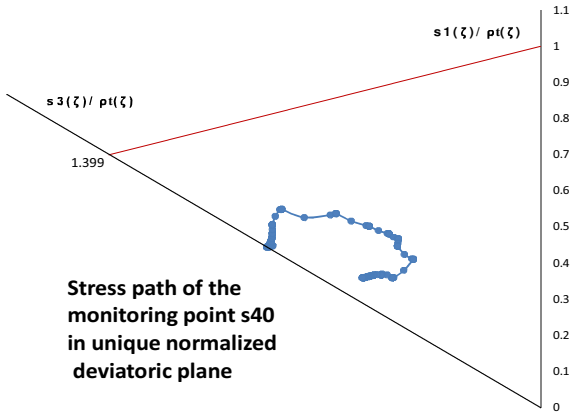

Figure 3.26. Stress path of point s40 in unique normalized deviatoric plane for soil type 3 during active loading.

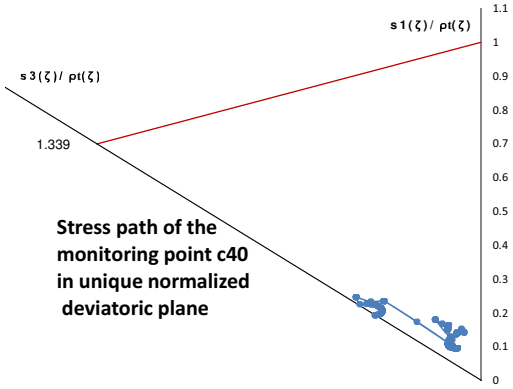

Figure 3.27. Stress path of point c40 in unique normalized deviatoric plane for soil type 1 during static loading.

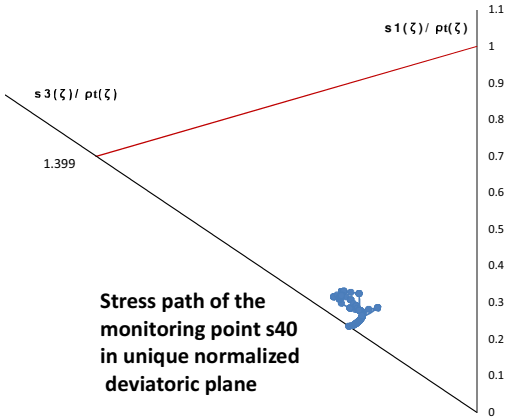

Figure 3.28. Stress path of point s40 in unique normalized deviatoric plane for soil type 1 during static loading.

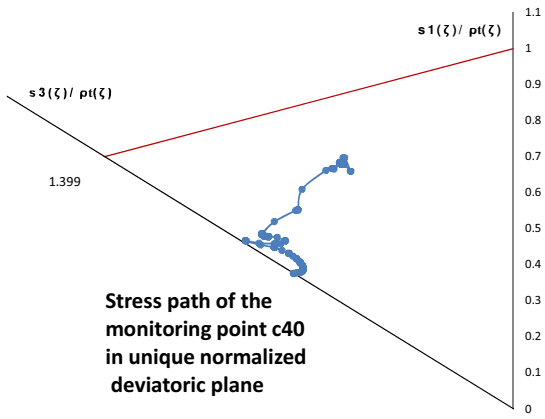

Figure 3.29. Stress path of point c40 in unique normalized deviatoric plane for soil type 2 during static loading.

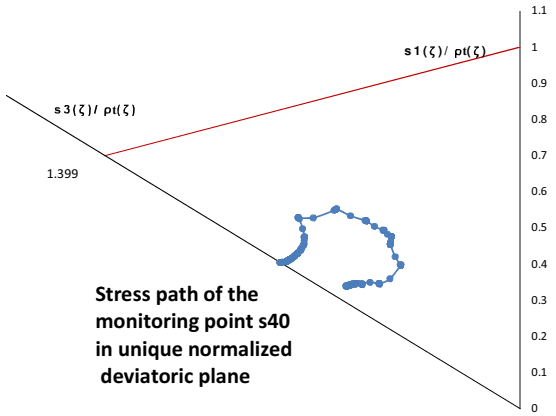

Figure 3.30. Stress path of point s40 in unique normalized deviatoric plane for soil type 2 during static loading.

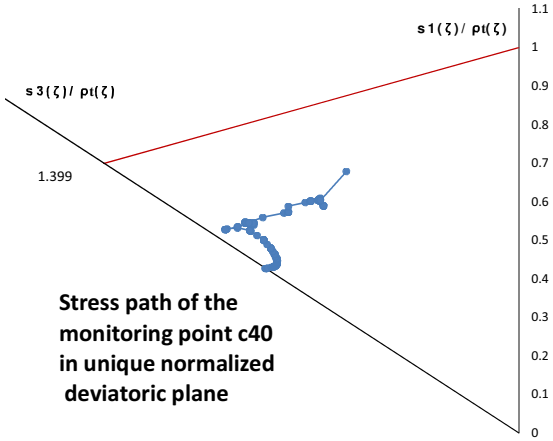

Figure 3.31. Stress path of point c40 in unique normalized deviatoric plane for soil type 3 during static loading.

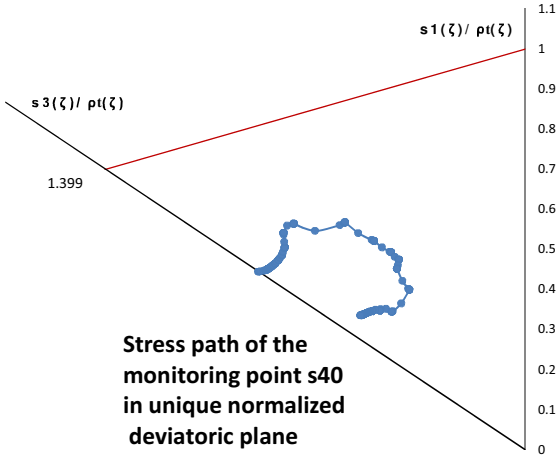

Figure 3.32. Stress path of point s40 in unique normalized deviatoric plane for soil type 3 during static loading.

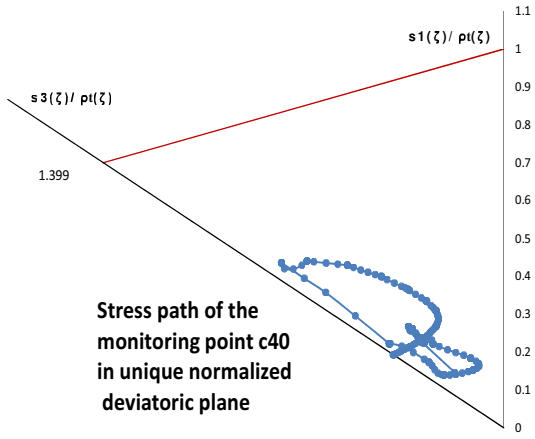

Figure 3.33. Stress path of point c40 in unique normalized deviatoric plane for soil type 1 during passive loading.

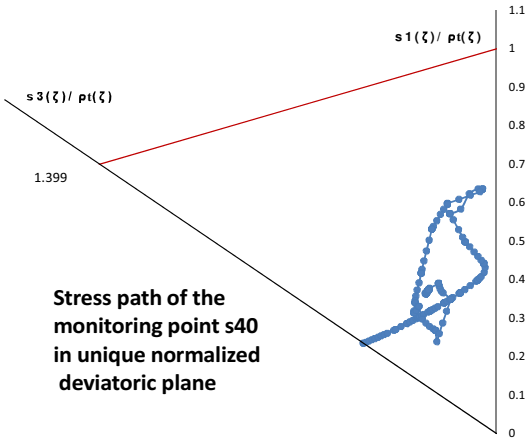

Figure 3.34. Stress path of point s40 in unique normalized deviatoric plane for soil type 1 during passive loading.

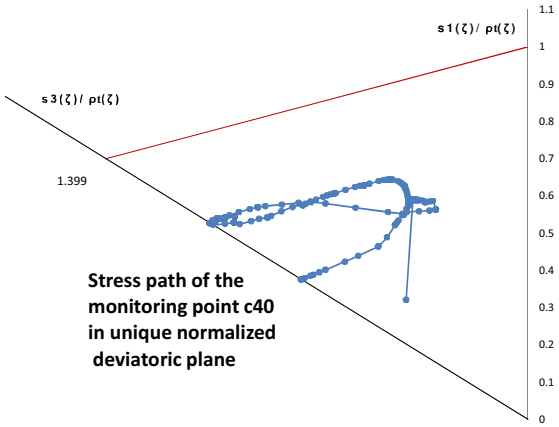

Figure 3.35. Stress path of point c40 in unique normalized deviatoric plane for soil type 2 during passive loading.

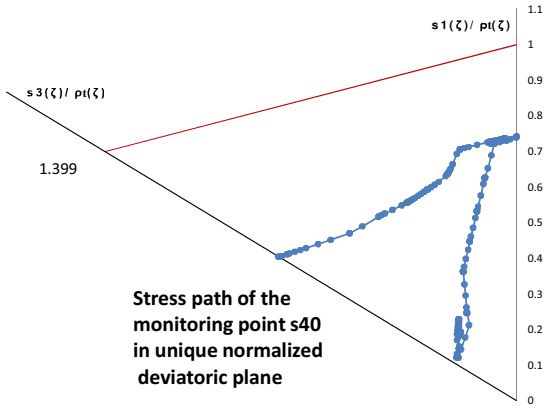

Figure 3.36. Stress path of point s40 in unique normalized deviatoric plane for soil type 2 during passive loading.

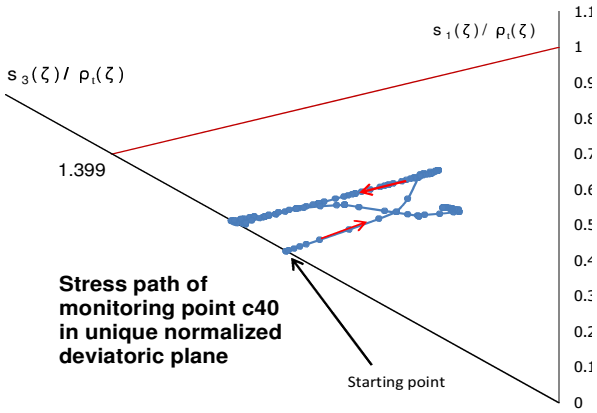

Figure 3.37. Stress path of point c40 in unique normalized deviatoric plane for soil type 3 during passive loading.

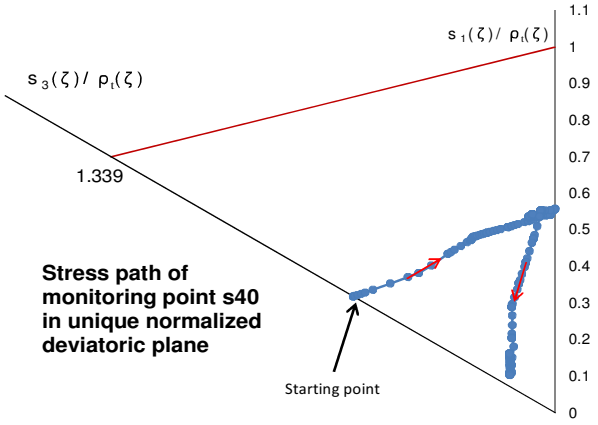

Figure 3.38. Stress path of point s40 in unique normalized deviatoric plane for soil type 3 during passive loading.

Among the nine analysis cases, the stress path of low-strength soil type 3 during high-intensity passive loading is assumed to be the most likely to touch or cross the yielding surface.

Fig. 3.37 and 3.38 present the normalized deviatoric stress paths of points c40 and s40 for soil type 3 in the case of passive loading. These figures show that the stress paths shift toward the yielding surface, although they are still inside the yielding curve. This means that the stress–strain behavior of the soil is still in the elastic condition for this case (soil type 3 and passive loading).

For all other soil types and loading cases, the stress paths drawn in a similar way were inside the yielding surface.

According to the figures presented in this section, in the case of EPB shield tunneling, where efforts are made to maintain the face pressure as close as possible to in situ earth and hydraulic pressure, the soil around the tunnel face is in the elastic domain.

3.4 Effect of EPB shield tunneling on the hydraulic condition of the soil

3.4.1 Drained and undrained condition of the soil during EPB tunneling

Drained or undrained condition of a soil during tunneling is a matter that has been discussed mostly in relation to stability of the open tunnel face (Anagnostou 1993, Vermeer et al. 2002).

In the analysis of saturated soils, both the generation and dissipation of pore pressures should, strictly speaking, be considered simultaneously by using the coupling analysis of consolidation theory. However, if the soil to be analyzed is of low permeability and the load is applied in a relatively short period, undrained deformation may be assumed for an appropriate analysis. On the other hand, if the permeability of the soil is high, or the load is applied very slowly, drained deformation can be assumed, and the pore pressure may be neglected. For the fully darined or undrained cases, the total stress analysis method is usually applied. That is, the soil is treated as a one-phase material (Song 1991).

Factors such as soil type and advance rate of the tunnel face can greatly affect the hydraulic condition of the ground. Pore water pressure generation by application of face pressure and then its dissipation changes the value and direction of the effective principal stresses which subsequently induces soil displacement. Depending on the soil type and advance rate of the tunnel face, soil stress–deformation behavior may vary from fully drained to fully undrained condition. Although analyses in saturated soil can be carried out by using soil–water coupling consolidation programs, they can also be accomplished by using the so called total stress method in either of the above cases.

In the following section, three significant factors—a) advance rate of the tunnel face, b) consolidation coefficient of the soil, and c) overburden depth of the tunnel—are considered first in conducting a parametric study and then proposing a numerical experimental equation for drained and undrained determination of soil stress–deformation behavior during EPB shield advancement in soil. In this part, an undrained analysis followed by a consolidation analysis in which generation and dissipation of excess pore water pressure is taken into consideration, were carried out using the PLAXIS program and the numerical model introduced in section 3.3.1.

3.4.2 Method

In EPB tunneling, the tunnel face is supported by excavated soil, water, and additives. At each loading step, face pressure is transmitted to the soil by pressurizing the excavation chamber through the transfer of thrust force into the bulkhead. As the face of the tunnel advances, the excavated soil and water enter the excavation chamber and then are mixed together with additives. Finally, the mixed materials are removed via a screw conveyor and transferred into a conveyor belt, from where it can be transported to the ground surface.

The main assumption here is that the tunnel face is a boundary through which pore water pressure can escape. This means that the excess pore water pressure generated owing to face pressure around the cutter head can be dissipated through the cutter head into the excavation chamber and then out of it through the conveyor belt in the form of muddy soil. At each loading step, for a constant advance rate of the tunnel face $(\Delta x/\Delta t)$, TBM moves forward by distance Δx during the time interval Δt.

Fig. 3.39 schematically represents the advance rate of the tunnel face at the first and second loading steps. Immediately after the face pressure acts on the saturated soil, pore water pressure is generated, after which the generated pore pressure starts to dissipate during time interval Δt. The degree of soil consolidation during this time depends on the advance rate of the tunnel face and the soil type. Pore water pressure values immediately after applying the face pressure and after time Δt can be obtained at the target section in each loading step. The target section, or so-called "monitoring section," refers to a location where the tunnel-induced displacements are measured in the field for safety and verification purposes (Fig. 3.39). Based on Fig. 3.39, for the first loading step, when the average distance of the TBM face from the monitoring section is x_1, the average excess pore water pressure at the monitoring section immediately after applying face pressure is u_{01} and after time Δt becomes u_1.

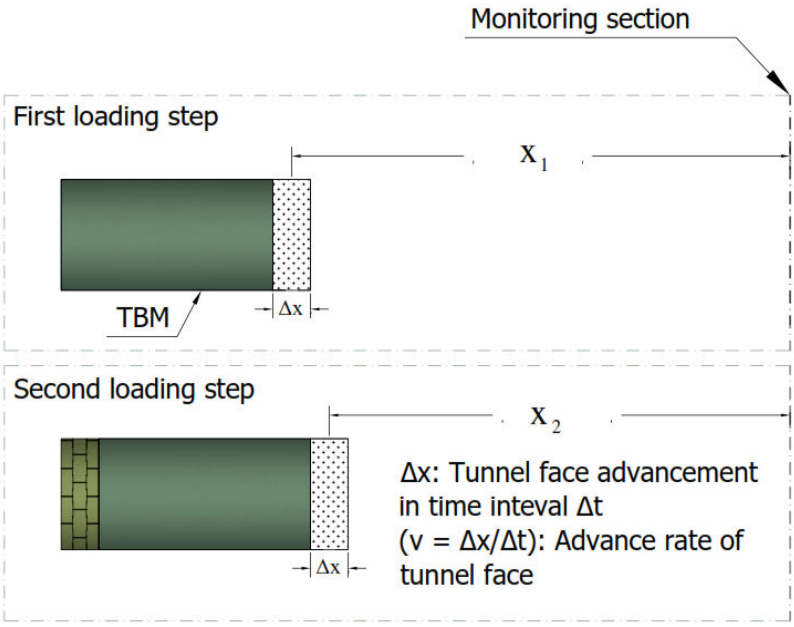

Figure 3.39. Shield tunnel face advancement toward monitoring section.

Therefore, the average degree of consolidation at the monitoring section in the first loading step $(x = x_1)$, U_1, can be expressed as

$$U_1 = \frac{u_{01} - u_1}{u_{01}} \times 100(\%) \tag{3.1}$$

For all other loading steps, similar procedures are taken to evaluate the degree of consolidation.

3.4.3 Parametric study

In this section, a parametric analysis is presented to evaluate the influence of three parameters on the hydraulic behavior of the soil in the model introduced in section 3.3.1.

The parameters are as follows:

a) Soil coefficient of consolidation, c_v (m²/day)
b) Advance rate of the tunnel face, v (m/day)
c) Overburden depth of the tunnel, H (m)

These parameters are monitored during a 20-m advancement of the TBM from step 1 (y = + 20 m) to step 10 (y = + 40 m). During this 10-step advancement, values of excess pore water pressure at the monitoring section (y = +40 m) are obtained, and then the average degree of consolidation is calculated at each step by using Eq. (3.1). The values of the three parameters employed in the analyses are listed in Table 3.4, and the results of the numerical analyses are shown in Figs. 3.40 through 3.51. The vertical black lines in these figures display the standard deviations of the degree of consolidation over the tunnel cross section of the monitoring section. Effects of the each one of the parameters are considered as follow:

a) Influence of soil coefficient of consolidation

The smaller value of the coefficient of consolidation produces a longer time for consolidation to occur. To investigate the effect of the soil coefficient of consolidation (c_v), the factor was varied across five values (Table 3.4). c_v is obtained as follows:

$$c_v = \frac{k}{\gamma_w.(\frac{1}{K'} + Q)} \tag{3.2}$$

where γ_w is the unit weight of the pore fluid, k is the coefficient of permeability, K' is the drained bulk modulus of the soil skeleton, and Q represents the compressibility of the fluid.

By neglecting the compressibility of fluid in comparison with soil skeleton, assuming soil bulk modulus value of $K' = 3.89 \times 10^3$ kN/m^2, and also five values of coefficient of permeability as $k = 8.64 \times 10^{-4}, 8.64 \times 10^{-3}, 8.64 \times 10^{-2}, 8.64 \times 10^{-1}$, and $8.64 \times 10^{+1}$ m/day, five values of consolidation coefficient are obtained as shown in Table 3.4.

In each step, by varying c_v and keeping the two other parameters fixed, the average degree of consolidation is obtained as the tunnel face moves toward the monitoring section.

Typical values of c_v for various soil types are shown in Table 3.5.

Table 3.4. Values of parameters employed in the parametric study

Parameters	Values
Advance rate of tunnel face	1, 2, 5, 10, and 20 m/day
Soil coefficient of consolidation	0.3361, 3.361, 33.61, 3361, and 33.61×10^{3} m²/day
Overburden depth	12 m, 18 m

Table 3.5. Typical values of the coefficient of consolidation (Carter and Bentley, 1991)

Soil	Classification	coefficient of consolidation (c_v) m²/yr
Boston blue clay	CL	12±6
Organic silt	OH	0.6-3
Glacial silt	CL	2.0-2.7
Chicago silty clays	CL	2.7
Swedish medium	CL-CH	0.1-1.2 (Laboratory)
Sensitive clay		0.2-1.0 (Field)
San Francisco bay mud	CL	0.6-1.2
Mexico city clay	MH	0.3-0.5

With two values for the overburden ratio (H) and five values for the advance rate of the tunnel face (v), a total of ten numerical analyses were conducted. Figs. 3-40 through 3–49 illustrate the results of these analyses. In Fig. 3-40, for example, keeping values of v and H fixed at 1 m/day and 12 m, respectively, the average degree of consolidation is shown for different values of c_v. The horizontal axis shows the distance of the tunnel face from the monitoring section (y = + 40 m), and the vertical axis represents the average degree of consolidation value according to Eq. (3.1).

In Fig. 3-40, the average degree of consolidation increases as the tunnel face approaches the monitoring section for all values of c_v. This increase occurs when the tunnel face is closer to the monitoring section for soil cases with lower values of c_v.

On the other hand, in the case of high c_v values, say $c_v = 33.61\times10^{3}$ m²/day, the generated excess pore water pressure at the monitoring section dissipates quickly regardless of the distance of the tunnel face from the monitoring section (within the range of 20 m), indicating that the drained nature of the soil. Similar behavior is noticeable in Figs. 3–41 through 3–49.

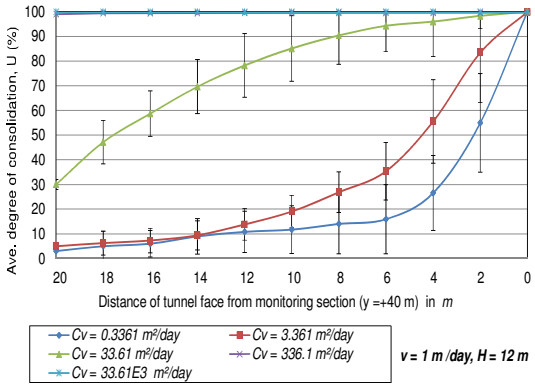

Figure 3.40. Average degree of consolidation at monitoring section (y = +40 m) assuming v =1 m/day, H = 12 m.

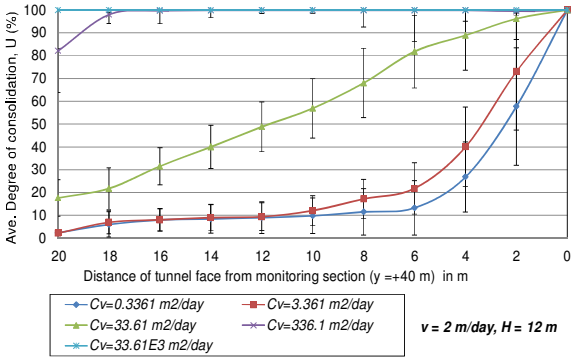

Figure 3.41. Average degree of consolidation at monitoring section (y = +40 m) assuming v =2 m/day, H = 12 m.

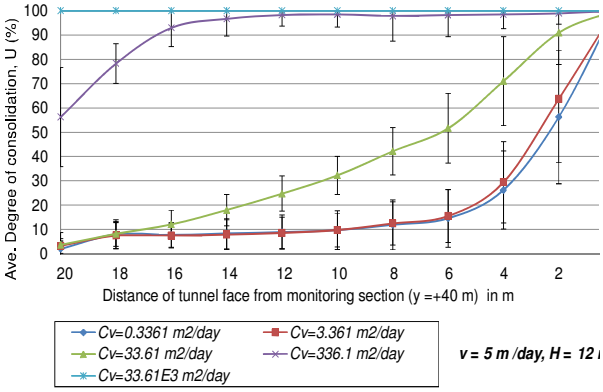

Figure 3.42. Average degree of consolidation at monitoring section (y = +40 m) assuming v =5 m/day, H = 12 m.

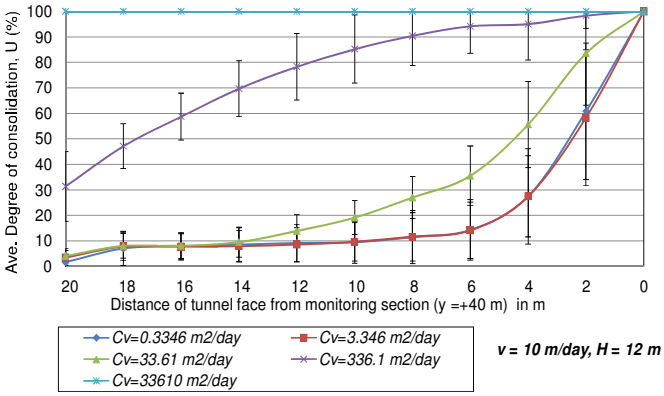

Figure 3.43. Average degree of consolidation at monitoring section (y = +40 m) assuming v =10 m/day, H = 12 m.

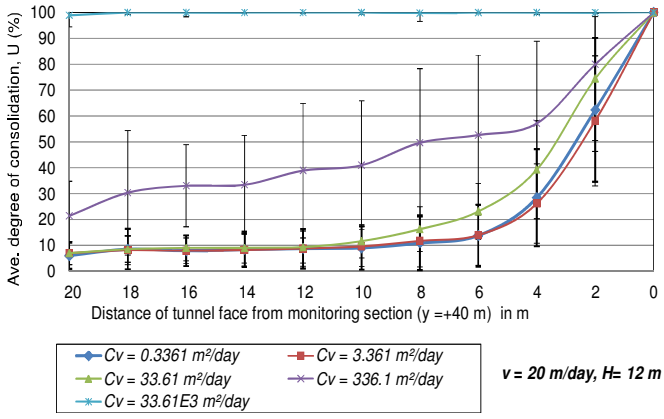

Figure 3.44. Average degree of consolidation at monitoring section (y = +40 m) assuming v =20 m/day, H = 12 m.

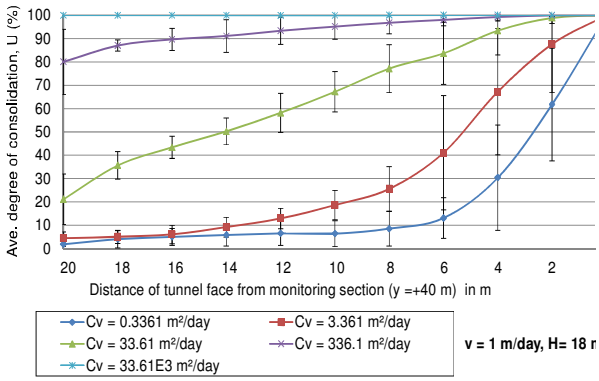

Figure 3.45. Average degree of consolidation at monitoring section (y = +40 m) assuming v =1 m/day, H = 18 m.

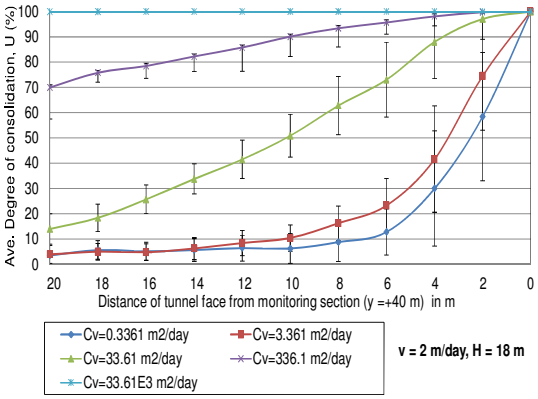

Figure 3.46. Average degree of consolidation at monitoring section (y = +40 m) assuming v =2 m/day, H = 18 m.

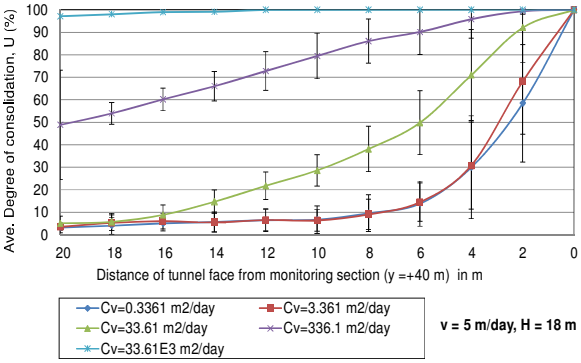

Figure 3.47. Average degree of consolidation at monitoring section (y = +40 m) assuming v =5 m/day, H = 18 m.

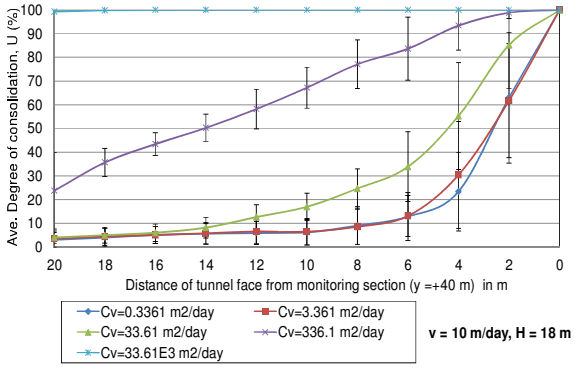

Figure 3.48. Average degree of consolidation at monitoring section (y = +40 m) assuming v =10 m/day, H = 18 m.

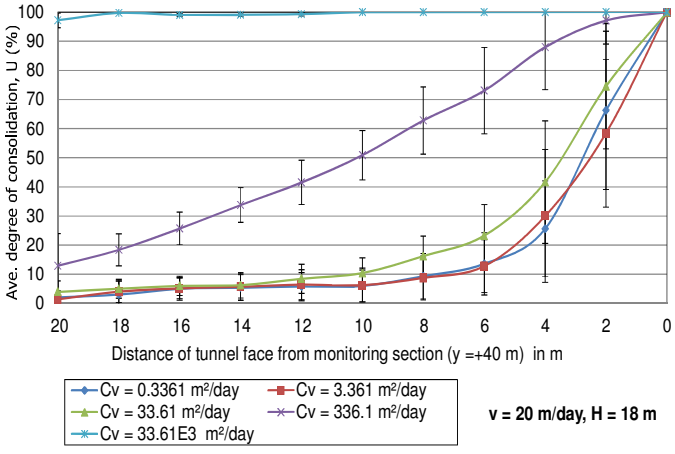

Figure 3.49. Average degree of consolidation at monitoring section (y = +40 m) assuming v =20 m/day, H = 18 m.

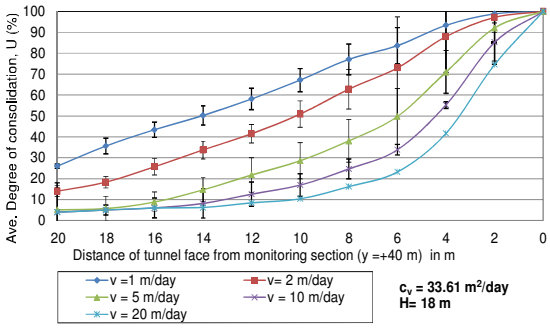

Figure 3.50. Average degree of consolidation at monitoring section (y = +40 m) assuming c_v =33.61 m²/day, H = 18 m.

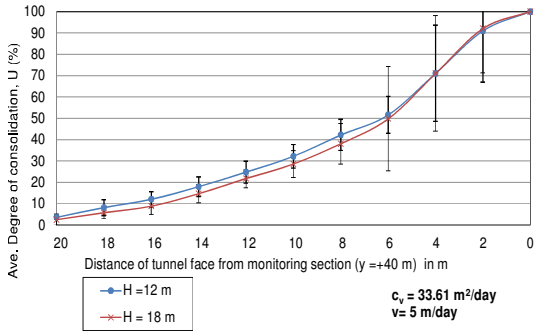

Figure 3.51. Average degree of consolidation at monitoring section (y = +40 m) assuming c_v =33.61 m²/day, v = 5 m/day.

b) Influence of advance rate of tunnel face

To examine the influence of the advance rate of the tunnel face, v, the factor was varied across five values of 1, 2, 5, 10, and 20 m/day (Table 3.4). In Fig. 3.50, for example, *v* changes while c_v and *H* were kept constant at 33.61 m²/day and 18 m, respectively.

For the sake of brevity, variations of *v* with other values of c_v and *H* other than those in Fig. 3.50 are not shown.

To investigate the effect of *v* for other values of c_v and *H*, comparisons among Figs. 3.40 through 3.49 can also be made. Fig. 3.50 shows that a slower advance rate leads to a higher degree of consolidation at the monitoring section. This is expected because a slower tunnel face implies that more time is available for excess pore water pressure to dissipate. Fig. 3.50 also shows that *v* does not influence the dissipation rate of excess pore water pressure as significantly as does c_v while the tunnel face approaches the monitoring section. This issue has also been addressed by Anagnostou in 1993.

c) Influence of overburden depth

To investigate the influence of the overburden depth *H*, two values of 12 and 18 m (*1D* and *1.5D*, where *D* is the tunnel diameter) were assumed (Table 3.4). This parameter indicates the height of the soil deposit above the tunnel crown.

Fig. 3.51 shows that tunnel excavation at a greater depth slightly decreases the rate of excess pore water pressure dissipation at the monitoring section owing to the longer

drainage path, although its effect is far less than that of the two previous parameters. As the tunnel face approaches the monitoring section, the effect of H becomes negligible.

3.4.4 Numerical experimental equation for soil drainage determination during EPB tunneling

Investigating the results in Figs. 3-40 through 3-51 reveals that as the tunnel face approaches the monitoring section, not only pore water pressure generation increases, but also does the dissipation rate of pore water pressure which results in a higher degree of consolidation. Having the average degree of consolidation, i.e. U (%), as an approximate index for which more than this index, stress-deformation calculation can be performed by assuming fully drained condition, and less than this index, the fully undrained condition is used, (e.g. for U > 70%, drained analysis can be assumed as proposed by Veermer and Meier (1998)) a distance $\bar{x}$ corresponding to this U can be specified. For example, in Fig. 3.49, in the case of c_v = 336.1 m^2/day, v = 20 m/day, and H = 18 m, when U > 70% is assumed as the average degree of consolidation so that the drained condition can be applied, we obtain $\bar{x}$ ≈ 6.5 m.

This means that in the case of c_v = 336.1 m^2/day, v = 20 m/day, and H = 18 m, for distances of tunnel face less than 6.5 m from the monitoring section, the fully drained condition can be assumed. As illustrated in Fig. 3.52, if the distance of the tunnel face from the monitoring section is taken to be x_i, for a specific set of values for v, c_v, and H, theoretically it could be assumed that there is a distance $\bar{x}$ such that when the tunnel face distance from monitoring section is closer and farther than this value, the fully drained and fully undrained conditions, respectively, can be assumed for soil stress–deformation calculations at the monitoring section.

As already mentioned, v, c_v, and H influence the drainage condition of the soil. If the tunnel diameter (D) is also taken into account, it can be stated that $\bar{x} = f(v, c_v, D, H)$.

To clarify how $\bar{x}$, v, c_v, D, and H are related, a dimensional analysis is carried out, using the results of the parametric study. By using the Buckingham π theorem, three dimensionless parameters are constructed as follows:

$$\pi_1 = \frac{\bar{x}}{H},\ \pi_2 = \frac{H}{D},\ \pi_3 = \frac{c_v}{v \cdot D} \tag{3.3}$$

$$\frac{\bar{x}}{H} = f\left(\frac{H}{D}, \frac{c_v}{v \cdot D}\right) \tag{3.4}$$

Taking the degree of consolidation U (= 60%, 70%, and 80%) as an index, $\bar{x}$ values are read from the results of the analyses performed in section 3.4.3 (parametric study).

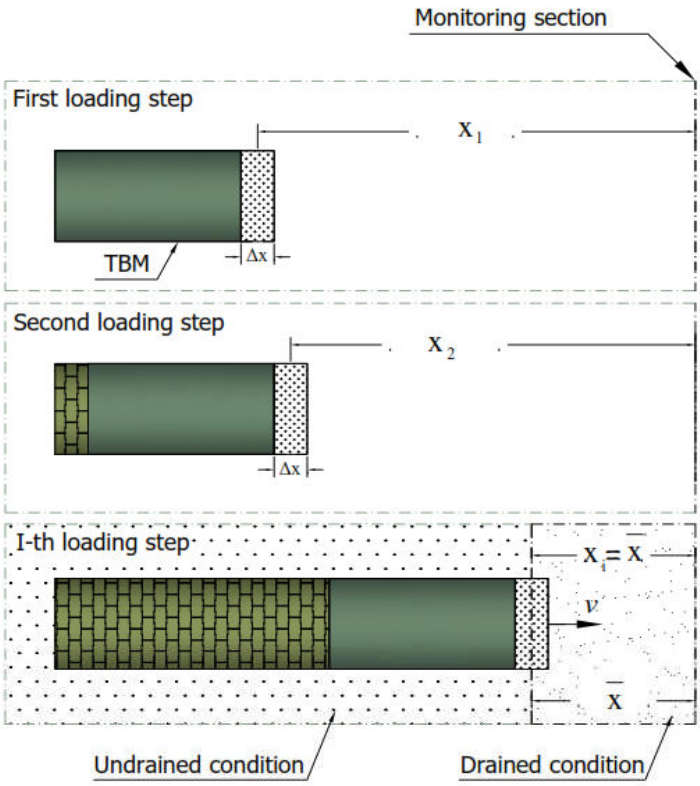

Figure 3.52. Drained-undrained condition with respect to advance rate of tunnel face and soil coefficient of consolidation.

By using these data and Eq. (3.3), the relationship between parameters π_1 and π_3 is obtained. The results are plotted in Figs. 3.53 through 3.58.

For example, for the case of degree of consolidation 60% (U = 60%), and overburden ratio $\pi_2 = H/D = 1$, relationship between parameters π_1 and π_3 parameters are shown in

Fig. 3.53. Figs. 3.53 through 3.55 display the values of π_1 plotted against π_3 for H/D = 1. For an overburden ratio of H/D = 1.5, the trends are displayed in Figs. 3.56 through 3.58.

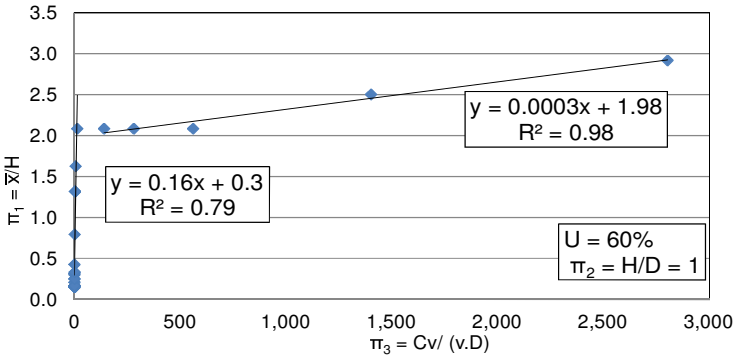

Figure 3.53. Dimensional analysis by plotting π_1 against π_3 for U = 60%, $\pi^2 = H/D$ = 1.

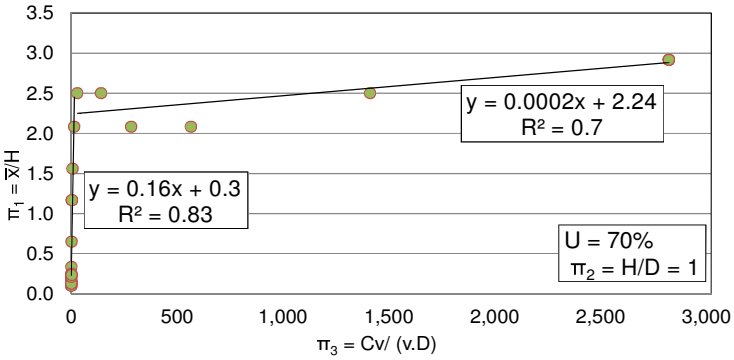

Figure 3.54. Dimensional analysis by plotting π_1 against π_3 for U = 70%, $\pi^2 = H/D$ = 1.

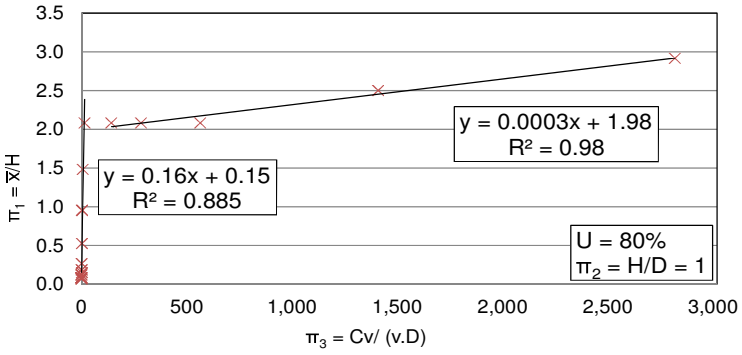

Figure 3.55. Dimensional analysis by plotting π_1 against π_3 for U = 80%, $\pi^2 = H/D$ = 1.

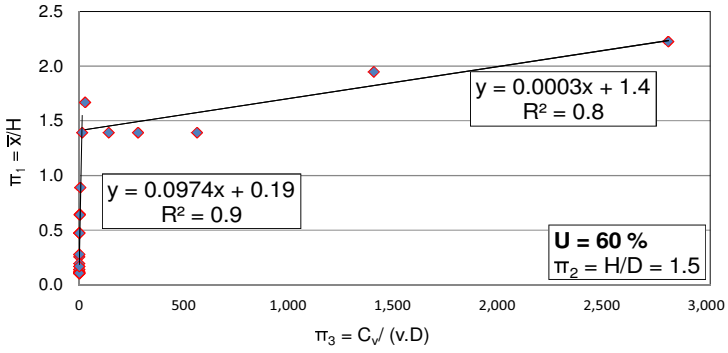

Figure 3.56. Dimensional analysis by plotting π_1 against π_3 for U = 60%, $\pi^2 = H/D$ = 1.5.

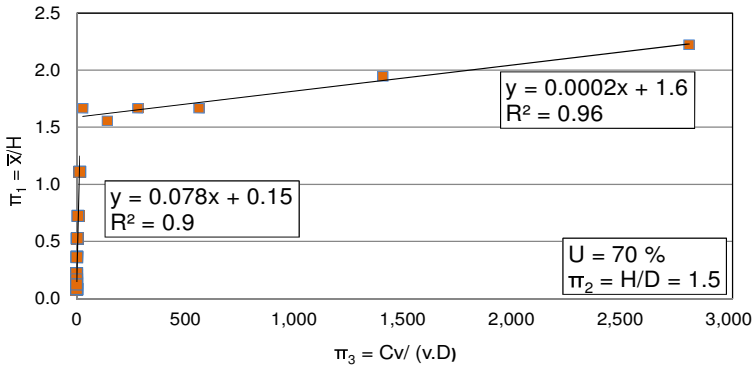

Figure 3.57. Dimensional analysis by plotting π_1 against π_3 for U = 70%, $\pi^2 = H/D$ = 1.5.

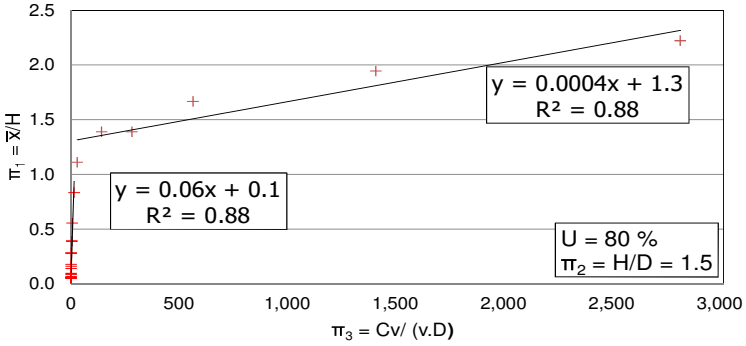

Figure 3.58. Dimensional analysis by plotting π_1 against π_3 for U = 80%, $\pi^2 = H/D$ = 1.5.

Fig. 3.59 shows π_1 plotted against π_3 for $\pi_2 = H/D$ = 1 and all average degrees of consolidation. A similar graph is also drawn for $\pi_2 = H/D$ = 1.5 and all degrees of consolidation in the same figure. The best fits of the data are obtained by bilinear regression.

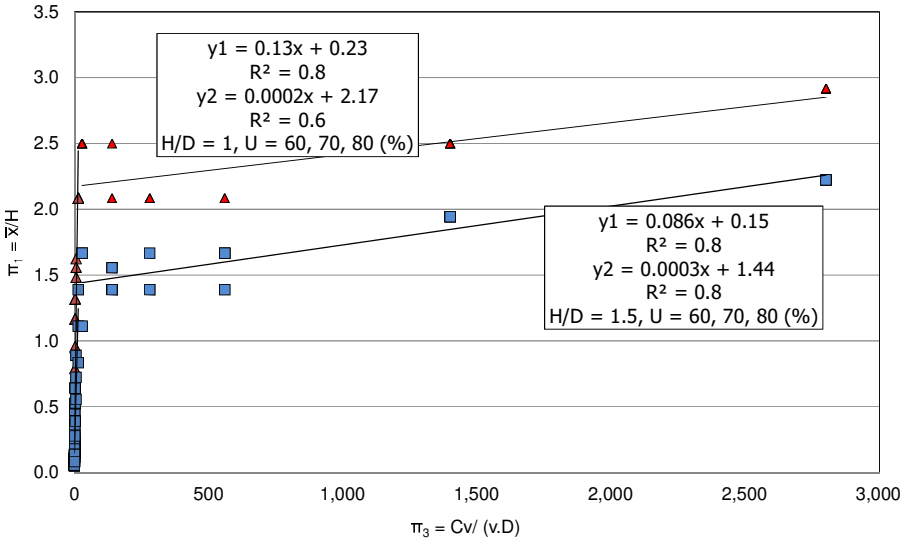

Figure 3.59. Dimensional analysis by plotting π_1 against π_3 for U = 60%, 70%, and 80%, with $\pi_2 = H/D$ = 1 and 1.5.

Fig. 3.59 shows that regardless of the value of U, the relationship between π_1 and π_3 for H/D = 1 is :

$$\frac{\bar{x}}{H} = 0.13(\frac{c_v}{v \cdot D}) + 0.23, \qquad 0 \le \pi_3 \le 15$$

$$\frac{\bar{x}}{H} = 0.0002(\frac{c_v}{v \cdot D}) + 2.17, \qquad \pi_3 \ge 15 \tag{3.5}$$

and for H/D = 1.5 is :

$$\frac{\bar{x}}{H} = 0.086(\frac{c_v}{v \cdot D}) + 0.15, \qquad 0 \le \pi_3 \le 15$$

$$\frac{\bar{x}}{H} = 0.0003(\frac{c_v}{v \cdot D}) + 1.44, \qquad \pi_3 \ge 15 \tag{3.6}$$

The more general form of the equation is

$$\frac{\bar{x}}{H} = a.(\frac{c_v}{v \cdot D}) + b \tag{3.7}$$

$$a = 0.13 - 0.088(\frac{H}{D} - 1), \; b = 0.23 - 0.16(\frac{H}{D} - 1) \qquad 0 \le \pi_3 \le 15$$

$$a = 2\times10^{-4}(\frac{H}{D})\text{ ، }\ b = 2.17-1.46(\frac{H}{D}-1) \qquad \pi_3 \geq 15$$

In above equation, v shows tunnel boring machine advance rate, c_v shows coefficient of consolidation, D is tunnel diameter, and H represents the height of the soil deposit above the tunnel crown. If x is taken as a general distance of TBM face from monitoring location, $\bar{x}$ is specified distance in which

If $x > \bar{x}$, the soil undrained deformation condition is assumed and the acting in-situ earth pressure and the soil Poisson's ratio can be obtained using soil total stress analysis. Poisson ratio in this case can be assumed as $\vartheta \sim 0.495$.

If $0 < x < \bar{x}$, the soil drained deformation condition is assumed and the acting earth pressure and the soil Poisson's ratio can be obtained using soil effective analysis. Poisson ratio in this case can be assumed as $0.3 < \vartheta < 0.45$.

In the case of accessibility to only of either drained or undraiend parameters of elastic modulus or Poisson ratio, using of relationship between drained and undrained parameters, the other two sets of parameters can be attained. In isotropic linear elastic materials, elastic modulus, Poisson ratio, and shear modulus can be connected to one another by formula $\mathrm{G} = \frac{\mathrm{E}}{2(1+\vartheta)}$. As the shear modulus parameter have identical value in both of drained or undrained analyses, by assuming Poisson ratio as above, so, based on equation $\frac{E'}{2(1+\vartheta')} = \frac{E_u}{2(1+\vartheta_u)}$ elastic modulus can be obtained for each analysis of drained or undrained case if we have the other ones.

Note that Eq. (3.7) is recommended for shallow tunnels in which the ratio of the overburden to tunnel diameter is between 1 and 2. Validation of the proposed experimental equation is shown in chapter 5.

3.5 Proposed simplified finite element method

Simplified 3D FEM simulation procedures of EPB shield tunneling have been proposed as follows based on the parametric study performed in section 3.4.3 and presented equation in section 3.4.4. It will be shown in chapter 5 that by the use of the simplified simulation procedures, the time period required to obtain the FEM simulation re-

sults of the same problem is shown to be reduced more than 50% compared with the soil-water coupling procedures. The steps for this simplified finite element analyses are as follow:

1) 3D finite element mesh of the analysis region including the monitoring section is prepared. The mesh boundary must be large enough from the tunnel and other construction that natural tunneling construction behavior can be simulated. In the case of complicated meshes, mesh generation programs could be used. In the case of relatively simple meshes, based on the known number of nodes, elements, restrained nodes numbers, tunnel configuration, using an excel program the mesh can also be constructed. Programs like Micro-AVS can be used to check the correctness of the mesh (Personal visualization system, Micro-AVS).
2) The soil constitutive model employed in the FEM calculation is an ideal elastic model.

   As it was mentioned in section 3.3 (Effect of EPB shield tunneling on the soil stress-path), in the case of EPB shield tunneling, where efforts are made to maintain the face pressure as close as possible to in situ earth and hydraulic pressure, the soil around the tunnel face is in the elastic domain. In this part, for simplicity and based on the results obtained in section 3.3, ideal elastic soil model is used.
3) By having the field parameters of (v, c_v, D, and H), and equation 3.7, $\bar{x}$ value is obtained for simple drainage determination.
4) According to the horizontal distance x between the TBM face and the monitoring section, the acting in-situ earth pressure and the soil Poisson's ratio are selected as follows by using the specific distance $\bar{x}$ using equation 3.7.

   If $x > \bar{x}$, the soil undrained deformation condition is assumed and the acting in-situ earth pressure and the soil Poisson's ratio can be obtained using soil total stress analysis.

   If $0 < x < \bar{x}$, the soil drained deformation condition is assumed and the acting earth pressure and the soil Poisson's ratio can be obtained using soil effective analysis.

By using the soil stress condition and the material properties mentioned above, the total stress FEM analysis is carried out without soil-water coupling.

5) The soil stress change due to the previous step TBM face pressure loading is used to obtain the in-situ earth pressure at the current step TBM face pressure loading.

Therefore, in this way, using of proposed simplified program method enable a simple total stress analysis under simple drainage condition instead of a complicated effective stress analysis considering soil-water coupling. Later on, soil displacement at any point in eh mesh including the monitoring location can be calculated.

3.6 Summary

In this chapter, effect of EPB shield tunneling on the soil stress path was investigated. Using the elastic perfectly plastic constitutive model with the Mohr–Coulomb failure criterion, the 3D stress distribution of the area near the crown and spring line of the tunnel investigated, after which the soil stress path with respect to the M–C yielding surface is presented. Based on the obtained graphs, it was demonstrated that the stress paths shift toward the yielding surface when tunnel working face approaches the monitoring section, although they are still inside the yielding curve. This means that the stress–strain behavior of the soil is still in the elastic condition. Therefore, it was concluded that in the case of EPB shield tunneling, where efforts are made to maintain the face pressure as close as possible to in situ earth and hydraulic pressure, the soil around the cutter head tends to be in elastic domain.

The effect of EPB tunneling on the hydraulic condition of the soil was also examined. Taking into account the three significant factors of a) advance rate of the tunnel face, b) consolidation coefficient of the soil, and c) overburden depth of the tunnel, a parametric study was conducted and a numerical experimental equation was presented for drainage determination of the soil during shield tunnel advancement. A numerical experimental equation is recommended for shallow tunnels in which the ratio of the overburden to tunnel diameter is between 1 and 2. It is used for simple drainage determination of soil during EPB tunneling.

Proposed simplified finite element method is described in the last section of this chapter. Using of the proposed simplified program method enables a simple total stress analysis under simple drainage condition instead of a complicated effective stress analysis considering soil-water coupling.

Validation of the proposed simplified finite element method is shown in chapter 5.

3.7 Appendix A (2D tunneling chart method proposed by Chen and Tseng, 2010)

Derivation of normalized deviatoric plane

Based on the Haigh–Westergaard principal stress space (Desai and Siriwardane 1984) (ξ, ρ_0, θ), the Mohr–Coulomb failure criterion can be presented as,

$$f(\xi,\rho_0,\theta) = \sqrt{2}\xi \sin\phi + \sqrt{3}\rho_0 \sin(\theta + \frac{\pi}{3}) + \rho_0 \cos(\theta + \frac{\pi}{3}) \sin\phi - \sqrt{6}c\cos\phi = 0 \tag{3.8}$$

where ξ lies on the hydrostatic axis within the deviatoric plane, as shown in Fig. 3.60.(a) ρ_0 and θ lie within the deviatoric plane away from the hydrostatic axis in stress space. The associated angle formed with the σ_1 axis is shown in Fig. 3.60.(b). Three parameters are given as,

$$\xi = \frac{\sigma_1 + \sigma_2 + \sigma_3}{\sqrt{3}} \tag{3.9}$$

$$\rho_0 = \sqrt{2J_2} \tag{3.10}$$

$$\cos 3\theta = -\frac{3\sqrt{3}}{2}\frac{J_3}{J_2^{\frac{3}{2}}} \tag{3.11}$$

where J_2 and J_3 are invariants of the stress deviator tensor given by,

$$J_2 = \frac{1}{3}(I_1^2 - 3I_2)$$

$$J_3 = \frac{1}{27}(2I_1^3 - 9I_1I_2 + 27I_3) \tag{3.12}$$

$$I_1 = \sigma_1 + \sigma_2 + \sigma_3$$

$$I_2 = \sigma_1\sigma_2 + \sigma_2\sigma_3 + \sigma_1\sigma_3$$

$$I_3 = \sigma_1\sigma_2\sigma_3$$

In Eq. (3.8), $\xi = 0$ implies that the hydrostatic pressure is 0, which corresponds to a deviatoric plane (π-plane) that contains the origin. At the π-plane, failure envelopes intersect the σ_1 and $-\sigma_3$ axes at ρ_{c0} and ρ_{t0}, respectively, as shown in Fig. A.1.b.; these parameters are defined as follows. The angle of inclination between ρ_{c0} and ρ_{t0} is 60°.

$$\rho_{t0} = \frac{2\sqrt{6}c.\cos\phi}{3+\sin\phi} \tag{3.13}$$

$$\rho_{c0} = \frac{2\sqrt{6}c.\cos\phi}{3-\sin\phi} \tag{3.14}$$

The deviatoric plane for each round of tunneling has a corresponding ξ, which can be mapped in the stress space. When the tunnel's working face arrive at each section, the corresponding tunneling stress can be plotted into different deviatoric planes. These planes are parallel with their respective ξ. The sizes of these planes are unequal. By normalizing all deviatoric planes into one plane, stress evaluation using a single chart becomes feasible for all rounds of tunneling.

To obtain the normalized deviatoric plane, $\sigma_1(\xi)$ and $\sigma_3(\xi)$ axes are replaced in the deviatoric planes by the normalized ratios $\sigma_1(\xi)/\rho_t(\xi)$ and $\sigma_3(\xi)/\rho_t(\xi)$, respectively, as illustrated in Fig. 3.61.

The failure envelope intercepts ρ_t along the σ_1 axis, a projection upon the deviatoric plane in the stress space, is normalized to unit length, where $\sigma_1(\xi)/\rho_t(\xi) = \rho'_t = 1$. By using of Eqs. (3.13) and (3.14), and the friction angle $\varphi = 30^\circ$ (refer to Table 3.1), the normalized length of $\sigma_3(\xi)/\rho_t(\xi) = \rho'_c = 1.399$ along the normalized axis of $\sigma_3(\xi)/\rho_t(\xi)$ is derived.

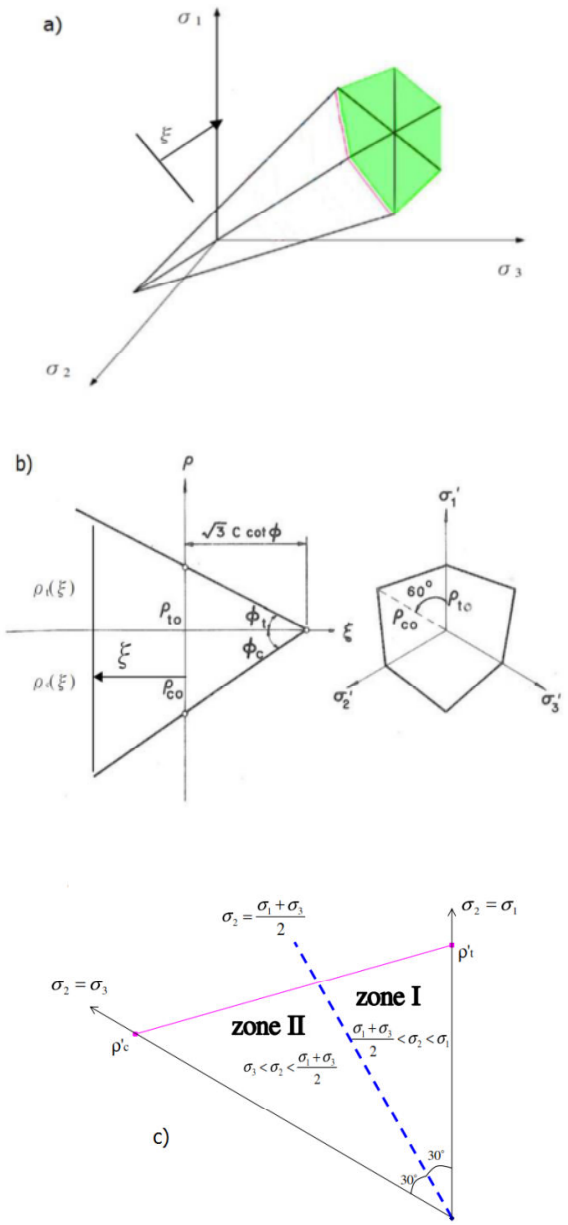

Figure 3.60. a) Mohr–Coulomb criterion; b) π-plane; c) relationship of principal stresses in deviatoric plane.

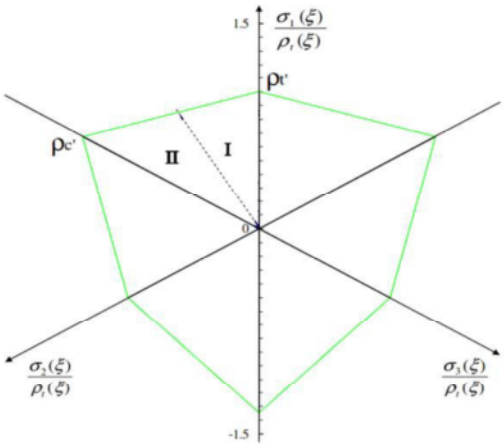

Figure 3.61. Unique normalized deviatoric plane.

References:

1) Fujita, K. : Use of Slurry and Earth Pressure Balance Shield in Japan, International Congress on Tunneling, pp. 383-406, 1981.
2) Nishitake, S. : Advanced technology realize high-performance earth pressure balanced shield. InFranchissements souterrains pour l'Europe, pp. 291-302, Rotterdam, 1990.
3) Stack, B. : Handbook of Mining and Tunnelling Machinery, John Wiley and Sons, U.K., 1982.
4) Yang, H., Shi, H., Gong, G. and Hu, G. : Earth pressure balance control for EPB shield, Science in China Series E: Technological Sciences, Vol. 52, No. 10, pp. 2840-2848, 2009.
5) Qu, F., Wu, L. and Sun, W. : Analysis of chamber pressure for earth pressure balance shield machine by discrete numerical model, Intelligent Robotics and Applications, Springer, pp. 402–411, 2009.
6) Thompson, J., Chai, J., Biggart, A. and Young, D. : Earth Pressure Balance Machines for the Silicon Valley Rapid Transit Project—Basis of Design, North American Tunneling Proceedings, pp. 168–176, 2008.
7) Anagnostou, G. : Modelling seepage flow during tunnel excavation, International Symposium-EUROCK 93, 1993.
8) Vermeer, P. A, Ruse, N. and Marcher, T. : Tunnel heading stability in drained ground, Felsbau, Vol. 20, No. 6, pp. 8–18, 2002.
9) Song. E. : Elasto-plastic consolidation under steady and cyclic loads, PhD Thesis, Delft University, Department of Civil Engineering and Geosciences, 1991.
10) Carter, M. and Bentley, S. P. : Correlations of soil properties, Pentech press publishers, 1991.
11) Vermeer, P. A. and Meier, C. P. : Stability and deformations in deep excavations in cohesive soils, Proceedings International Conference on Soil-Structure Interaction in Urban Civil Engineering, Darmstadt Geotechnics, Vol. 1, No. 4, 1998.
12) Desai, C. S. and Siriwardane, H. J. : Constitutive Laws for Engineering Material with Emphasis on Geologic Materials, 1984, Prentice-Hall, Vol. 11, 1984.
13) Personal visualization system, Micro-AVS: <http://www.cybernet.co.jp/avs/products/microavs/>

Chapter 4 Case study

4.1 Introduction

Considerable experience with earth-pressure shields has been gained in Japan, where this construction method was developed in 1960s (Stack 1982). Ground movements associated with EPB shield tunneling are still of great concern in a mixed ground and below existing tunnels, not only because of its potentially damaging effects to the overlying structures but also it pose serious threat to passengers in operation tunnels. In this case, all attempts must be made to act upon the settlement sources and prevent ground decompression. Field measurement data of soil displacement due to the underground tunneling not only help to achieve better understanding of the ground behavior, but it could be a beneficial database for making comparison with FEM results for future investigation.

In this chapter, a comprehensive shield tunneling case namely as "Yokohama Circular Northern Route" located in Yokohama, Japan, is presented. Project overview, geological and hydrological specification of the site, monitoring sections information, and recorded displacement data are reviewed.

4.2 Project Overview

Metropolitan Expressway Company is currently constructing the Metropolitan Expressway Yokohama Circular Northern Route (Northern Route below), an expressway of a length of approximately 8.2 km serving as a link between the Kohoku Interchange of the Third-Keihin Road and the Namamugi Junction of the Yokohama-Haneda Airport Line of Metropolitan Expressway in the northern section of the Yokohama Circular Route Road. Fig. 4.1 demonstrates the Yokohama Circular Northern Route shown by

thick red line as well as Kohoku Interchange of the Third-Keihin Road, Namamugi Junction, and Haneda Airport. Fig. 4.2 displays a close up aerial view of the site.

In the Northern Route, tunnels are constructed in approximately 70% of the route to reduce the number of houses to be relocated and preserve the surrounding environment. In this project, parallel tunnels are constructed for a length of 5.5 km in the tunnel section of the route mostly under private land. Diverging and merging sections are built at four locations in the tunnels also under private land. Large spaces are created from inside the shield tunnel under a maximum water pressure of 0.5 MPa without adopting trenching although no records are available on practical applications of the method. In order to decrease the number of houses for relocation and preserving the surrounding environment, 70% of the routes are constructed via tunnels.

Figure 4.1. Yokohama Circular Northern Route (reproduced from the http://hamarepo.com/story.php?story_id=1683#)

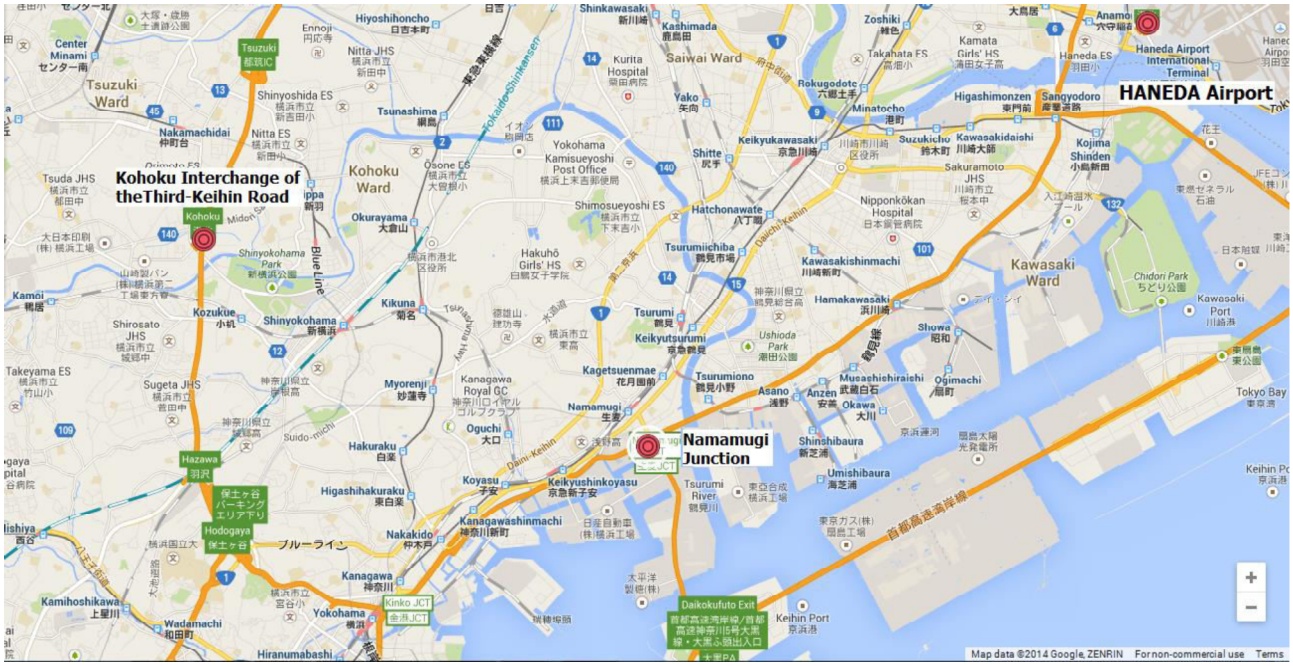

Figure 4.2. Plan view of the Kohoku interchange (starting point) and Namamugi Junction (End point) of the tunneling route (Photo was made by data from Google map, 2014).

These tunneling are constructed using side by side Earth Pressure Balance Machines. Overburden above tunnel varies between 11 to 57 m and clearance between twin tunnels is changing from 3.0 to 7.6 m.

The project started in 2011 and expected to be finished in 2014. With the development of the Northern Line communication with the inland and the sites of Tokyo Bay and along the Keihin coastal area and the Port of Yokohama are enhanced. It will also improve the living environment of the Yokohama area residents by distributing the traffic along the coastal area of Yokohama.

By completion of this project, the distance between Shin-Yokohama and Yokohama-Haneda Airport Line is expected to decrease to 10 minute facilitating the faster access to Haneda airport.

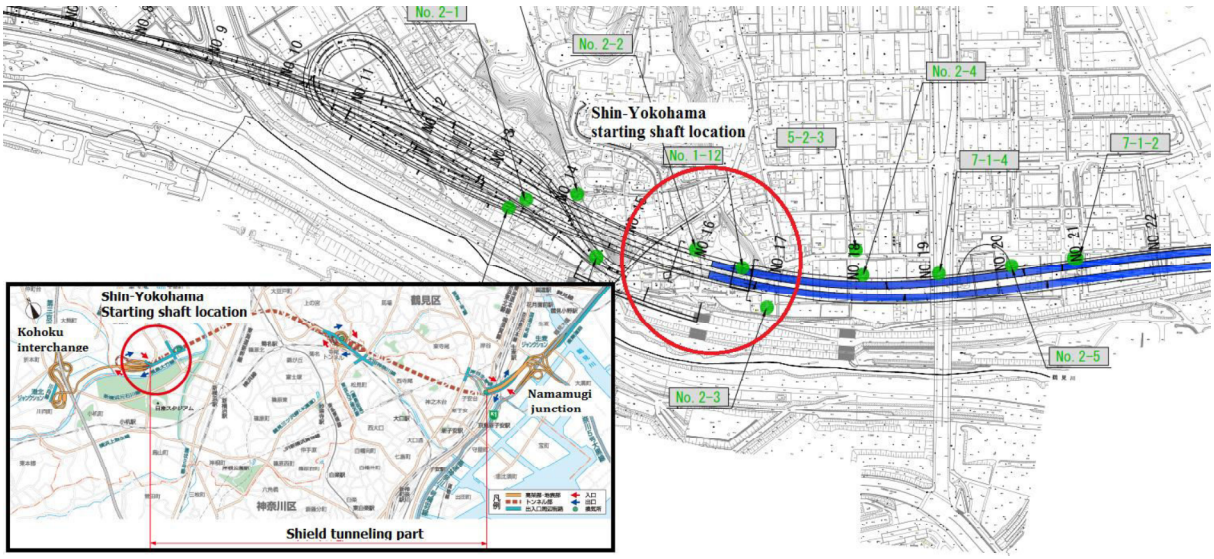

Figure 4.3. Starting shaft location in shin-Yokohama (data received from Metropolitan Expressway Co. Ltd)

Tunneling starting shaft locates in Shin-Yokohama area as shown in Fig. 4.3. Fig. 4.4 shows the entrance of the tunnel down the starting shaft.

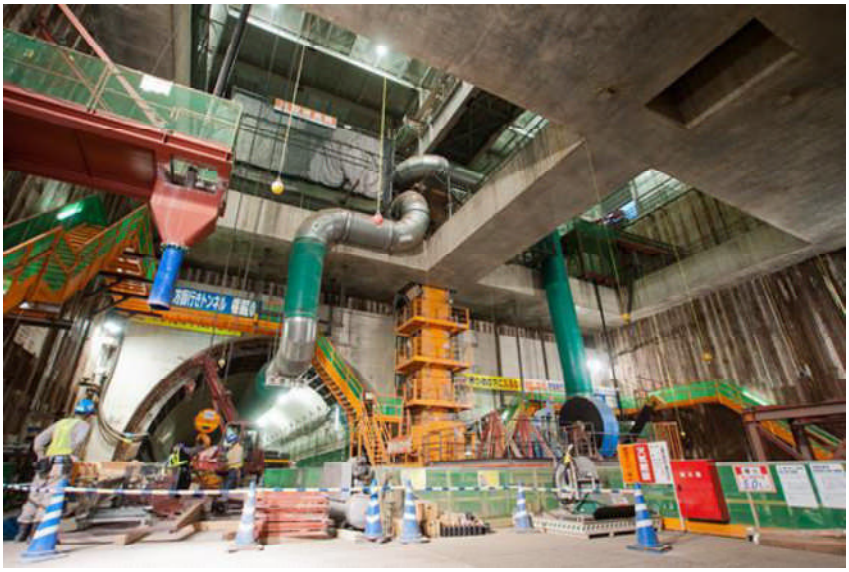

Figure 4.4. Entrance of tunneling route down through the shaft below the shin-Yokohama area (reproduced from the http://radiate.jp/20111111/kouza34/#)

The shield machines are being used for tunneling of this route have 12.49 m outer diameter, 11.5 m long, and 1,500-ton each. Fig. 4.5 illustrates the EPBMs.

Figure 4.5. Used EPB shield machines for tunneling of Yokohama Circular Northern Route (reproduced from the http://radiate.jp/20111111/kouza34/#)

4.3 Geological and hydrological specification of the site

Geological profile of the soil in the site is shown in Figs. 4.6 and 4.7. In Fig. 4.6 the longitudinal profile of the tunneling part of the route can be seen.

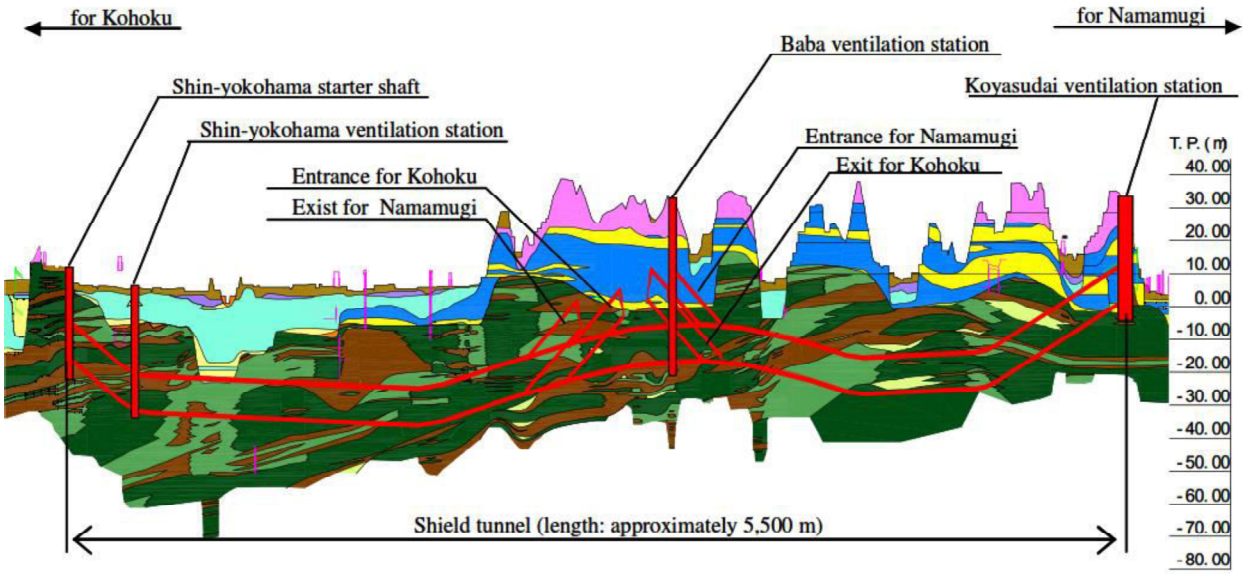

Figure 4.6. Geological profile (soil types are shown in Fig. 4.7) (data received from Metropolitan Expressway Co. Ltd).

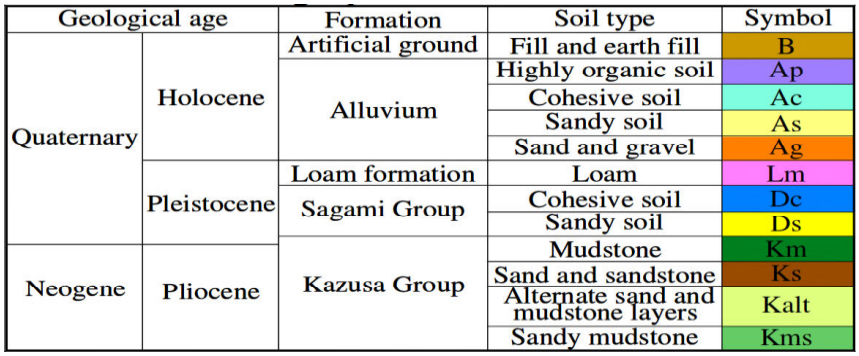

Figure 4.7. Stratigraphic classification (geological profile is shown in Fig. 4.6)

The shield machines advance through the ground mainly composed of mudstone (Km), sandy mudstone (Kms) and sand and sandstone (Ks), all of which have an N-value of 50 or higher. The soil parameters of this site and details of the stratification are summarized in Table 4.1.

Table 4.1. Soil parameters and stratification of studied site obtained from field tests[1].

Depth (m)	Symbol	Soil type	γ_t kN/m³	c kN/m²	Φ °	E_u MPa	ν_u	E' MPa	ν'	K_0	k m/day
0–1.5	*B*	Fill material	14.0	30	0	1.2	0.495	1.1	0.333	0.8[2]	8.64×10^{-3}
1.5–10	*Ac*	Cohesive soil	15.5	35	3	3.3		2.94		0.8[2]	8.64×10^{-3}
10–12.3	*As*	Sand	18.0	20	33	6.0		5.35		0.46[3]	8.64×10^{-1}
12.3–14.5	*Ks*	Sand and sandstone	19.5	60	42	324		289		0.33[3]	8.64×10^{-3}
14.5–17.5	*Kms*	Sandy mudstone	18.0	1840	10	551.5		492		0.16[4]	8.64×10^{-3}
17.5–19	*Ks*	Sand and sandstone	Same as *Ks* layer								
19–24	*Km*	Mudstone	18.5	2020	7	482	0.495	430	0.333	0.16[4]	8.64×10^{-3}
24–27	*Ks*	Sand and	Same as *Ks* layer								
27–28.5	*Kms*	Sandy mudstone	Same as *Kms* layer								
28.5–30	*Ks*	Sand and sandstone	Same as *Ks* layer								
30–31	*Kms*	Sandy mudstone	Same as *Kms* layer								
31–33.5	*Ks*	Sand and	Same as *Ks* layer								
33.5–55	*Km*	Mudstone	Same as *Km* layer								

[1] In Table 5, γ_t is the total unit weight, c is the cohesion, Φ is the friction angle, E_u is the undrained Elastic modulus, E' is the drained Elastic modulus, ν_u is the undrained Poisson's ratio, ν' is the drained Poisson's ratio, K_0 is the lateral earth pressure at rest, and k is the permeability of soil.

[2] The value is based on 'standard specifications for shield tunneling', Japan Society of Civil Engineers.

[3] The value is based on Jaky's equation, $K_0 = 1 - \sin\Phi$.

[4] A value derived from experience in the field has been used.

Thickness, elastic modulus and Poisson ratio for tunnel lining is also shown in Table 4.2. The rings length is this case is 2 m.

Table 4.2. Lining specification of the tunnel

Thickness (mm)	E (MPa)	v
400	33000	0.17

The unconfined compressive strength is 1000 kN/m^2 or higher for Km and Kms. The ground is hard. An alluvium with an N-value of approximately 3 reaches the tunnel crown below ground level near the Tsurumi River and National Highway Route No. 1. The parallel shield tunnels composed of rings with an outer diameter of 12.3 m and an inner diameter of 11.5 m have a length of 5.5 km between the Shin-Yokohama starter shaft and Koyasudai ventilation station. Two shield tunnel boring machines are used for excavation. The starter shaft is located in a quiet housing area. The tunnels are excavated mostly under private land from the starter shaft to the receiving shaft.

OCR values obtained from consolidation tests on samples taken from boreholes show that all samples are over consolidated. OCR value in Ks and Km (refer to Table 4.1) layers is observed to be higher than 10.

Hydrological condition of the site along the tunnel route is monitored through the water level observation in boreholes and test pits. Based on these data, ground water level is assumed to be 2 m below the ground surface in 350 meter from launching shaft along the tunnel route. Permeability values are also shown in Table 4.1.

4.4 Monitoring sections

In order to verify the safety of underground construction, three monitoring sections called MS1, MS2, and MS3 were located along the tunnel lines after about 15, 50, and 180 m from the launching shaft location. The tunnel excavation is being done in two separate lines, west line and east line as shown in Fig. 4.8. This figure displays the layout of the site plan, launching shaft, monitoring sections, west and east tunnel lines, and tunnel ring numbers (shown by R).

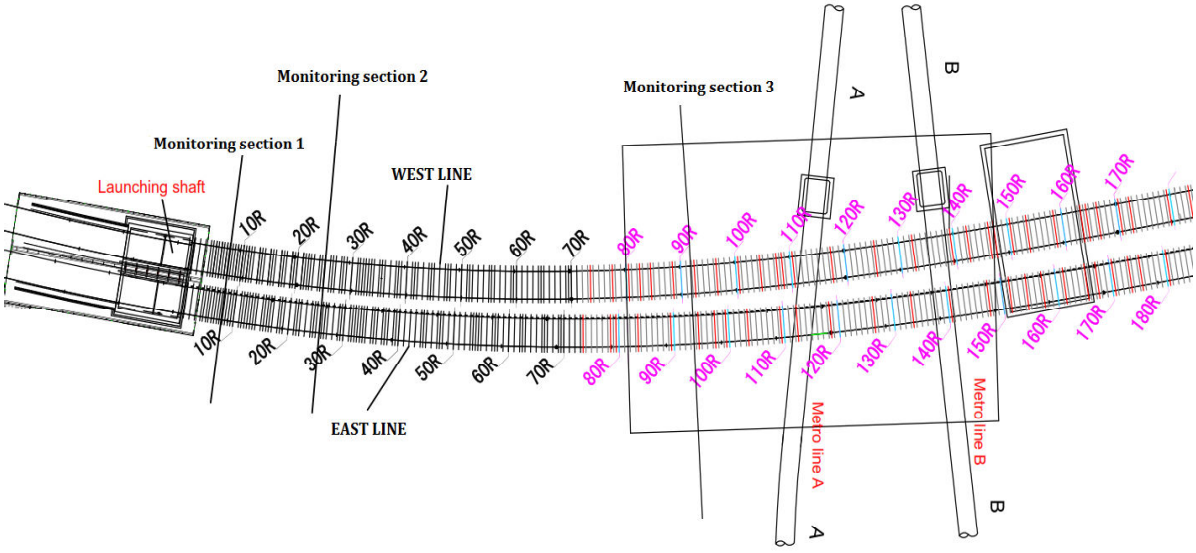

Figure 4.8. Layout of the approximate first 350 m of the tunneling routes (west and east lines), ring numbers (shown by R), launching shaft, and monitoring locations (MS1, MS2, and MS3).

The measurement points in the monitoring sections are monitored for vertical soil displacement before, during, and after the passing of tunnel lines. Measurement points in three monitoring sections of monitoring sections MS1, MS2, and MS3 are displayed in Figs. 4.9 through 4.11. After passing of MS3, the EPBMs intersect almost perpendicularly with two other subway lines named Metro line A, and B as shown in Fig 4.8.

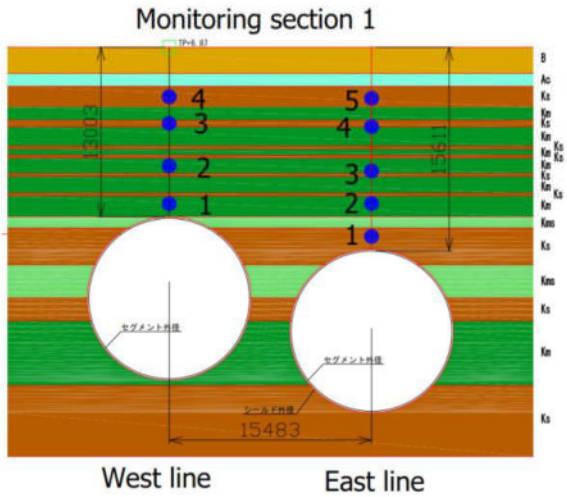

Figure 4.9. Measurement points in monitoring section 1 (MS1).

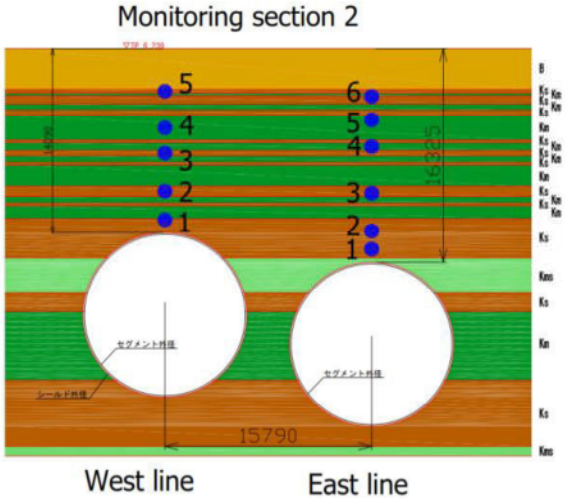

Figure 4.10. Measurement points in monitoring section 2 (MS2).

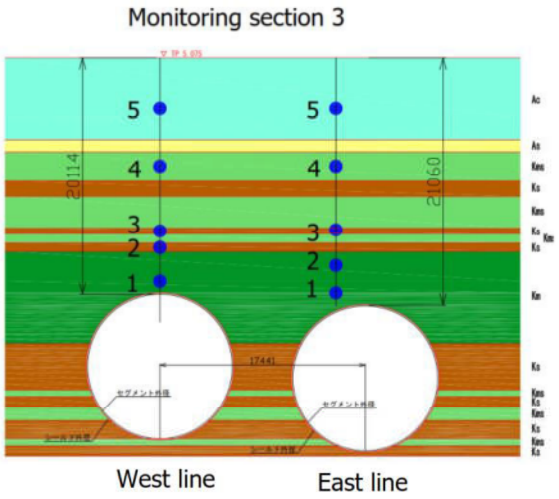

Figure 4.11. Measurement points in monitoring section 3 (MS3).

4.5 Measurement data

Value of vertical displacements in monitoring points as shown in Figs. 4.9 to 4.11 are measured by measurement devices for controlling the safety of construction before arrival, during passing of TBM through the monitoring sections.

Figure 4.12. Date of excavation, ring numbers (shown by R), and monitoring sections.

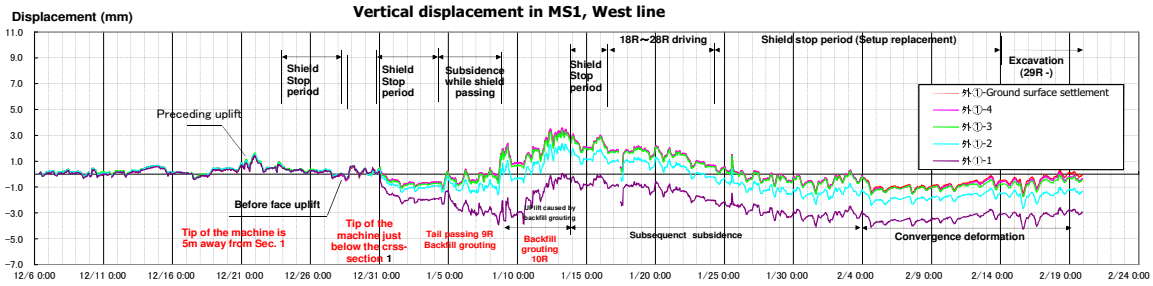

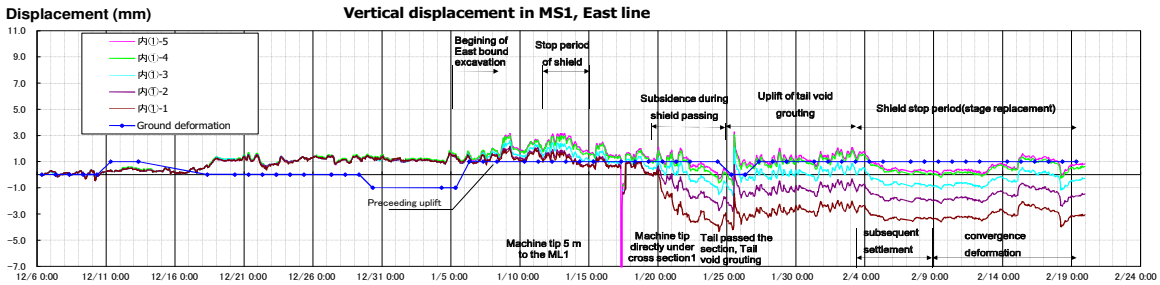

Figure 4.13. Measurement of vertical soil displacement by date of construction in monitoring points of MS1 (west and east lines).

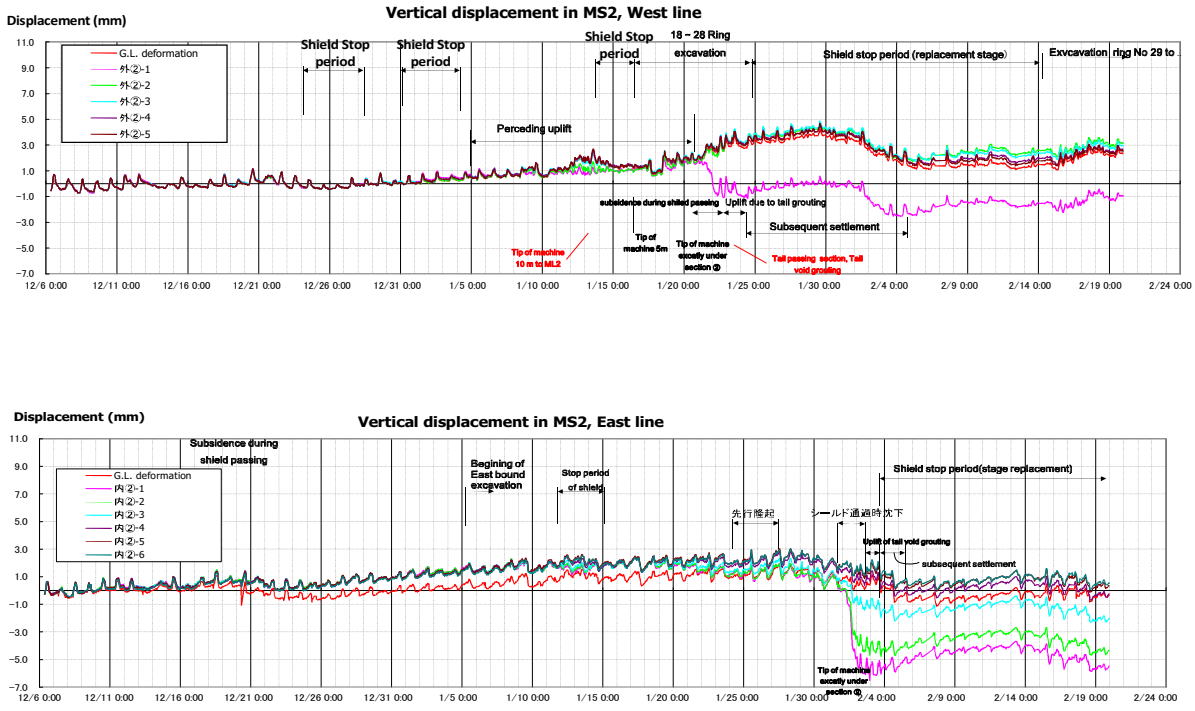

Figure 4.14. Measurement of vertical soil displacement by date of construction in monitoring points of MS2 (west and east lines).

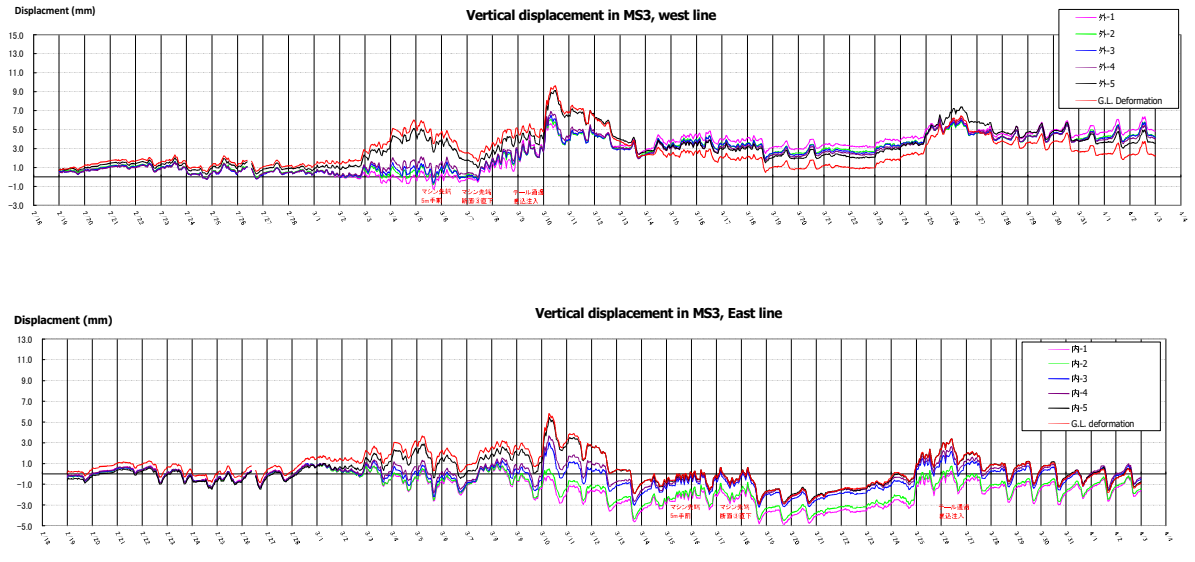

Figure 4.15. Measurement of vertical soil displacement by date of construction in monitoring points of MS3 (west and east lines).

Date of tunnel construction by ring numbers as well as MS1, MS2, and MS3 are shown in Fig. 4.12 for almost 210 m from along the tunnel route from launching shaft. The vertical displacements by date of excavation are shown in Fig. 4.13 for monitoring section 1, in Fig. 4.14 for monitoring section 2, and in Fig. 4.15 for monitoring section 3.

4.6 Summary

In this chapter, a comprehensive shield tunneling case namely as “Yokohama Circular Northern Route” located in Yokohama, Japan, was introduced. Overview of the project, geological and hydrological specification of the site, recorded vertical displacement of three monitoring sections namely as MS1, MS2, and MS3 were presented.

References:

1) Stack, B. : Handbook of Mining and Tunnelling Machinery, John Wiley and Sons, U.K., 1982.

Chapter 5 Comparison and verification

5.1 Introduction

In chapter 3, a parametric study was performed and based on the parametric study results; an experimental equation was presented for drainage determination of the soil. Then, a simplified finite element analyses method was proposed for tunnel induced deformation by determining the drainage condition of the ground around the TBM instead of complicated water-soil coupling analysis. Verification of the proposed simplified FEM method is shown in this chapter.

By using of the case study data introduced in chapter 4, shield tunneling advancement simulation of this case study is carried out by using of simplified FEM method. Vertical soil displacement of the monitoring points is calculated, and then the calculated displacement results are compared with field data measurement. The results are shown in this chapter.

In this chapter, at the first, FEM numerical model of the tunnel construction site introduced in chapter 4 is explained. The displacement of the measurement points in the monitoring section induced by EPB tunneling is calculated by a 3D FEM program. Finally, the vertical displacement of the measured data and the computational results of the FEM are compared.

Furthermore, a comparison is made to obtain the difference between computation time of analyses for cases of analyses performed with soil-water coupling method and simplified proposed FEM procedure.

5.2 FEM numerical model

3D FEM analyses were carried out using the FE program developed by Komiya et al. (1996). Details of the relevant FE formulation are given in the literature (Akagi and Komiya 1996). In order to create the finite element analysis of the case introduced in chapter 4, following items were taken into consideration:

1- The 3D FEM considered for verification focuses only to the area of that includes a 120-m long section (60 rings) that starts from ring No. 80 and ends at ring No. 140, as illustrated in Fig. 5.1 (80R to 140R) including MS3. The dates and ring numbers shown in Fig. 5.1 reveal that the average advance rate of the tunnel face in west line is around 4 to 16 m/day and 6 to 16 m/day in the east line. The groundwater level is between 2.2 to 2.8 m below the ground surface. In this part, only the data of case study (presented in chapter 4) related to monitoring section 3 (MS3) are considered. The measurement points in the monitoring section 3 (MS3) are monitored for vertical soil displacement before, during, and after the passing of tunnel lines. Fig. 4.11 showed the layout and location of settlement gauges at MS3. The soil parameters of the site and details of the stratification are detailed in chapter 4 in Table 4.1.

   A 3D model with a monitoring section 3 (MS3)—whose width, length, and height are 128, 136, and 55 m, respectively—was developed as shown in Fig. 5.2.

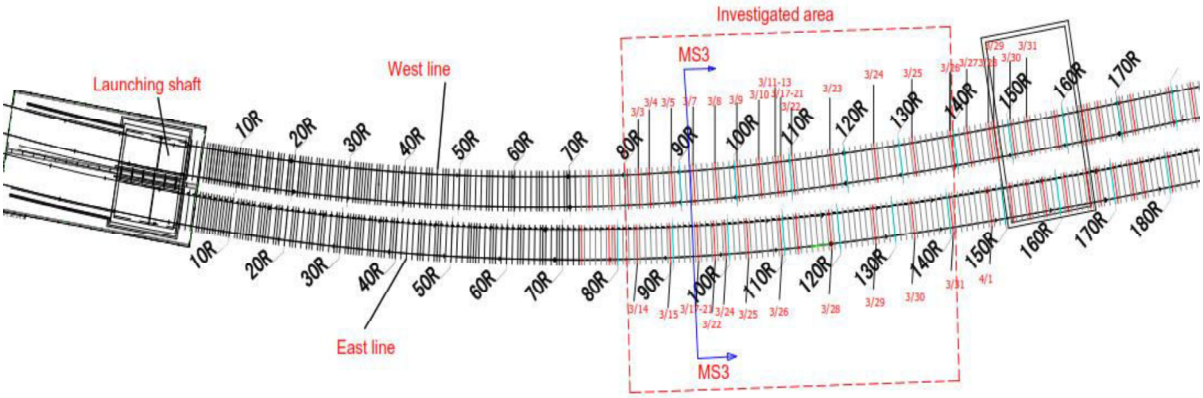

Figure 5.1. Layout of the site plan, launching shaft, west and east lines including MS3 (investigated are shown in this figure).

2- The stress path analysis performed in section 3.3 showed that during EPB tunneling, the ground ahead of the tunnel tends to be in the elastic zone. Therefore, in this case, a linear elastic soil model is also employed.

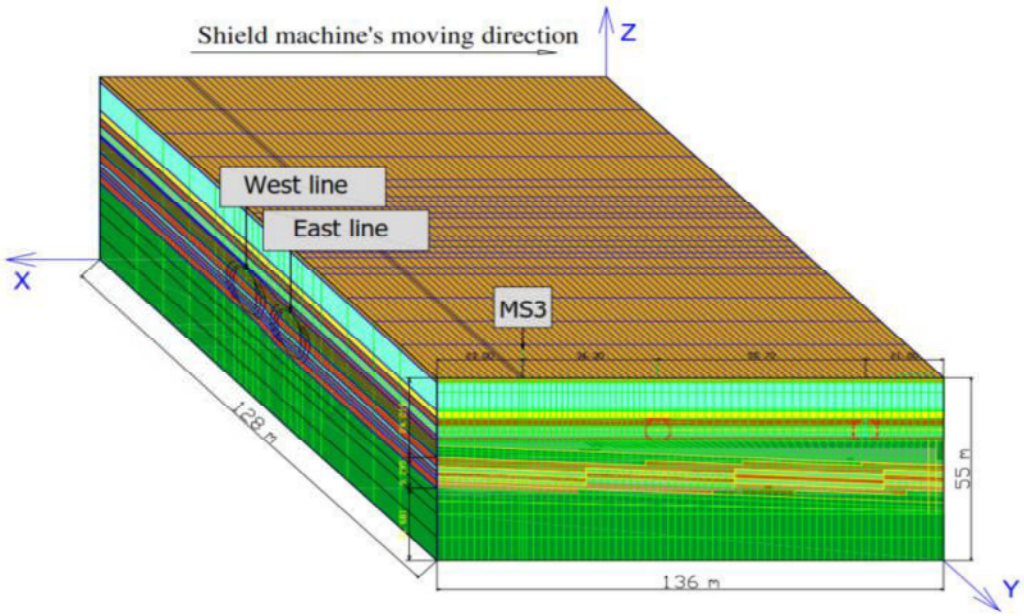

Figure 5.2. Developed 3D FEM mesh of the case study introduced in chapter 4.

3- The proposed Eq. (3.7), obtained by the results of the parametric study, can be used for drainage determination during tunnel face advancement on the basis of parameters *v*, c_v, and *H/D*. The proposed equation used to obtain $\bar{x}$ value for drainage determination as follow:

Step 1: The values of parameters *v*, c_v, and *H/D* are determined. For this case study, average *v* is ~10 m/day for the west line and ~11 m/day for the east line (Fig. 5.1). A c_v of 3.36 m^2/day is obtained by using Eq. (3.2). The coefficient of permeability is set to 8.64×10^{-3} m/day according to Table 4.1, and the soil bulk modulus is set to $K' = 3.89\times10^{3}$ kN/m^2. *H* of the tunnel lines varies between 20 to 26 m, whereas *H/D* varies between 1.6 and 2.08; therefore, *H/D* is set to the average value of 1.84.

Step 2: By using the data introduced in the previous step and substituting them into Eq. (3.7), we determine the value of $\pi_3 = \frac{c_v}{v \cdot D}$ and then calculate the constants a and b.

$$\pi_3 = \frac{c_v}{v \cdot D} = 0.026$$

$$a = 0.13 - 0.088(\frac{H}{D} - 1) = 0.056$$

$$b = 0.23 - 0.16(\frac{H}{D} - 1) = 0.095$$

Substituting the above values into the initial equation and solving for $\bar{x}$ gives $\bar{x}$ = 2.23 m. Owing to the similarity of v in both lines, the same value of $\bar{x}$ = 2.23 m is obtained for both lines.

(i) If x is considered to be tunnel face distance from monitoring section 3 (MS3),

For $x > \bar{x} =$ 2.23, the soil undrained deformation condition is assumed and the acting in-situ earth pressure and the soil Poisson's ratio can be obtained using soil total stress analysis.
For $0 < x < \bar{x} =$ 2.23, the soil drained deformation condition is assumed and the acting earth pressure and the soil Poisson's ratio can be obtained using soil effective analysis.

The input parameters of the soil layers for this model are the same as those listed in Table 4.1. Depending on the soil drainage condition (drained or undrained), the elastic modulus and Poisson's ratio (E', ν' or E_u, ν_u) as well as other parameters listed in Table 4.1 are used.

In the model, the difference between the face pressure and actual in situ soil pressure in front of the tunnel, as well as the difference between the grouting pressure and in situ soil pressure at the back of tunnel, are taken as input forces in each step. For drained and undrained conditions, the in situ soil pressure is calculated on the basis of effective and total stresses. Furthermore, the stress and strain of

the elements induced by face pressure and the tail grouting in each step are stored to be used in the next analysis step.

(ii) The displacement at MS3 is calculated and then plotted against the tunnel face distance from MS3.

Vertical displacements of field data are compared with the computational results of FEM at MS3. Fig. 5.3 illustrates the comparison results.

5.3 Comparison and verification

5.3.1 General

In this part, first, comparison of soil vertical displacement between the field measurement and FEM results using simple proposed FEM procedure is presented. Next, in order to find out the computation time difference between the simple proposed FEM procedure and a complete soil-water coupled program, the numerical model introduced in section 3.3.1 is analyzed by both of simple proposed FEM procedure and a complete soil-water coupled program (PLAXIS).

5.3.2 Vertical soil displacement comparison

Fig. 5.3 represents the vertical displacement of 5 points at MS3 for FEM results and field measurement data in both west and east lines as a function of the distance of the TBM face from this section.

The moments at which the face and tail of the TBM pass MS3 are also indicated. Before arrival of the TBM face at MS3, the vertical displacement of measurement points in both lines are around zero in the FEM output; the same trend, albeit with a slight heave, is detected in field data.

A few meters before arrival of the TBM face at MS3, the vertical displacement noticeably rises in the FEM output for both lines and specifically in the west line in the field data. This is because the face pressure of the TBM is increasingly perceived by measurement point as the tunnel face approaches the section. During passing of the TBM tail

in both lines, the vertical displacement noticeably increases in the FEM output and field data because the tail void grouting pressure is radially applied to the surrounding soil.

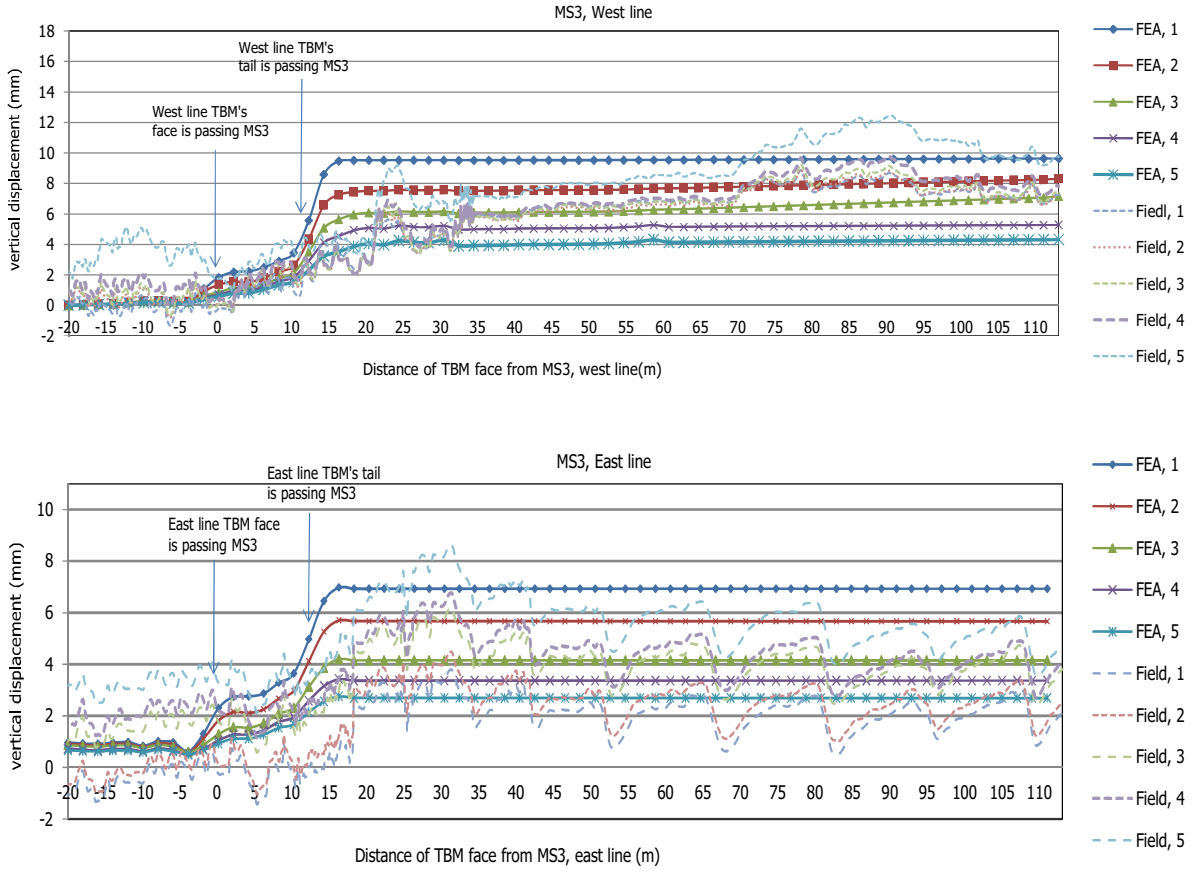

Figure 5.3. Comparison of FEA results with field measurement data for monitoring section MS3.

After passing of the TBM tail through MS3, the FEM results show almost constant vertical displacement, whereas the field data display some upward and downward fluctuations of vertical displacement, which may be due to the post grouting effect of the lining segments around MS3 after the passage of TBM through the section. The maximum anticipated vertical displacement at MS3 in the west line of the FEM output and field data are almost identical (~10 mm); in contrast, the displacement for the east line calculated by FEM is about 7 mm, with a measured value in site of approximately 8 mm. The results show that the values of vertical displacement anticipated by FEM analyses highly conform to the field measurement data. Hence, good prediction of vertical soil displacement can be achieved with the proposed Eq. (3.7) to determine the drainage condi-

tion by use of a simple total stress analysis without soil–water coupling of the soil during EPB tunneling.

5.3.3 Comparison of computational time

In order to compare computation time of analysis performed by simple proposed 3D FEM procedure and also 3D soil-water coupled program, the model introduced in section 3.3.1 is used.

The 3D Model was introduced in Fig. 3.2. In the model, a tunnel of diameter D = 12 m in a uniform soil deposit with an overall thickness of 4D = 48 m, a width of 2.5D = 30 m, and a length of 6.67D = 80 m is assumed. Numerical analyses simulation of 10 m tunnel advancement is analyzed in the y-direction for 5 steps (from y = +20 m to y = +30 m in Fig. 3.2). On each step, the shield machine moves forward by Δy = +2 m. The length of the TBM is assumed to be 10 m which lies from y = +10 m to y = +20 m before the start of simulation. The tunnel is assumed to be excavated by the EPB shield method. The mesh of this model was constructed in the both of proposed 3D FEM procedure program and also 3D soil-water coupled program. Schematic of loading steps, type of analyses in soil-water coupling analyses program is shown in Fig. 5.4.

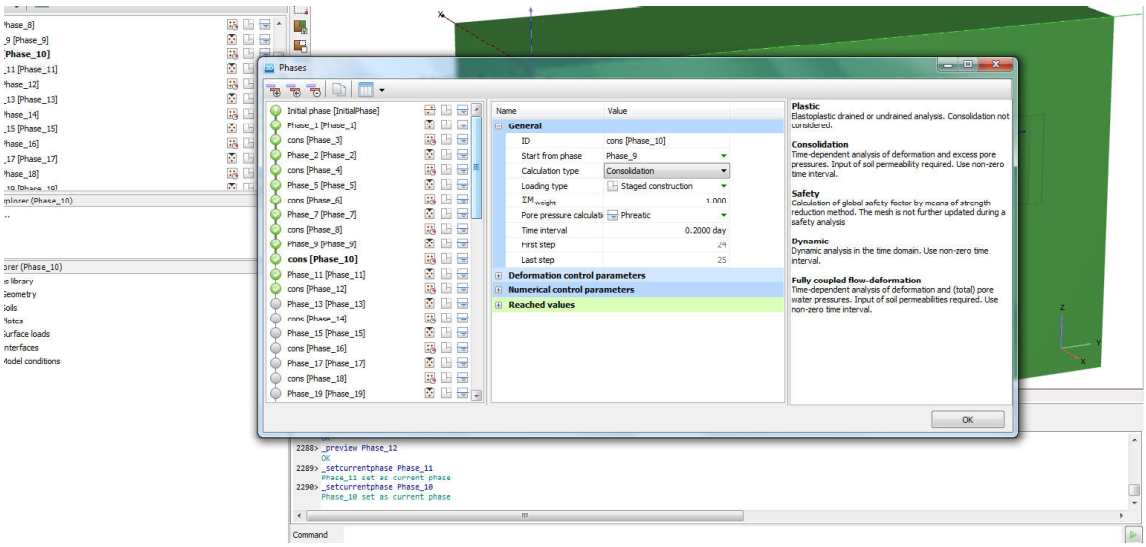

Figure 5.4. Schematic of loading steps and type of analyses in soil-water coupling analyses program (PLAXIS).

Analyses conditions in both cases are compared in concise format as shown in Table 5.1.

Table 5.1. Comparison of computation time of analyses between soil-water coupling program and the program using presented simplified FEM procedure

Parameters	Soil-water coupling program	Program using proposed simplified FEM procedure
Mesh dimensions	80 m, 30 m, and 40 m in X, Y, and Z direction respectively	80 m, 30 m, and 40 m in X, Y, and Z direction respectively
Tunnel	Diameter: 12 m Half of it is modeled.	Diameter: 12 m Half of it is modeled.
soil	Model: Mohr-Coloumb Elastic Modulus: 289 Mpa Poisson ratio: 0.33 Cohesion: 1 kPa Friction angel: 0 degree Dilatancy: 0 degree Unsaturated specific weight: 17.5 kN/m^3 Saturated specific weight: 19.5 kN/m^3 Initial void ratio: 0.5 Drainage type: Undrained	Model: Linear elastic Elastic Modulus: 289 Mpa Poisson ratio: 0.33 Drainage type: Drained and Undrained depending to distance from monitoring section
lining	Model: Linear elastic Elastic Modulus: 3.1×10^4 Mpa Specific weight: 27 kN/m^3 Thickness: 25 cm	No lining is used.
TBM	Model: Linear elastic (modeled as a plate) Diameter: 12 m Length: 10 m	TBM body has not been modeled but TBM's jack forces are applied to nodes. Diameter: 12 m Length: 10 m
Advancement pattern	10 m advancement from y = +20 m to y = +30 m in y direction	10 m advancement from y = +20 m to y = +30 m in y direction
Step No. of loading and analyses	No. of loading steps: 5 steps In each step, shield machine advances 2 m in *Y* direction. In each step, a plastic analysis and then a consolidation analysis are performed. (Fig. 5.4)	No. of loading steps: 5 steps In each step, shield machine advances 2 m in *Y* direction. Depending on the drainer or undrained condition, effective or total stress analyses are performed.
Approximate computation time	**10 minutes**	**5 minutes**

Tunnel advancement simulation in the case of soil-water coupling analysis is performed using PLAXIS 3D program. In the case of proposed simplified FEM procedure, analyses are performed using the program developed by Komiya and Akagi. (1996).

The computer which ran both of above cases has a processor of Intel Core i7-2640 M with CPU of 2.8 GHz on 64 bit operating system.

Approximate time of calculation for each of above cases is also shown in Table 5.1. It can be seen that approximate of 10 minutes needs for the calculation of the 10 m tunneling advancement simulation by using of soil-water coupling 3D PLAXIS program, while the time needed for the same mesh to be computed by simplified proposed 3D FEM procedure is about half of former one. Therefore, 50% saving in time could be anticipated by using of the proposed simplified FEM procedure.

5.4 Summary

As it was shown in chapter three, a parametric study was performed and based on the parametric study results; an experimental equation was presented for drainage determination of the soil during shield machine advancement. Later on, a simplified finite element method of calculation was proposed for tunnel induced deformation by using presented numerical equation for drainage determination of the ground around the TBM instead of complicated water-soil coupling analysis. Verification of the simplified FEM method was shown in this chapter. By using of the case study data, shield tunneling advancement simulation of the case study was carried out by simplified FEM method and then vertical displacement of the monitoring points were calculated. Calculated displacement results by FEM were compared and demonstrated with field data measurement in this chapter.

In this chapter, at the first, FEM numerical model of the studied site was explained. Soil displacement of the measurement points in the monitoring section induced by EPB tunneling was calculated by a 3D FEM program. Finally, vertical displacement of the measured data and the computational results of the FEM were compared.

The results show that the values of vertical displacement anticipated by FEM analyses highly conform to the field measurement data. Hence, good prediction of vertical soil displacement can be achieved by using of simplified FEM program along with the proposed Eq. (3.7) to determine the drainage condition.

Furthermore, a comparison is made to obtain the difference between computation time of analyses for cases of analyses performed with soil-water coupling method and simplified proposed FEM procedure. It was seen that 50% saving in time could be anticipated by using of the proposed simplified FEM procedure.

References:

1) Akagi, H. and Komiya, K. : Finite element simulation of shield tunneling processes in soft ground, International Symposium on Geotechnical Aspects of Underground Construction in Soft Ground, pp. 447–452, 1996.

Chapter 6 Conclusion

6.1 Achieved results

The current study deals with earth pressure balanced machine advancement method. An EPB machine advancement simulation using simplified FEA method was presented. Presented simplified numerical analysis method in this case is mainly used for settlements predictions of the soil due to the tunneling construction. Simplified FEM simulation procedure enables a simple total stress analysis under simple drainage condition instead of a complicated effective stress analysis considering soil-water coupling.

This study is divided into three main parts; in the first part, effect of EPB shield tunneling on the soil effective stress path is investigated. By using of the 2D tunneling chart method, the normalized deviatoric stress paths of the two points in the crown and spring line of the tunnel at one monitoring section were presented for three different soil types and three different loading cases. In total, nine analyses cases were performed in this part.

In the second part, effect of EPB tunneling on the drained and undrained behavior of the soil is examined. Three significant factors of—a) advance rate of the tunnel face, b) consolidation coefficient of the soil, and c) overburden depth of the tunnel—are considered first in conducting a parametric study and then proposing a numerical experimental equation for drained and undrained determination of soil stress–deformation behavior during EPB shield advancement in soil.

In the last part, a comprehensive EPB shield tunneling simulation case study is introduced. The shield tunneling case study namely as “Yokohama Circular Northern Route” locates in Yokohama, Japan.

The proposed FEM procedures have been verified by comparing the 3D FEM analysis results of EPB shield tunneling with the field measurement record obtained from the large diameter and the deep EPB shield tunneling within the stiff ground.

The results obtained in this research are summarized as follows:

1. A simplified FEA simulation procedure for stress-deformation calculation of EPB tunnel advancement is proposed which enables a simple total stress analysis under simple drainage condition instead of a complicated effective stress analysis considering soil-water coupling. It was concluded that 50% saving in time could be anticipated by using of the proposed simplified FEM procedure.
2. In the case of EPB tunneling, the face pressure is kept as close as possible to the sum of the in situ soil and hydraulic pressures. Here, by conducting stress path analyses with three soil types under three types of face pressure conditions (active, static, and passive load cases), the soil around the tunnel face in EPB tunneling was found to be in the elastic domain.
3. To investigate the effects of EPB tunneling on the drainage condition of the soil, a parametric study of the soil coefficient of consolidation, advance rate of tunnel face, and overburden depth was conducted.

   This analysis showed that in the case of high values of coefficient of consolidation, the generated excess pore water pressure at the monitoring section dissipates quickly regardless of the distance of the tunnel face from the monitoring section indicating the drained nature of the soil.

   Slower advance rate leads to a higher degree of consolidation at the monitoring section. This is expected because a slower tunnel face implies that more time is available for excess pore water pressure to dissipate.

   Tunnel excavation at a greater depth slightly decreases the rate of excess pore water pressure dissipation at the monitoring section owing to the longer drainage path, although its effect is far less than that of the two previous parameters. As the tunnel face approaches the monitoring section, the effect of overburden depth (*H)* becomes negligible.

4. An empirical formula was presented for simple drainage determination of soil around TBM during tunneling. This equation along with simplified FEM was used for displacement calculation of shield tunneling.
5. The proposed numerical experimental equation was verified in an EPB tunneling case, using recorded field observations and considering the results of stress path analyses indicating that the soil condition remains in the elastic zone during EPB tunneling. The results showed that good prediction of soil vertical displacement could be achieved by using the proposed numerical experimental equation.

References:

LIST OF PUBLISHED PAPERS

JOURNAL PAPERS

Numerical analysis of the effect of earth pressure balanced shield tunneling on soil stress–deformation behavior, JSCE Journal, Geotechnics, vol. 2, pp. 224-238, Oct. 2014, Alireza Afshani, Hiroshi Dobashi, Kazuhito Komiya and Hirokazu Akagi.

CONFERENCE PAPERS

Approach to Numerical Simulation of Shield Tunneling and Its Evaluation by Comparison with Field Data, International Symposium on Tunneling and Underground Space Construction for Sustainable Development, Seoul, Korea, March 2013, Alireza Afshani, Hiroshi Dobashi, Shinji Konishi, Kazuhito Komiya and Hirokazu Akagi.

Shield Tunneling Advancement Simulation Using 3D FEM Considering Distance Factor and Its Validation, 18th Southeast Asian Geotechnical and Inaugural AGSSEA Conference, Singapore, pp. 431-437, May 2013, Alireza Afshani, Hiroshi Dobashi, Shinji Konishi, Kazuhito Komiya, Hirokazu Akagi, and Kaho Orihara.

Shield Tunneling Advancement Simulation Using 3D FEM Considering Distance Factor and Its Validation, 3rd International Conference on Computational Methods in Tunneling and Subsurface Engineering, Bochum, pp. 75-84, May 2013, Alireza Afshani, Hiroshi Dobashi, Shinji Konishi, Kazuhito Komiya and Hirokazu Akagi.

Advancement simulation of parallel tunnels and their interchange with two other subway lines using a new FEM approach, a case study, The 2nd international conference on geotechnics for sustainable development, Hanoi, Vietnam, November 2013, Alireza Afshani, Hiroshi Dobashi, Kazuhito Komiya and Hirokazu Akagi.

Stress-path and drainage analysis of soil during earth pressure balanced shield tunneling, Eighth International Symposium on Geotechnical Aspects of Underground Construction in Soft Ground, Seoul, August 2014, Alireza Afshani and Hirokazu Akagi.